Evaluation of Linear DC Motor Actuators for Control of Large Space Structures

by

Eric Nelson Ide

thesis submitted to the Faculty of the

Virginia Polytechnic Institute and State University

in partial fulfillment of the requirements for the degree of

Master of Science

in

Electrical Engineering

APPROVED:

Douglas K. Lindner, Chairman

A. A. (Louis) Beex

Stanoje Bingulac

May, 1988

Blacksburg, Virginia

Evaluation of Linear DC Motor Actuators for Control of Large Space Structures

by

Eric Nelson Ide

Douglas K. Lindner, Chairman

Electrical Engineering

(ABSTRACT)

This thesis examines the use of a linear DC motor as a proof mass actuator for the control of large space structures. A model for the actuator, including the current and force compensation used, is derived. Because of the force compensation, the actuator is unstable when placed on a structure. Relative position feedback is used for actuator stabilization. This method of compensation couples the actuator to the mast in a feedback configuration. Three compensator designs are proposed. The physical limits of the LDCM place limits on the bandwidth of the closed loop actuator.

A ten mode finite element model of a flexible space structure was used in simulations to examine all aspects of the actuator's performance. The performance of the actuator is compared for the three compensator designs. The actuator bandwidth is seen to be important in the actuator's effectiveness. Increasing actuator bandwidth resulted in a saturation nonlinearity in the actuator. The excitation capability of the actuator was examined to determine the authority of the actuator. The damping of the mast modes was examined to determine the effect of the feedback configuration of the actuator/mast system. Root locus techniques were used to explain changes in the vibrational modes of the structure due to the actuator compensation. Disturbance analysis was performed to quantify the effect of corrupted measurements on the purity of force generated by the actuator.

Acknowledgements

I would like to thank the members of my committee: Dr. D. K. Lindner, Dr. A. A. Beex, and Dr. S. Bingulac. My advisor, Dr. Lindner, gave me ideas and direction throughout the course of my research. Dr. Bingulac provided insight into the numerical aspects of my research.

I give my deepest appreciation to Karl and Karen Reichard. They have been my best friends, riding partners, party buddies, and everything else I have needed over the last two years.

I thank Karl, Mike B., Mike D., Dick, Jasti, Susan, Hein, Steve, Ann, Bill, Felix, and all the other students in the signals and systems area for their friendship and comraderie in making the last two years a memorable experience.

Table of Contents

List of Illustrations

List of Tables

1.0 Introduction

As space structures increase greatly in size, it becomes impossible to treat them as rigid bodies. The light, flexible materials used in these structures can result in modes of vibration as low as 0.1 Hz. These low frequency modes have very little structural damping. In order to use these large structures as platforms for equipment which require accurate pointing, such as space telescopes, the vibration of the structure must be suppressed.

Passive damping is an alternative which may be considered for future large space structures, however, studies of the requirements of large space structures, including a space station concept, have concluded that the mass of passive dampers becomes prohibitively large for large space structures [1]. It follows that active damping systems must be developed.

To actively damp the vibrations of a structure, force or torque must be applied to the structure. While this is easily accomplished on the earth, in space, it is a significant problem. The lack of an earth reference to push on places unique constraints on the actuators used to generate control forces or torques. Many types of actuators have received attention as feasible for use in active damping systems for large space structures.

A representative list includes piezoelectric transducers, gyrodampers, reaction wheel actuators, and reaction mass actuators. The work which has examined these actuators has generally dealt with simplified systems. For example, actuator dynamics and non-linearities have been ignored, and perfect measurements have been assumed to be available.

This thesis examines a linear DC motor (LDCM) for use as a proof mass actuator for vibration suppression in a large space structure. This thesis differs from previous work examining actuators in that it gives a complete description of the aspects of use of a linear DC motor actuator. The configuration of the actuator/structure system resulting from actuator stabilization loops is considered. The effect of the physical limits of the actuator on the actuator compensation is considered. The effect of the closed loop actuator dynamics is considered. Disturbances associated with measurements within the system are considered.

Three actuator designs are presented. Simulations are performed coupling ten actuators to a ten mode finite element model of a flexible space structure. The performance of the three compensator designs is compared. The excitation capability of the actuator is examined to determine actuator authority. Actuator compensation is seen to affect the vibrational modes of the structure. Root locus techniques are used to explain changes in the structure's vibrational modes for the three compensator designs. Digital relative position measurements and noisy accelerometer measurements cause noise in the force generated by the actuator. Comparing the different aspects of performance for the three compensator designs highlights the important implementation issues for the LDCM actuator.

The following few paragraphs give a brief outline of recent research into actuators for vibration suppression of large space structures. Transducers which produce and measure strain show promise in vibration damping. Since the generation of strain does

not require an inertial reference to push against, these actuators may be applied in a space environment. Studies which have applied piezoelectric transducers to both measure and generate strain on cantilever beam show that these transducers work well in damping small oscillations [2]. This type of system could be coupled with another which damps large vibrations. These transducers are seen to easily implement rate feedback.

Large structures may have a large number of modes which need to be controlled. Some research is examining distributed-parameter vibration control systems to compare with systems using discrete actuators. Distributed piezoelectric-polymer actuators have been applied to a cantilever beam. These studies have concluded that it is possible to use distributed actuators to control all modes of the structure with no model truncation [3].

A gyrodamper is another type of actuator which does not require an inertial reference to push against. A gyrodamper is a momentum transfer device. A pair of control moment gyros is configured to have the two axes of rotation in the same plane. By changing the angle between the two axes, gyro momentum is transferred to the structure by applying a torque to it. Studies have shown that gyrodampers may be applied to large space structures with rate feedback and may achieve moderate amounts of damping [4].

Reaction actuators are another method of generation force for control of space structures. These actuators push against the inertia of a mass. Placing a force (torque) against a mass places an equal and opposite force (torque) against the structure. There are two types of reaction actuator. Reaction wheel actuators use a motor to apply torque to a flywheel and, hence, to a structure. Proof mass actuators are the linear equivalent of a reaction wheel actuator.

Experimental studies have compared a reaction wheel actuator to a proof mass actuator for vibration suppression of a cantilever beam [5]. This work was performed

by simulation. The conclusions state that actuator placement is important in determining actuator effectiveness. The reaction wheel actuator was concluded to be more effective than the proof mass actuator for the tested actuator location. The proof mass actuator used in this study consisted of a mass excited by two DC motors with cams attached to the shaft. Several other proof mass actuators with different dynamics and performance which have been studied.

A pivoted proof mass actuator has been proposed for use in vibration suppression in large space structures [6]. This actuator consists of a mass attached to the structure by a hinge. For small amounts of proof mass motion, the arc described by the proof mass approximates linear motion. Actuator dynamics were derived and concluded to be important in the application of this actuator.

A linear magnetic drive proof mass actuator has been proposed and a prototype built. Studies have placed the prototype actuator on a cantilever beam for model generation [7]. Simulations have also been performed to examine the effectiveness of this actuator in application to a large space structure [8]. The relationship between actuator bandwidth and the structure mode frequencies was investigated to determine gain limitations for stability of rate feedback control.

Other work has concentrated on actuator compensation to make the linear drive proof mass actuator positive real [9]. The same work looked at using the proof mass actuator for limiting-performance/minimum-time control of large space structures.

Much has been done in examining actuators capable of generating control forces (torques, strains) for space structures. Much of this work has concluded that the actuator dynamics are an important consideration in control design for large space structures [4],[7],[8]. It has also been concluded that the actuator/structure interactions must be considered in control design [1].

This thesis examines a linear DC motor for use as a proof mass actuator. The purpose is to fully characterize the LDCM actuator, especially the actuator dynamics and actuator/structure interactions.

Chapter two describes the linear DC motor actuator. The physical limits of the actuator, stroke length and power supply current, are seen to place limits on the amount of force the actuator can generate. This chapter also presents a model for the LDCM. The current and force compensation used in the actuator is explained. This compensation removes the effect of back emf and friction from the force generated by the actuator.

Chapter three looks at placing the LDCM actuator on a large space structure. A model for a large space structure obtained from NASA is presented. The actuator is seen to be unstable when placed on the structure. Because relative position measurements are the only ones available in space, the actuator stabilization couples the actuator to the mast in a feedback configuration.

Chapter four explains the compensation used for actuator stabilization. The actuator bandwidth is seen to be limited by the physical limits of the LDCM actuator. Three compensator designs are presented: a lead compensator, position-velocity feedback, and wide bandwidth position-velocity feedback. It is shown that increasing the actuator bandwidth will give the actuator a saturation nonlinearity.

Chapter five evaluates the performance of the LDCM actuator. The performance of the actuator with the three different compensator designs is compared to show the characteristics of each compensator design. The actuator is evaluated for both excitation of the structure and for the amount of damping it adds to the structure. The actuator bandwidth is seen to affect its ability to follow input commands and excite the structure. The three actuator compensator designs are shown to add different amounts of damping to the structure. Root locus techniques are used to explain this difference.

This analysis explains the actuator-structure interactions which arise from the feedback configuration of the mast and actuator. Chapter five also shows the effects of disturbances within the system. The measurements used for actuator compensation: a digital relative position measurement obtained from an optical encoder and an acceleration measurement corrupted by noise, are seen to cause noise in the force generated by the actuator.

Chapter six gives a summary and presents conclusions. An appendix gives listings of the computer programs used for the simulations.

2.0 The Linear DC Motor

A linear DC motor can be used to generate the control forces necessary for vibration suppression in flexible space structures. The linear DC motor operates similarly to a rotary DC motor with some important differences. This chapter gives a description of the linear DC motor and explains its important limitations.

2.1 Motor Description

Figure 1 shows a drawing of a typical permanent magnet linear DC motor (LDCM). An LDCM is made up of two major parts: the base of the motor which contains the motor coils and drive circuitry and the bar which contains permanent magnets to generate the motor flux. The bar is supported by bearings and moves through the center of the base. Because it is a permanent magnet motor, the amount of force the base coils apply to the bar is directly proportional to the magnitude of the current in the coils.

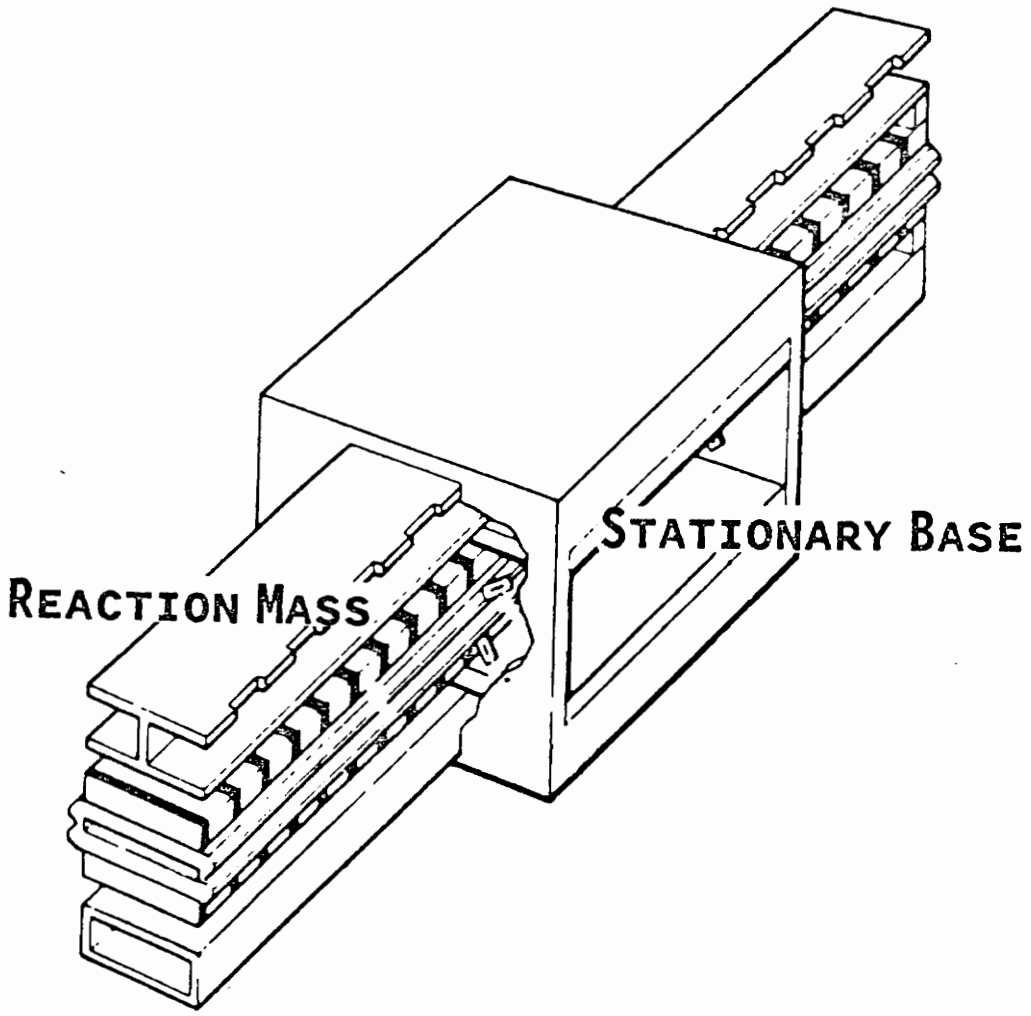

Figure 1. Picture of LDCM Actuator.

The LDCM design used for this analysis was equipped with two measurement devices; an accelerometer and an optical encoder. The accelerometer is mounted on the LDCM bar and allows measurement of the force applied to the bar. The force applied to the motor bar may be different from the force applied to the base due to friction. The optical encoder is mounted on the motor bar. It allows measurement of the displacement of the motor bar relative to its center. The optical encoder consists of a grid mounted on the bar and circuitry on the base which counts the number of grid teeth which have passed by. The output of the encoder is a signal proportional to the number of teeth. The encoder output is a quantized measurement which will jump an increment in output each time a tooth is counted. The nominal optical encoder resolution is 1 mm.

2.2 *Physical Limits*

The LDCM actuator has two physical limits which affect its performance: a current limit and a stroke limit. The motor drive circuitry and power supply have a limit on the current they can supply. Since the force generated by the LDCM is proportional to the motor current, this places an upper limit on the amount of force the motor can generate. If the current commanded from the power supply is higher than the limit, the current will saturate at the limit level. Commanding an amount of current essentially commands an amount of force to be applied. Giving a force command larger than the force limit will cause the applied force to saturate at the limit level.

The LDCM will have an available stroke equal to the length of the motor bar. Trying to achieve a displacement of the motor bar larger than the available stroke will cause the bar to strike a stop at the end of its stroke. It is important to keep this from

happening because damage could occur to the motor. Also, striking the stop would cause an impulse to be imparted into the motor base. The force limit, stroke limit, and bar mass are shown below for the two types of LDCM.

	Type I	Type II
Force Limit	30 N	15 N
Stroke Limit	±15 cm	±7 cm
Bar Mass	11.4 kg	6.8 kg
Nominal Encoder Resolution	1 mm	1 mm

2.3 *Force Generation*

The physical limits of the LDCM, current and stroke, both have an impact on its use in generating control forces. The current limit places a limit on the amount of force the LDCM can generate. The stroke limit also limits the amount of force the LDCM can generate at a given frequency. The bar mass will also be seen to affect the amount of force the LDCM can generate at a given frequency.

Consider applying a sinusoidal force to the LDCM bar,

$$f = F \sin \omega t \ , \tag{2.3.1}$$

where f is the force applied to the bar, F is the magnitude of the applied force and ω is the frequency at which the force is applied. Newton's Law relates the force applied to the acceleration,

$$a = \frac{f}{m} = \frac{F}{m} \sin \omega t \ . \tag{2.3.2}$$

The displacement generated from this acceleration is

$$\delta = -\frac{F}{m\omega^2} \sin \omega t \ . \tag{2.3.3}$$

This relationship shows that, if the magnitude of the force applied at a frequency is too great, the displacement generated will be too large and the LDCM bar will strike the end of its travel. Taking the magnitude of this relationship and substituting the stroke limit, d, gives a relationship for the maximum force allowed at a frequency to keep from violating the stroke limit,

$$f_{\max\ (STROKE)} = md\omega^2 \ . \tag{2.3.4}$$

Notice that both the stroke limit, d, and the bar mass, m , affect the amount of force which can be applied at a frequency ω .

The LDCM, as well, cannot give more force than the current limit allows. The maximum force generated versus frequency is shown in Figure 2. This plot shows the effect of the two mechanisms which limit the amount of force the LDCM can generate: the LDCM stroke limit and the power supply current limit. The frequency ω_B, shown in the plot, is the frequency where the effect of the two mechanisms intersect. At frequencies below ω_B, the stroke limit limits the available force. At frequencies above ω_B, the power supply current limit limits the available force. Changing the motor bar mass, the current limit, or the motor stroke limit would change ω_B.

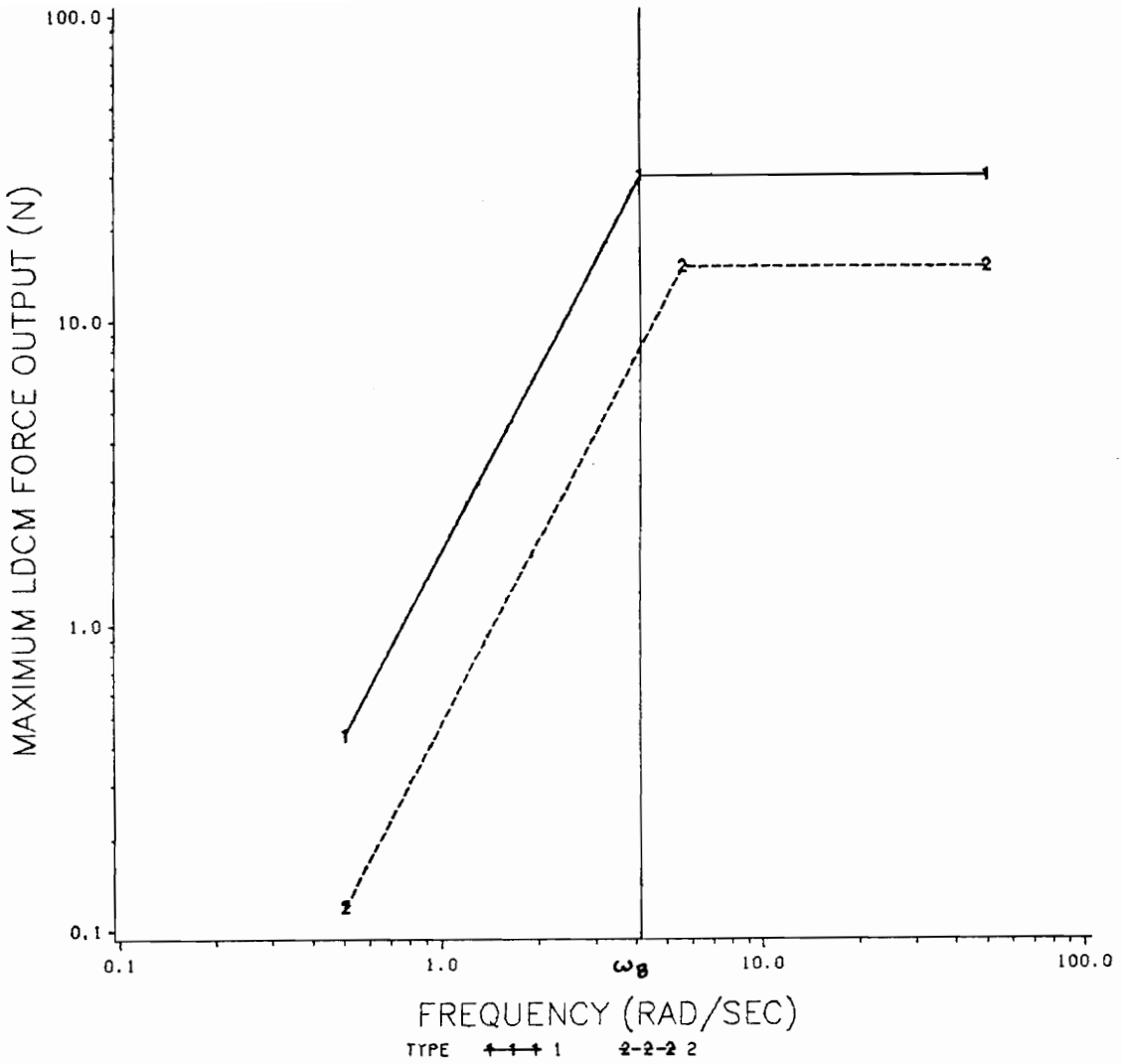

Figure 2. Maximum Force Output for the LDCM Actuator.

2.4 *Motor Model*

A model for the motor can be derived from the circuit diagram of the linear DC motor shown in Figure 3 [10]. Because the flux of a permanent motor is constant, the motor current is directly proportional to the force generated by the coils,

$$f = K_F i \ , \tag{2.4.1}$$

where K_F is the motor constant. The back emf is directly proportional to the relative velocity between the motor base and the motor bar,

$$v_b = K_F v_R(t) \ . \tag{2.4.2}$$

Writing the equation from the circuit diagram gives

$$-v_m + R\, i(t) + L \frac{d\, i(t)}{dt} + K_F v_R(t) = 0 \, . \tag{2.4.3}$$

The relative velocity is the velocity between the LDCM base and bar. On a space structure, neither the base nor the bar is stationary so the relative velocity is

$$v_R(t) = \dot{y} - \dot{p} \ . \tag{2.4.4}$$

where $\dot{y}$ is the velocity of the motor bar and $\dot{p}$ is the velocity of the base. Both must be measured in the same inertial coordinate system. Combining these equations, adding the proof mass dynamics,

$$f = m\ddot{y} \ , \tag{2.4.5}$$

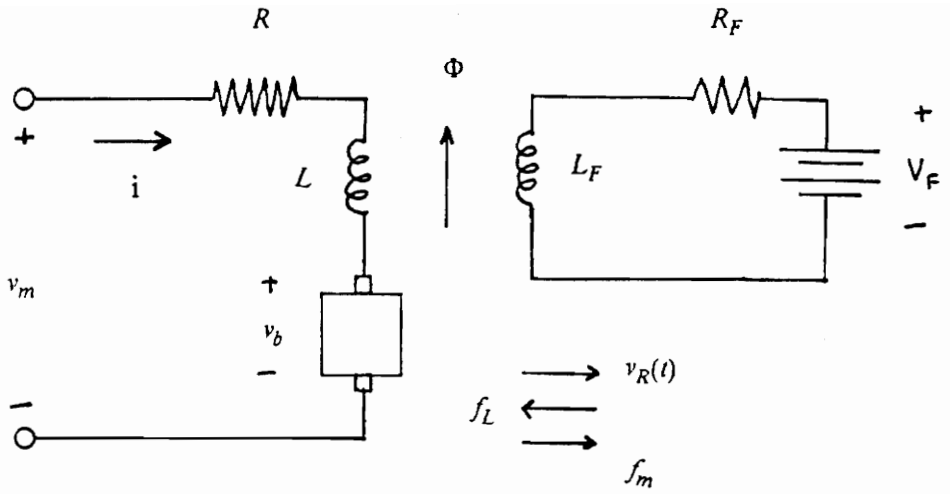

Figure 3. Circuit Diagram of Linear DC Motor.

v_m = motor voltage
i = motor current
R = motor coil resistance
L = motor coil inductance
v_b = back emf due to relative base/bar motion
f_m = force generated by motor
f_L = load force
$v_R(t)$ = relative velocity between motor base and bar
R_F = resistance representing field coils
L_F = inductance representing field coils
Φ = constant flux generated by permanent magnets

and simplifying gives the block diagram in Figure 4. This is a block diagram of the LDCM model.

2.5 *Current Compensation*

The LDCM actuator includes current compensation. This is the same for both types of actuator. The current compensation is used to reduce the phase lag caused by the motor's dynamic performance. The current compensation also is used to reduce the effect of the base velocity, $\dot{p}$, on the generated force.

Figure 5 shows the block diagram of the current loop. The current is measured by adding a small sensing resistor in series with the motor. The current is fed back with compensation so that the motor current will follow current input commands in spite of the motor dynamics. The compensation was chosen also to reduce the effect of the motor base velocity on the output force.

Figure 6 shows Bode plots of i/i_c and $f/\dot{p}$ for the current loop. The i/i_c plot shows that the current loop has unity gain and zero phase to above 1000 rad/sec. The $f/\dot{p}$ plot shows that, at frequencies below 1000 rad/sec, the component in the force due to the base velocity is well attenuated. The actuator will be used at frequencies well below 1000 rad/sec.

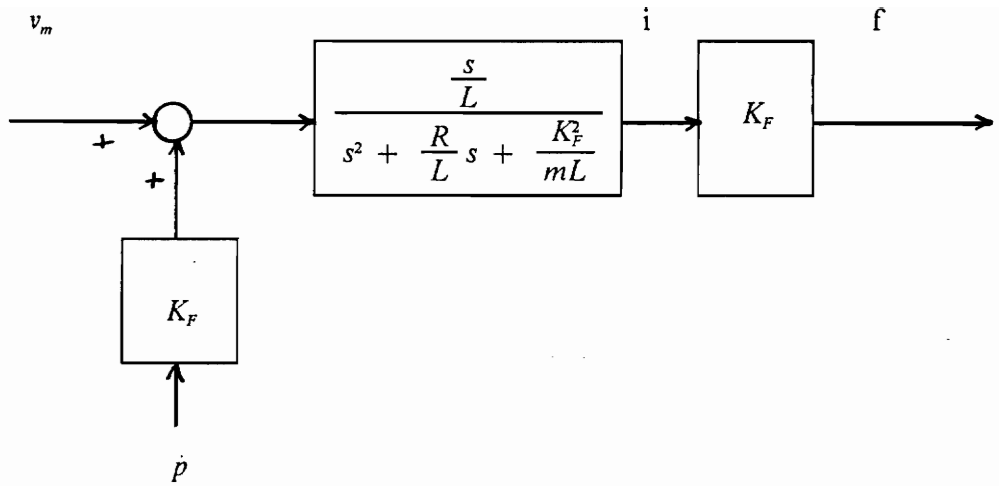

Figure 4. Block Diagram of Motor Model.

v_M = motor voltage
$\dot{p}$ = base velocity
f = motor force
i = motor current
m = mass of proof mass
R = motor coil resistance
L = motor coil inductance
K_F = motor force constant

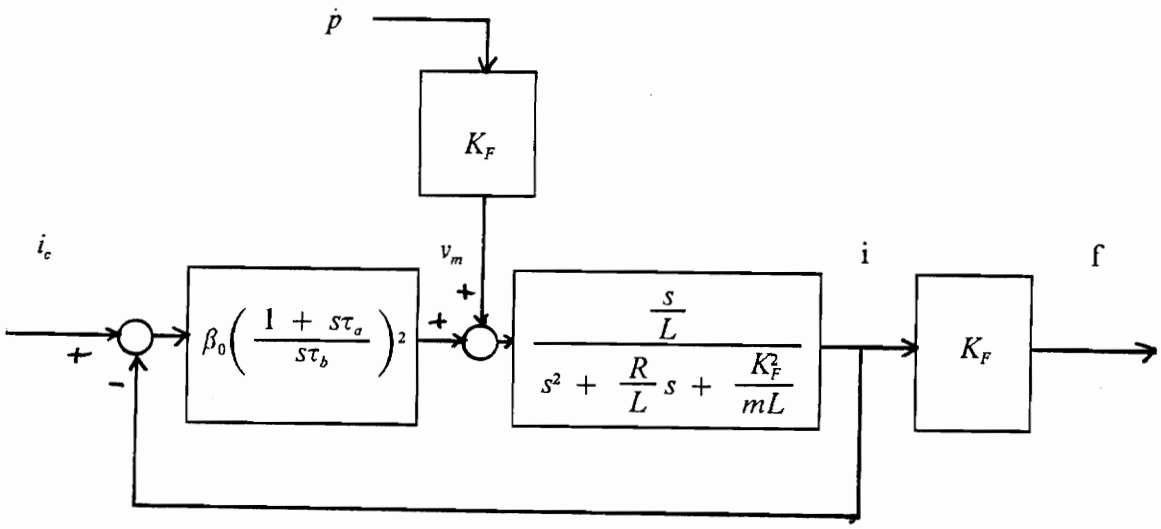

Figure 5. Block Diagram of Current Loop.

$\dot{p}$ = base velocity
i_c = commanded current
i = motor current
v_M = motor voltage
f = force applied to motor bar
K_F = 20.4 N/Amp
R = 14 Ω
L = 6 mH
m = 11.6 kg Type I, 6.8 kg Type II
β_0 = 28 Ω
τ_a = 1.8×10^{-4} s
τ_b = 1.0×10^{-4} s

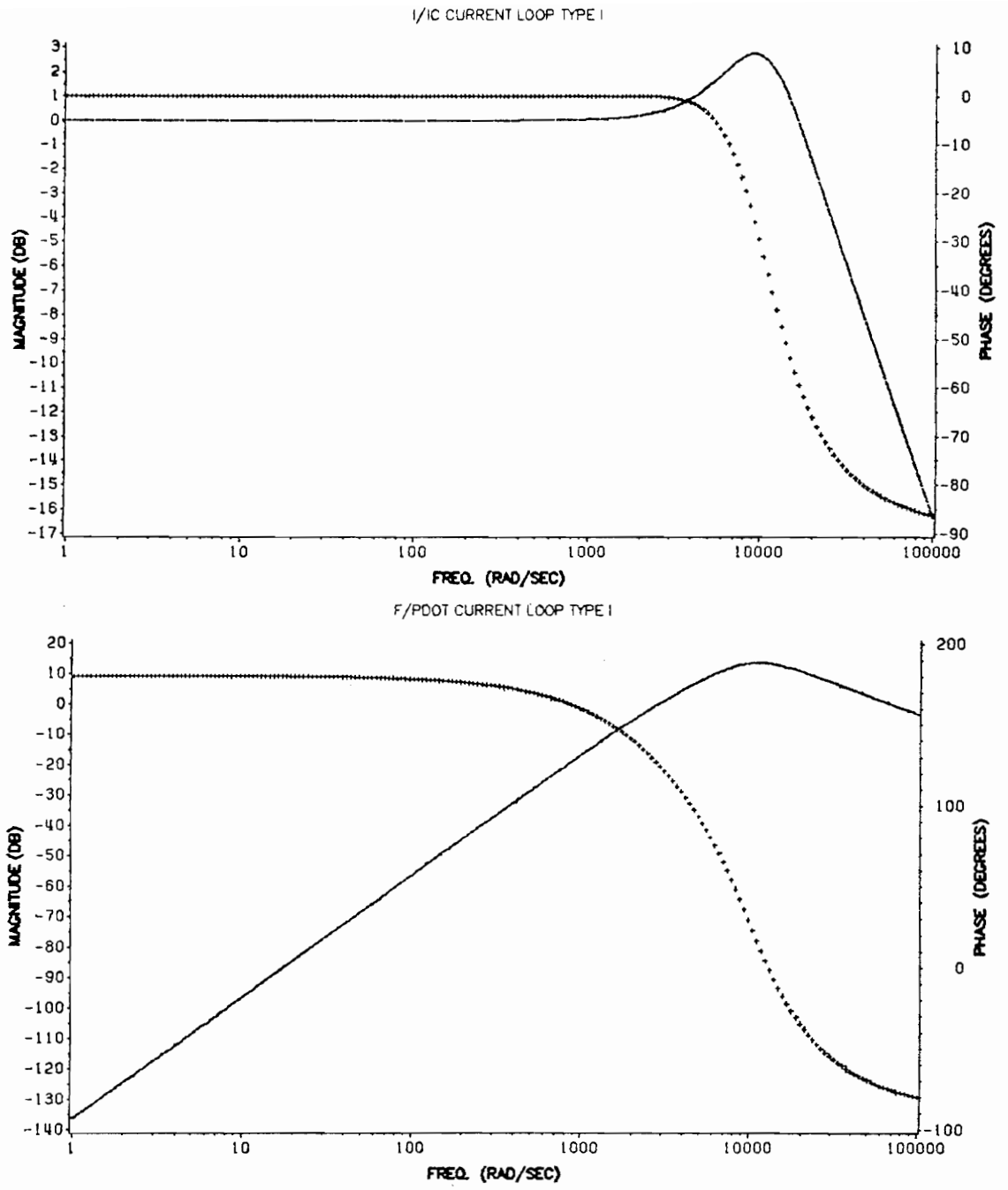

Figure 6. Bode Plots of i/ic and f/pdot, Current Loop.: Top, i/i_c; Bottom, $f/\dot{p}$

2.6 *Force Compensation*

The LDCM actuator is also equipped with force compensation. This is the same for both types of actuator. The force compensation serves two purposes. First, it reduces the effect of friction in the motor and guarantees that the actuator will apply the commanded force to the motor bar. Second, it further reduces the force component due to base velocity. The force compensation will also reduce cogging due to motor commutation.

Figure 7 shows a block diagram of the force loop. The force applied to the LDCM bar is measured by an accelerometer mounted on the bar. The accelerometer poles are above 3000 rad/sec. This is well above the frequencies where the actuator will be used. The accelerometer output is multiplied by the mass of the motor bar to give the measured force. This is fed back with compensation.

Figure 8 shows Bode plots of f/f_c and $f/\dot{p}$ for the force loop. Figure 9 shows a Bode plot of $f/f_{friction}$ for the force loop. The f/f_c plot shows that the force loop has unity gain and zero phase to 100 rad/sec. The actuator will be used at frequencies below 100 rad/sec. The $f/\dot{p}$ shows that the force component due to $\dot{p}$ is attenuated more than 100 dB at frequencies below 100 rad/sec. The $f/f_{friction}$ plot shows that disturbances due to friction are attenuated by more than 25 dB at frequencies below 100 rad/sec.

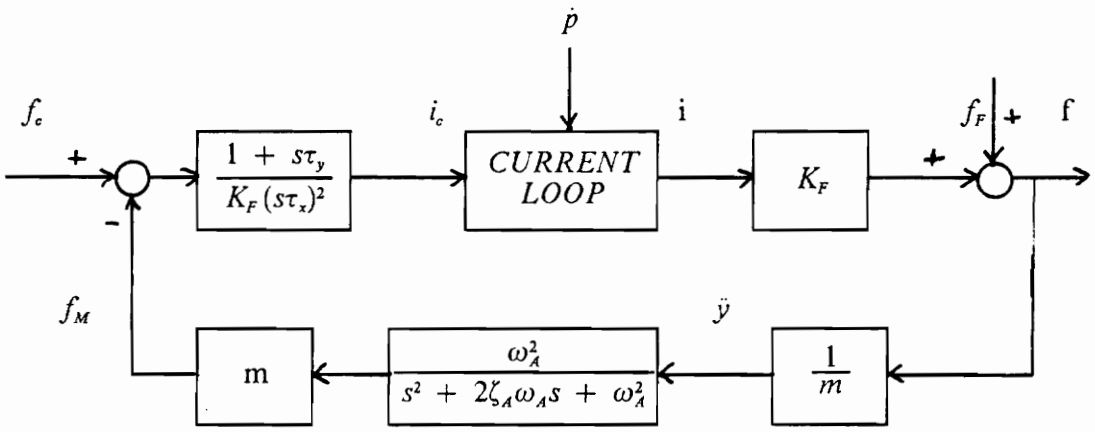

Figure 7. Block Diagram of Force Loop.

f_c = commanded force
f_M = measured force
f = force generated
f_F = friction force
$\dot{p}$ = base velocity
i_c = commanded current
i = motor current
$\ddot{y}$ = acceleration of motor bar
$\omega_A = 1000\pi\ s^{-1}$
$\zeta_A = 0.7$
$\tau_y = 2.27 \times 10^{-3}$ s
$\tau_x = 1.51 \times 10^{-3}$ s
$K_F = 20.4$ [N/Amp]

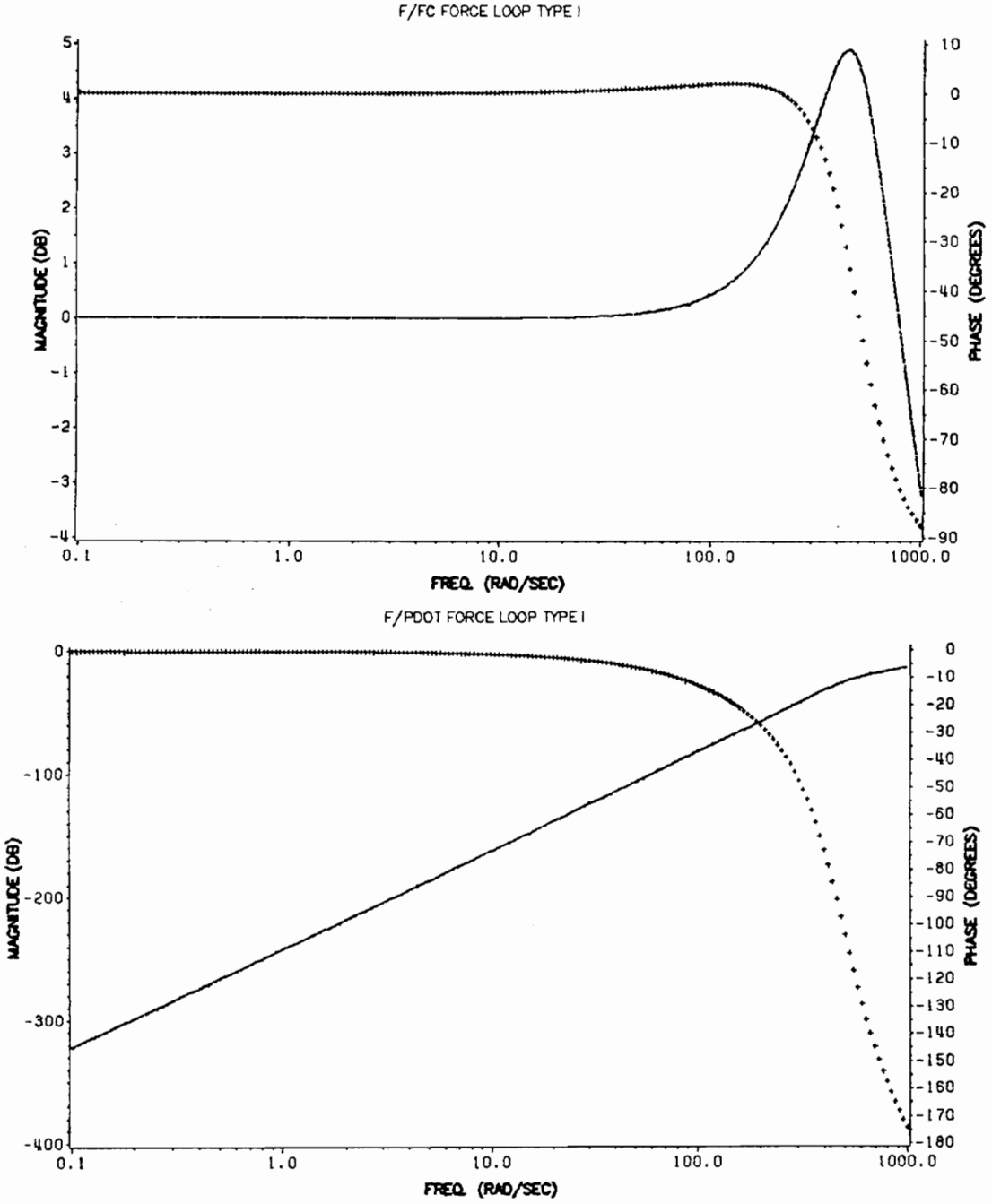

Figure 8. Bode Plots of f/fc and f/pdot, Force Loop.: Top, f/f_c; Bot, f/p

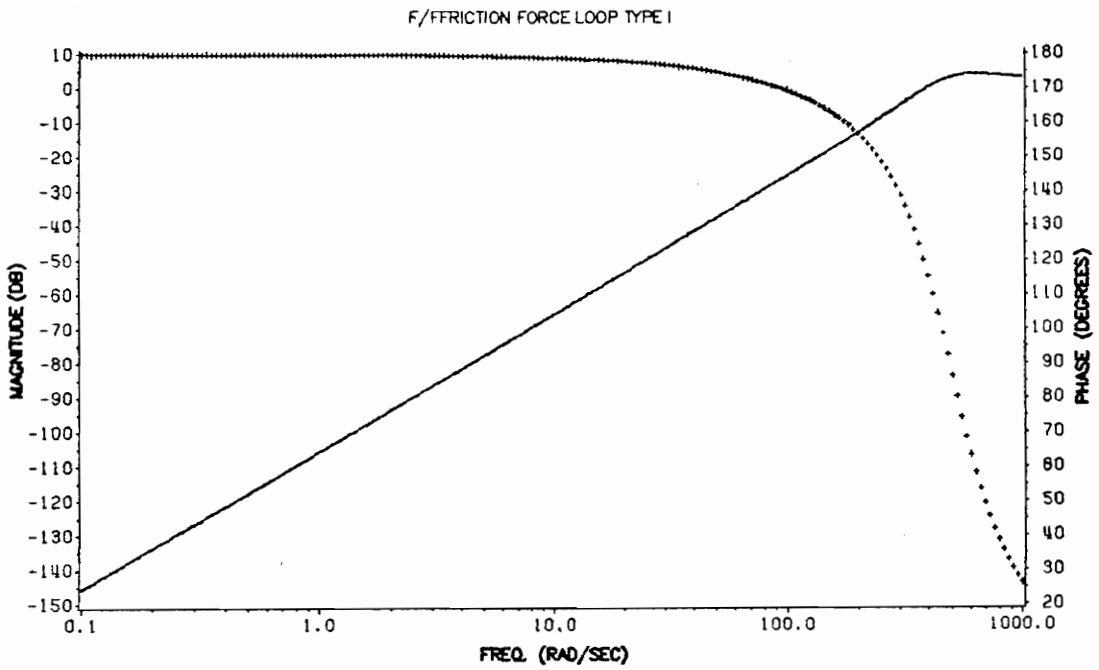

Figure 9. Bode Plots of f/ffriction, Force Loop.: f/f_F

2.7 *Summary*

This chapter has described the important physical features of the LDCM actuator. The physical limits, actuator stroke and power supply current, were seen to affect the amount of force the actuator can generate. The current and force compensation placed around the motor reduced the effects of friction and back emf. Since the loop responses are flat to 100 rad/sec, all dynamics due to the motor may be ignored below 100 rad/sec.

3.0 The Structure-Actuator System

The LDCM has been proposed for use as an actuator for control of large space structures. For this application, the LDCM will function as a proof mass actuator. The base will be attached to a structure with the motor bar free to move. Commanding a force on the motor bar (proof mass) will place an equal and opposite force on the motor base and hence the structure. The LDCM actuator has been proposed for use in exciting structural vibrations for experimental purposes and for use in damping structural vibrations. To evaluate the effectiveness of the LDCM actuator in these uses, a proposed flexible space structure with LDCM actuators mounted on it was examined.

3.1 Structure

The proposed structure that will be used in this analysis comes from the NASA Control of Flexible Structures (COFS) program. The COFS program examines the behavior of large flexible space structures. One proposed experiment of the COFS pro-

gram would use the space shuttle to carry an extendable mast in a canister in the cargo bay. The structure would be extended for experiments. The structure would be excited into vibration with LDCM actuators. Identification experiments would be done, then the LDCM actuators would damp the vibration of the structure.

3.1.1 Mast Description

The proposed mast is 60 meters long with a one meter triangular cross section. Figure 10 shows a drawing of the COFS mast extending out of the shuttle cargo bay. A cross section of the mast is also shown. A right hand cartesian coordinate system is used in referring to the mast. The x axis points toward the rear of the shuttle. The z axis points out of the cargo bay along the mast.

In between the sections of the mast are bays where actuators and instrumentation may be located. The bays are numbered starting from number one at the base of the structure in the cargo bay to number 54 at the tip of the mast. Ten LDCM actuators are located on the COFS mast. Figure 11 shows the actuator locations and configurations. Four type I actuators are located at the tip in a square configuration as shown. The actuators are referred to by the numbers shown. Actuators one and three may be used to excite the tip of the mast in the y direction. Actuators two and four can be used to excite the tip in the x direction. The combination of all four can be used to excite torsional modes. The other six actuators are located in pairs at bays 46, 28, and 10 in the orthogonal configuration shown. This configuration allows the actuators at any of the three bays to excite the structure in both the x and y directions. The actuators which can excite the mast in the x direction are referred to as actuators 6, 8, and 10, respec-

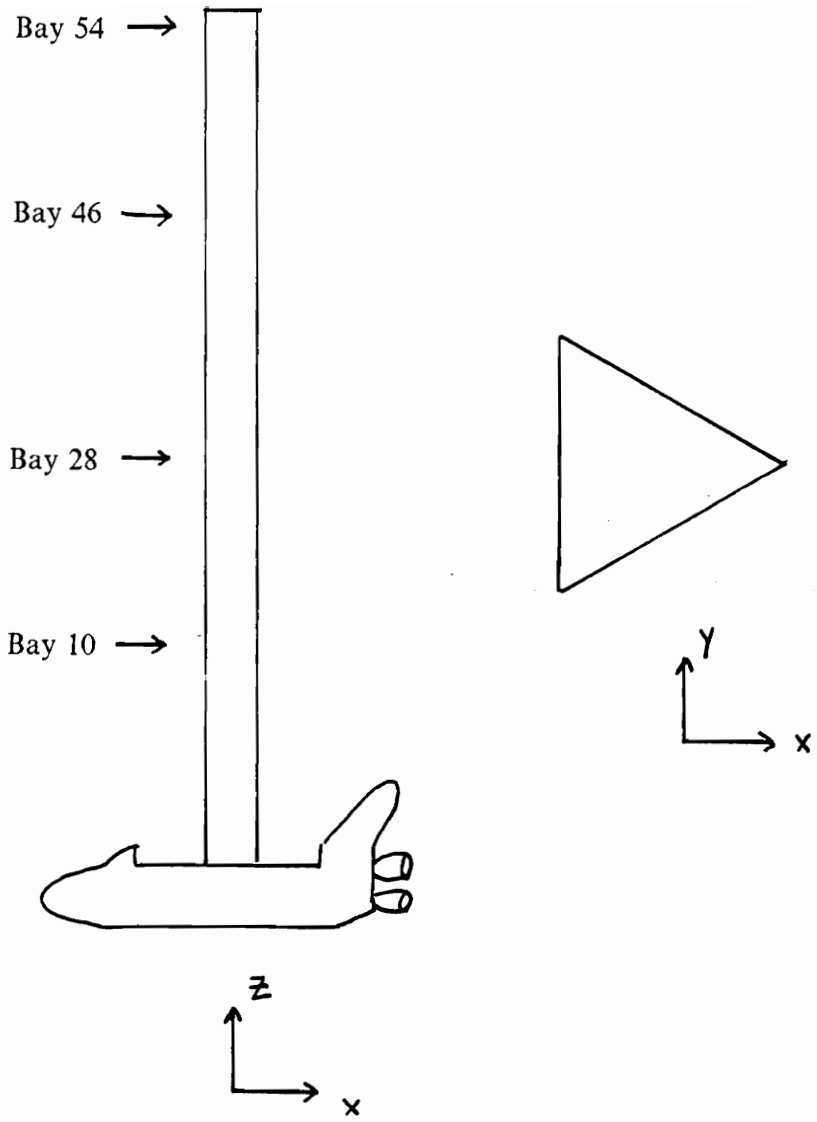

Figure 10. COFS Mast and Cross Section

Bay	Actuators	Number
54	4 Type I	1, 2, 3, 4
46	2 Type II	5, 6
28	2 Type II	7, 8
10	2 Type II	9, 10

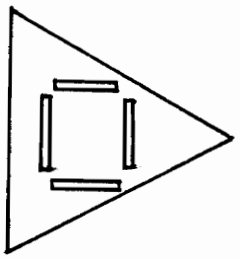

Actuator
Configuration
Bay 54

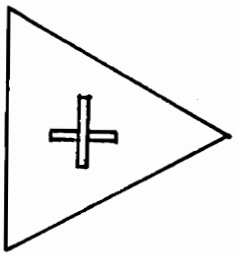

Actuator
Configuration
Bays 46, 28, 10

Figure 11. Actuator Locations and Mounting Configurations.

tively. The actuators which can excite in the y direction are referred to as numbers 5, 7, and 9, respectively.

3.1.2 Mast Model

NASA supplied data for modelling the COFS mast. Ten modes were used in our model. Four modes were included for bending in each the x direction and in the y direction. Two modes were included for torsional vibration. Table 1 shows the data NASA supplied for the mast model. The mode frequencies and mode shape coefficients were determined by finite element analysis. The amount of damping associated with each mode was assumed by NASA to be the amount shown in the table. Our analysis focused on the modes between one and fifty rad/sec. The finite element analysis was performed assuming the actuator bases were mounted on the structure, therefore, the numbers from NASA correctly modeled the mast with the actuators mounted on it.

Each mode of the mast was modelled as a second order differential equation of the form,

$$\dot{q}_i = \begin{bmatrix} 0 & 1 \\ -\omega_i^2 & -2\zeta_i\omega_i \end{bmatrix} q_i + \begin{bmatrix} 0 \\ \alpha_{ij} \end{bmatrix} f_j = A_i q_i + B_{ij} f_j \qquad (3.1.1)$$

where

ω_i = natural frequency of i^{th} mode

ζ_i = structural damping of i^{th} mode

α_{ij} = mode shape coefficient corresponding to i^{th} mode and j^{th} actuator location

Table 1. Table of Modes.

Mode	Freq.	Mode Shape Coefficient				Assumed Damping
	(rad/s)	Bay 54	Bay 46	Bay 28	Bay 10	(%)
1 x	1.175	.0486	.0373	.0149	.000874	0.2
1 y	1.5205	.0375	.0263	.0048	-.0048	0.2
2 y	8.168	-.0240	.0193	.0639	.0206	0.3
2 x	8.545	-.0243	.0194	.0647	.0213	0.3
1 torsion	9.1106	.0887	.0795	.0461	.0194	0.5
3 y	23.688	.0164	-.0487	.0117	.0489	0.5
3 x	24.693	.0167	-.0493	.0111	.0505	0.5
2 torsion	32.107	-.0496	.0122	.1161	.0739	0.5
4 y	41.469	-.0103	.0516	-.0553	.0665	0.5
4 x	42.977	-.0107	.0530	-.0567	.0683	0.5

$$q_i = \begin{bmatrix} \textbf{Position component of state} \\ \textbf{Velocity component of state} \end{bmatrix}$$

f_j = force input at j^{th} actuator location

Position and velocity of the mast due to each mode is obtained with the output matrices,

$$p_j = [\beta_{ij} \quad 0]\, q_i = C_{pj}\, q_i \tag{3.1.2}$$

$$v_j = [0 \quad \beta_{ij}]\, q_i = C_{vj}\, q_i \tag{3.1.3}$$

where

p_j = Position of mast at j^{th} actuator location

v_j = Velocity of mast at j^{th} actuator location

β_{ij} = mode shape coefficient of i^{th} mode at j^{th} actuator location

q_i = state corresponding to mode.

To get the composite behavior of the mast due to all ten modes, an augmented model was used of the form

$$\begin{bmatrix} \dot{q}_1 \\ . \\ . \\ \dot{q}_N \end{bmatrix} = \begin{bmatrix} A_1 & 0 & . & . \\ 0 & A_2 & . & . \\ . & . & . & 0 \\ . & . & 0 & A_N \end{bmatrix} \begin{bmatrix} q_1 \\ . \\ . \\ q_N \end{bmatrix} + \begin{bmatrix} B_{11} & . & . & B_{1M} \\ . & . & . & . \\ . & . & . & . \\ B_{N1} & . & . & B_{NM} \end{bmatrix} \begin{bmatrix} f_1 \\ . \\ . \\ f_M \end{bmatrix} \tag{3.1.4}$$

$$\begin{bmatrix} p_1 \\ . \\ . \\ p_M \end{bmatrix} = [C_{p1} \quad . \quad . \quad C_{pM}] \begin{bmatrix} q_1 \\ . \\ . \\ q_N \end{bmatrix}$$

$$\begin{bmatrix} v_1 \\ \cdot \\ \cdot \\ v_M \end{bmatrix} = [C_{v1} \quad \cdot \quad \cdot \quad C_{vM}] \begin{bmatrix} q_1 \\ \cdot \\ \cdot \\ q_N \end{bmatrix}$$

where A_i, B_{ij}, C_{pj}, C_{vj} are the matrices for the i^{th} mode and j^{th} actuator location. M is the number of actuators and N is the number of modes included in the model.

3.2 *Open Loop System*

The LDCM actuator is to be used on the COFS mast, therefore, the actuator and mast dynamics must be combined to examine the system. Figure 12 shows a representation of the LDCM actuator mounted on the COFS mast. The position of the proof mass (LDCM bar) measured in an inertial reference frame is referred to as y. The inertial position of the mast is referred to as p. The relative position of the proof mass, δ, is the difference between the two, $y - p$.

Placing a force on the proof mass with the motor coils will place an equal and opposite force on the mast,

$$f_{ST} = -f_{PM} \cdot \tag{3.2.1}$$

where f_{ST} is the force placed on the mast and f_{PM} is the force placed on the proof mass. Combining this equation with the equations of motion of the mast and proof mass,

$$f_{PM} = m\ddot{y} \ , \tag{3.2.2}$$

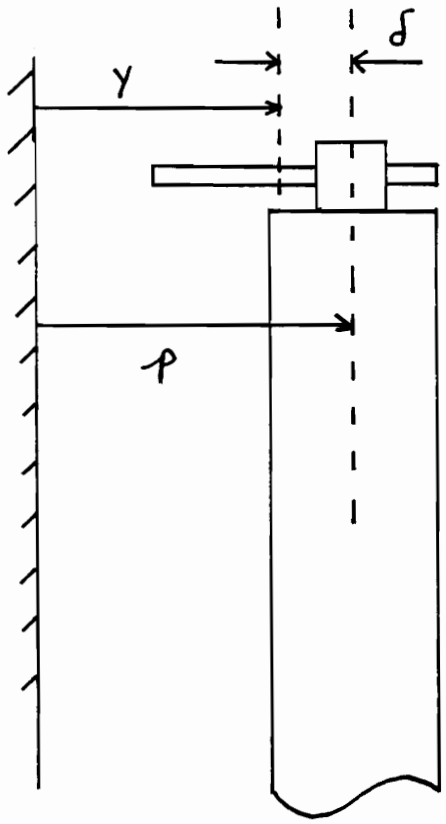

Figure 12. Representation of Actuator Mounted on Structure.

y = position of proof mass in inertial reference frame
p = position of mast in inertial reference frame
δ = relative position of proof mass

gives the open loop system shown in the block diagram in Figure 13.

The mast is stable, however, the proof mass is not. In order to have a stable system, compensation must be added to the proof mass actuator.

3.3 Proof Mass Stabilization

There are two fundamental approaches which may be used to stabilize the proof mass. The first method is to feed back the inertial position of the proof mass. The second method is to feed back the relative position of the proof mass. Each approach has both advantages and disadvantages.

For the system of the LDCM actuator mounted on the COFS mast, both approaches may be represented by the same block diagram, shown in Figure 14. The LDCM actuator has the proof mass relative position measurement available. The relative position feedback approach is represented when the switch is left open. This corresponds to directly feeding back the relative position measurement. The inertial position feedback approach is represented when the switch is closed. If the mast inertial position, p, could be measured, it could be added to the proof mass relative position measurement to give the proof mass inertial position.

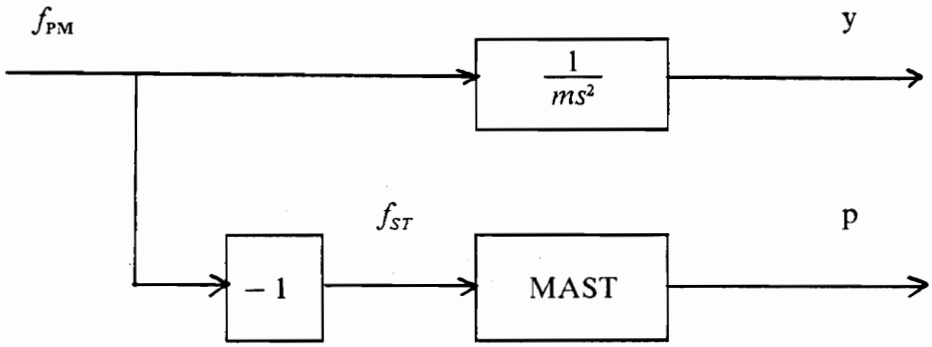

Figure 13. Block Diagram of Uncontrolled System.

f_{PM} = force generated by proof mass actuator
f_{ST} = force applied to structure
p = inertial position of mast
y = inertial position of proof mass

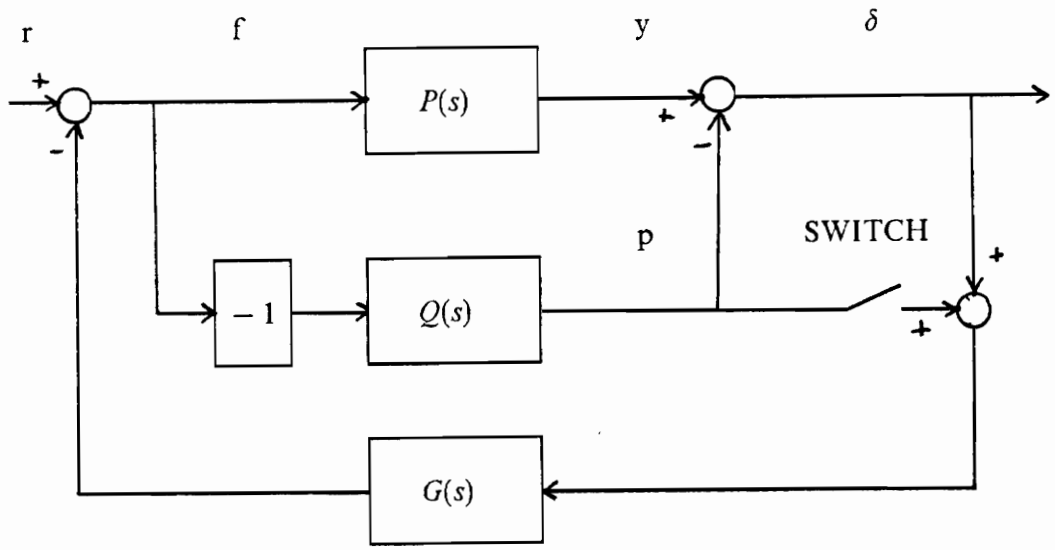

Figure 14. Block Diagram of the Two General Compensation Schemes

r = reference command input
f = force generated by proof mass
$G(s)$ = compensation
$P(s)$ = transfer function of proof mass dynamics
$Q(s)$ = transfer function of structure dynamics
y = proof mass inertial position
p = mast inertial position
δ = relative position of proof mass

3.3.1 Inertial Position Feedback

A system with inertial position feedback has certain characteristics. The proof mass follows reference commands in the inertial reference frame. For example, if the mast was excited and the proof mass was given a zero command, the proof mass would stay stationary in space and the mast would slide over it. A zero command corresponds to commanding zero force on the proof mass.

The advantage of this configuration is that the compensation of the proof mass does not affect the mast. This allows the mast and proof mass to be compensated separately.

There are several disadvantages to this configuration. First, this approach does nothing to keep the LDCM within its stroke limit. Some method other than actuator compensation must be used to limit the mast deflection. Second, there are problems with rigid body movements of the structure. A zero command causes the proof mass to be stationary in the inertial reference frame. In rigid body moves, the structure would slip past the proof mass. This could leave the proof mass away from the center of its stroke leaving a reduced amount of actuator stroke available for use. Third, it is not possible to easily measure the mast inertial position to form the proof mass inertial position from the proof mass relative position measurement.

3.3.2 Relative Position Feedback

A system with relative position feedback has different characteristics than one with inertial position feedback. Commanding the proof mass causes the proof mass to have

a displacement from the structure. A zero reference command tells the proof mass to follow the structure.

There are several advantages to this configuration. First, a zero command tells the proof mass to follow the structure, therefore, the proof mass will follow the structure through even large rigid body moves. Second, limiting the relative position command will automatically limit the deflection of the proof mass and keep it within the LDCM stroke limit. Third, the proof mass relative position measurement is available for feedback on the LDCM actuator.

There is a disadvantage to this configuration. Feeding back the proof mass relative position places the mast in the feedback path. This causes the actuator to be linked to the structure in a feedback configuration.

3.4 Summary

This chapter described the mast actuator system. A finite element model containing ten modes was used to model the mast behavior for the frequency range one to fifty rad/sec. The LDCM actuator is unstable when mounted on the COFS mast. Relative position feedback is the most feasible approach because of the availability of the relative position measurement. Because the relative position feedback approach was used, the actuator stabilization couples the actuator to the mast in a feedback configuration.

4.0 LDCM Compensation

Because of the availability of the relative position measurement in the LDCM actuator, the relative position feedback approach was used to stabilize the LDCM actuator. This will allow easy limitation of the actuator stroke. This configuration also places the mast in the feedback path, therefore, the actuator compensation will change the characteristics of the mast behavior. This chapter details the design of the actuator compensation.

4.1 Design Goals

There are two important considerations in the design of the compensation. First, it is important for the mast actuator system to have a stable relative position response. This will guarantee that the relative position will tend to zero. This will always leave the full stroke of the actuator available for use.

Second, it is important to keep the proof mass relative position within the LDCM stroke limit. If the relative position exceeds the stroke limit, the proof mass will strike the stop. By striking the stop, an impulse will be applied to the mast and vibrations will be excited.

While giving a stable relative position response and keeping the proof mass relative position within the LDCM stroke limit, there two design strategies. First, the actuator compensation could be designed to keep the force generated by the actuator below the LDCM force limit. This would give the actuator linear performance. Second, the actuator compensation could be designed to ignore the LDCM force limit. This could result in force saturation if the force requested by the compensation was more than the LDCM force limit.

4.2 Compensator Designs

Several simplifications were used during the actuator compensator design. The structure was assumed to be stationary during the compensator design so

$$\delta = y \ . \tag{4.2.1}$$

The accelerometer dynamics were ignored because the accelerometer has high bandwidth compared to the frequencies being used. A unity gain was used for the force loop because it has unity gain and zero phase to frequencies above the frequencies of use. For performing the actuator compensation design, the optical encoder was assumed to give a perfect, continuous measurement of the proof mass relative position.

The physical limits of the LDCM actuator, force and stroke, motivate the compensator design. The maximum force output of the LDCM was shown in chapter two. Since the actuator will be compensated by a relative position loop, it is appropriate to look at the maximum relative position available. Since the proof mass position is related to the force applied by $\frac{1}{ms^2}$, multiplying the plot in Figure 2 by $\frac{1}{ms^2}$ will give the maximum relative position available due to the physical limitations of the LDCM. This plot is shown in Figure 15.

The actuator compensation was designed to give the actuator relative position response the same shape as Figure 15. The actuator poles were placed to give the magnitude of the relative position response unity gain out to a frequency ω_c. Above ω_c, the magnitude response was given double pole rolloff. This was achieved by giving the closed loop actuator a pair of complex poles at a characteristic frequency of ω_c with $\zeta = 0.707$. The poles of the open loop actuator are both at the origin.

With the actuator relative position response of this form, placing a limiter on the reference input command will deep the actuator within its stroke limit. Choosing ω_c, the bandwidth of the compensated actuator, will determine the magnitude of the force signals the actuator must generate.

To look at the effect of the actuator bandwidth on the force signals, consider the block diagram shown in Figure 16. This block diagram shows a general method of compensating the proof mass actuator with a relative position loop. To look at the force signals required, look at the transfer function from δ_c to f,

$$\frac{f}{\delta_c} = \frac{G(s)}{1 + P(s)\,G(S)} \quad . \tag{4.2.2}$$

This transfer function may be simplified as follows

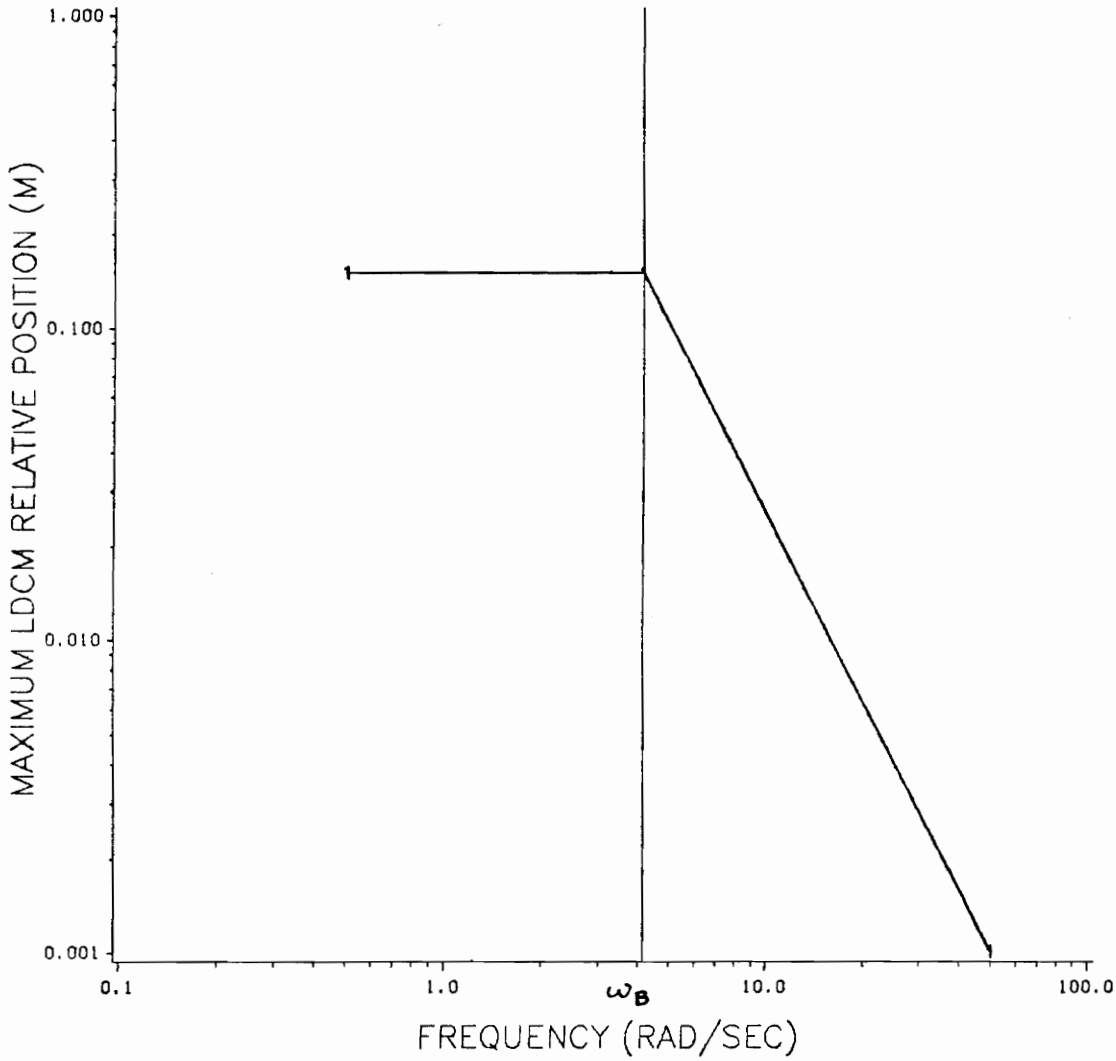

Figure 15. Maximum LDCM Relative Position, Type I Actuator.

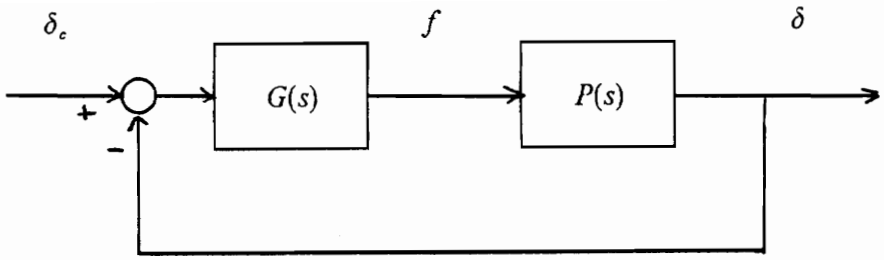

Figure 16. Block Diagram of General Relative Position Compensation.

δ_c = reference input command
f = force signal
δ = proof mass relative position
$G(s)$ = actuator compensation
$P(s)$ = proof mass dynamics

$$\frac{f}{\delta_c} = \frac{P(s)\,G(s)}{1 + P(s)\,G(S)} \times \frac{1}{P(s)} \quad . \tag{4.2.3}$$

Substituting gives

$$\frac{f}{\delta_c} = \frac{\delta}{\delta_c} \times ms^2 \quad . \tag{4.2.4}$$

At frequencies below ω_C, δ/δ_c is desired to be unity, therefore, the force signal is quadratically dependent of frequency. The frequency where the magnitude of the force signals equals the LDCM force limit is defined to be ω_B. This is the point shown on the plots shown in Figure 2. Choosing a value for ω_C, the bandwidth of the closed loop actuator, relative to ω_B decides between the two design strategies mentioned earlier.

Choosing $\omega_C = \omega_B$ will keep the magnitude of the signals below the LDCM force limit. This will give the actuator linear performance as long as the input command magnitude is less than the stroke limit of the LDCM. The linear performance is an advantage of this design strategy, however, there is also a disadvantage. The relative position response rolls off at frequencies above ω_B. Most of the mast mode frequencies are above ω_B so this design strategy will give poor excitation of modes with frequencies greater than ω_B.

Choosing $\omega_C > \omega_B$ will give the compensated actuator higher bandwidth, however, for full stroke input commands, the force signals will exceed the LDCM force limit at frequencies higher than ω_B. The second design strategy is to give the closed loop actuator bandwidth equal to the highest mode frequency. For this strategy, full stroke input commands at frequencies above ω_B will cause force saturation of the LDCM actuator. The actuator will behave in a nonlinear manner for full stroke input commands above ω_B in frequency.

Since the magnitude of the force signals depend on the input command magnitude, the input could be limited to keep force saturation from occurring. At frequencies above ω_B, limiting the relative position command to

$$\delta_{c\ limit} = \frac{f_{limit}}{m_{\text{proof mass}}\ \omega^2_{excitation}} \tag{4.2.5}$$

will keep the actuator from saturating in force. This design strategy will always have a nonlinearity present, either force saturation or a frequency dependent input command limit.

Three actuator compensator designs were used for analysis. Design one is a lead compensator design. Design two is a position-velocity feedback design. Both designs one and two were given bandwidth to keep the actuator within its force limit and give linear behavior. Design three is a wide bandwidth form of design two. It was given bandwidth equal to the highest mast mode frequency of interest. The designs shown are for type I actuators. The parameters for type II actuators are shown on the block diagrams when they are different from the type I parameter values.

4.2.1 Design One: Lead Compensator

Design one is a lead compensator design. The relative position of the proof mass is fed back through a lead compensator. Figure 17 shows a block diagram of this design.

Figure 18 shows a root locus of the pole placement for this design. The actuator poles are placed to give the force characteristic the correct shape to keep the actuator

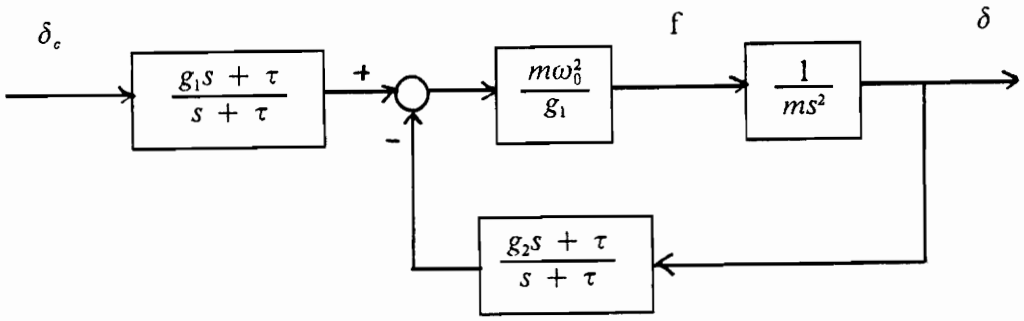

Figure 17. Block Diagram of Lead Compensator.

δ_c = command input
δ = relative position of proof mass
f = generated force
m = 11.6 kg Type I, 6.8 kg Type II
ω_0 = 4.681 Type I, 6.063 Type II
$g_1 = 3$
$g_2 = 6$
$\tau = \frac{3}{\sqrt{2}} \omega_0$

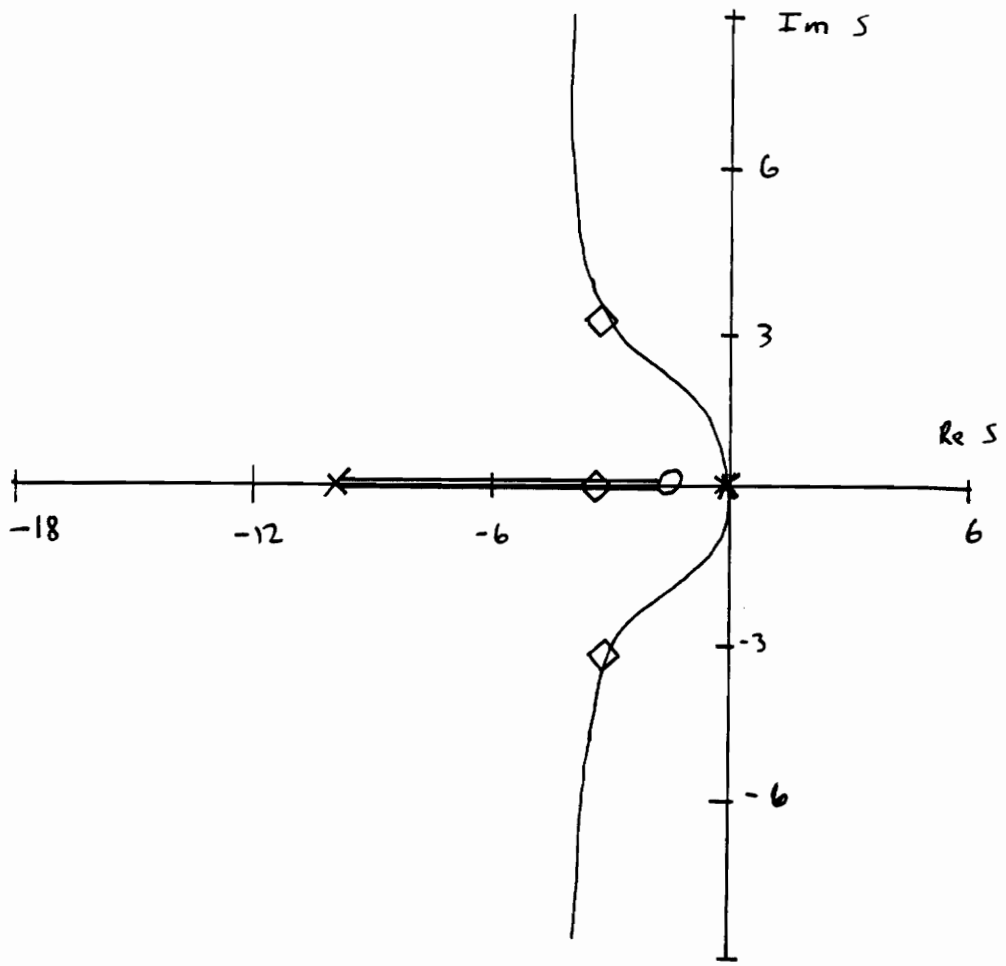

Figure 18. Root Locus of Lead Compensator Design.

O = zero location
X = open loop pole location
◇ = closed loop pole location

within both its stroke and force limits. A precompensator cancels the pole and zero the the lead compensator leaves on the real axis.

Figure 19 shows Bode plots of f/δ_c and δ/δ_c for a type I actuator of this design. Examining the f/δ_c plot shows that, for a command magnitude of 12 cm, the force characteristic matches the maximum generated force curve in Figure 2 for a type I actuator. This guarantees that this actuator design will behave in a linear fashion.

The δ/δ_c plot shows that specifying the force characteristic automatically specifies the relative position characteristic, δ/δ_c. Comparing the mode frequencies to the δ/δ_c plot shows that, at the higher mode frequencies, the actuator will have low relative position response. It will be shown later that this means this design will have poor excitation ability at the higher mode frequencies.

4.2.2 Design Two: Position Velocity Feedback

Design two is a position velocity feedback design. Figure 20 shows a block diagram of this design. The proof mass relative position measurement is fed back with constant gain. Notice that if the mast is stationary, the proof mass relative position equals the proof mass inertial position.

The output of the proof mass accelerometer is passed through a block with the transfer function

$$\frac{s}{s^2 + 2\zeta_r\omega_r s + \omega_r^2} \quad . \tag{4.2.1}$$

This transfer function approximates an integrator. This realization was used because an ideal integrator cannot be built. The approximation is good above ω_R rad/sec. The

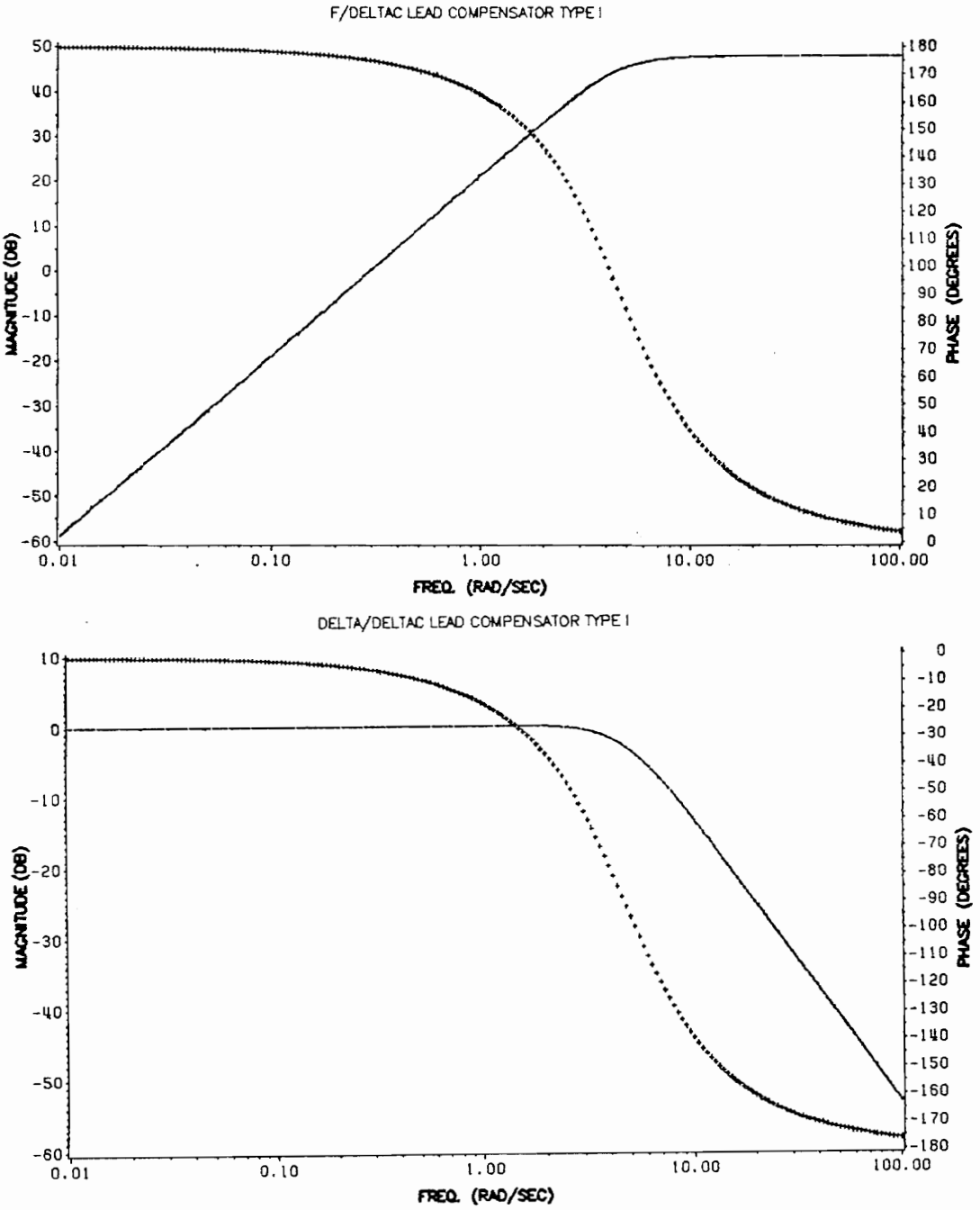

Figure 19. Bode Plots of Lead Compensator Performance.: Top, f/δ_c; Bottom, δ/δ_c

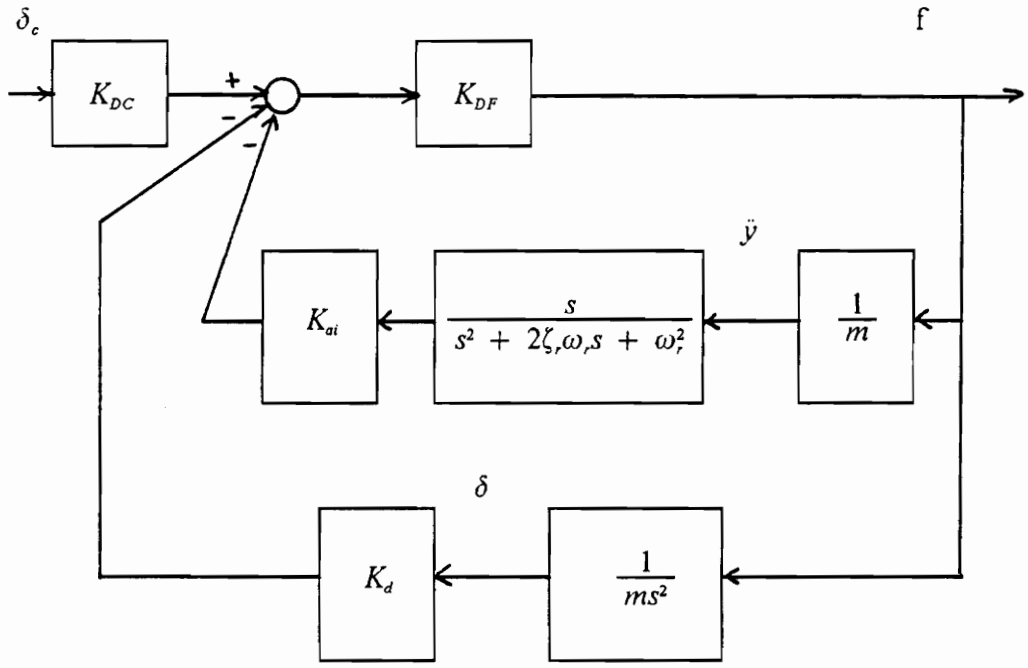

Figure 20. Block Diagram of Position Velocity Loop

δ_c = relative position command
δ = proof mass relative position
f = generated force
$\ddot{y}$ = proof mass acceleration
K_{DC} = 1.0
K_{DF} = 250.0
K_{ai} = 0.303 Type I, 0.2339 Type II
K_d = 1.1439 Type I, 1.109 Type II
ζ_r = .707
ω_r = 0.1 π
m = 11.6 kg Type I, 6.8 kg Type II

system will be used above this frequency. Below ω_R rad/sec, this block approximates a differentiator so that low frequency signals will be attenuated. The output of this block approximates the inertial velocity of the proof mass. This output is fed back with constant gain.

Notice that, with a perfect integrator and stationary mast, the two feedback signals would be the inertial position and velocity of the proof mass. This design is essentially a state feedback design. The two feedback gains were calculated using state feedback pole placement techniques. As explained earlier, the poles were placed to guarantee linear operation. The feedback gains for the two types of actuators are shown on the block diagram.

Figure 21 shows Bode plots of f/δ_c and δ/δ_c for this design. Like design one, the f/δ_c plot matches the plot in Figure 2 to guarantee linear operation. The δ/δ_c plot shows that this design also has bandwidth lower than the higher mode frequencies.

4.2.3 Design Three: Wide Bandwidth Position Velocity Feedback

Design three is a wide bandwidth version of design two. The configuration is the same as design two. The feedback gains allow easy placement of the actuator poles to increase the bandwidth of the relative position loop. The actuator poles were placed using state feedback techniques to make the actuator relative position bandwidth the same as the highest mode frequency. The gains required to do this are

K_{DC} = 68 Type I, 41 Type II

K_{ai} = 2.5 Type I, 1.5 Type II

K_d = 69 Type I, 42 Type II

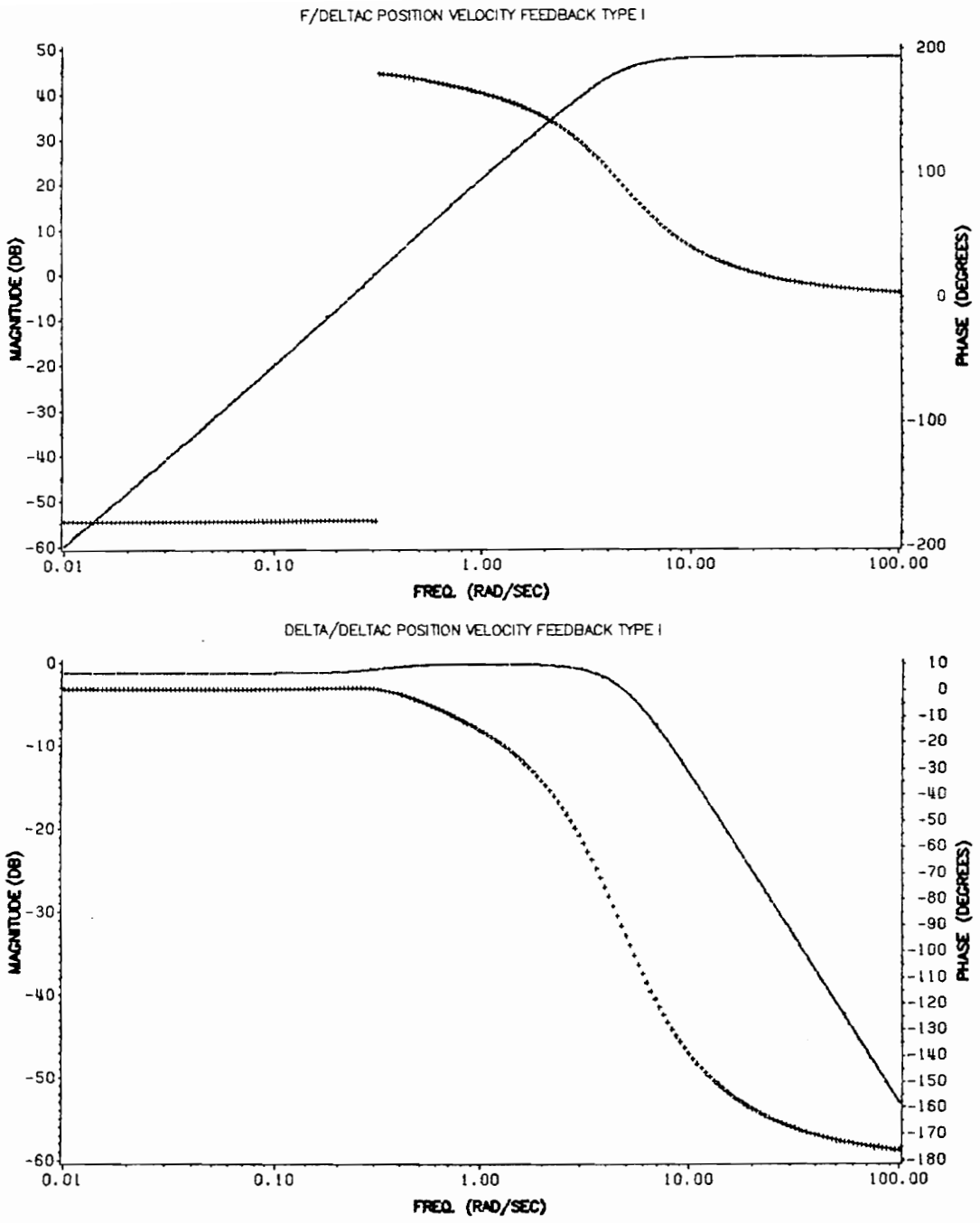

Figure 21. Bode Plots of Position Velocity Loop Performance.: Top, f/δ_c; Bottom, δ/δ_c

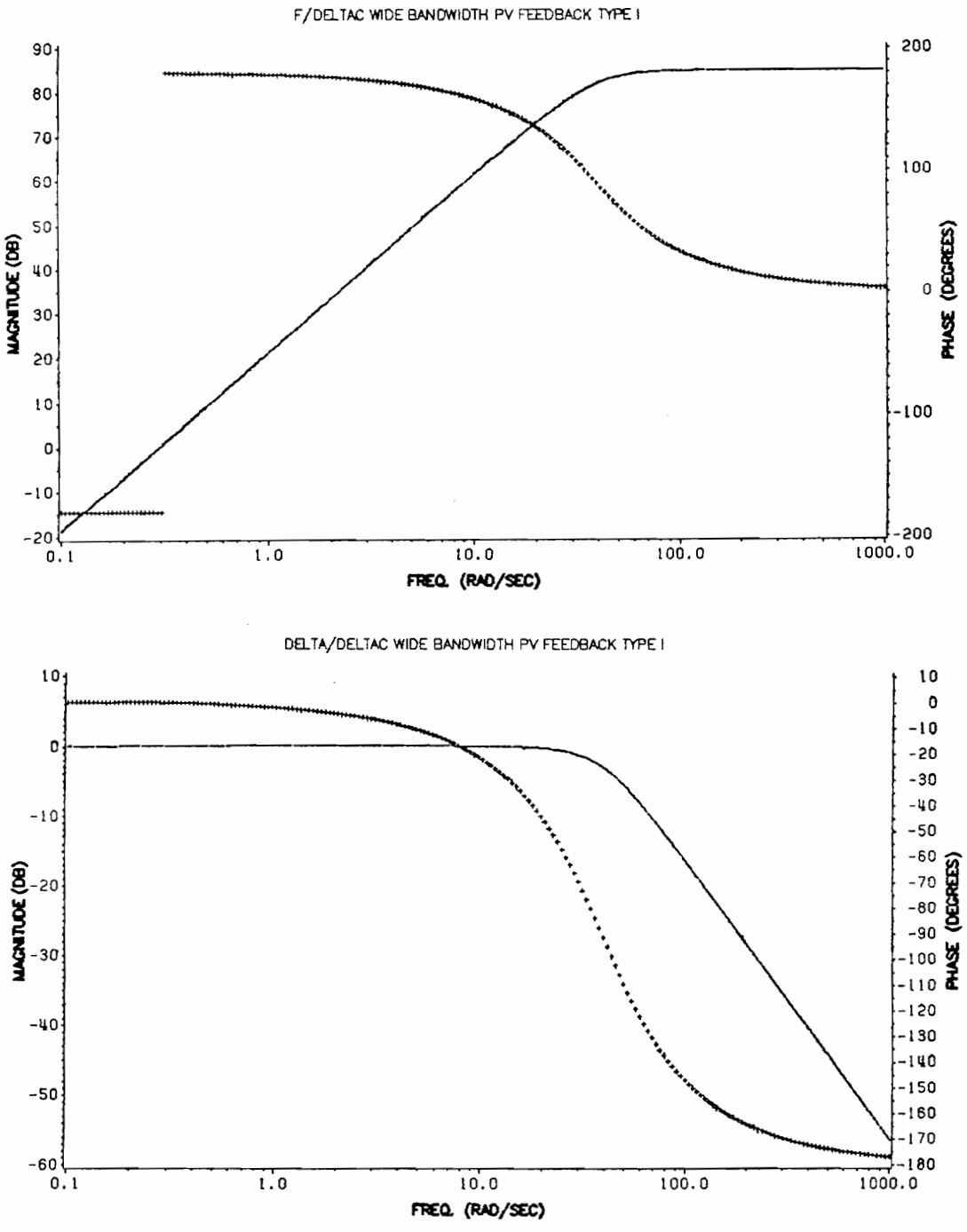

Figure 22. **Bode Plots of Wide Bandwidth Position-Velocity Loop Performance:** Top, f/δ_c; Bottom, δ/δ_c

Figure 22 shows plots of f/δ_c and δ/δ_c for this design. This design keeps the LDCM within its stroke limit. Force saturation will occur for full stroke commands at higher excitation frequencies.

The Bode plot of δ/δ_c shows that this design has relative position bandwidth equal to the frequency of the highest mode. This design should have larger relative position response at higher frequencies than the other two designs. Further analysis will show that the nonlinearity present in this design will have an effect on its relative position response.

4.3 Comments On Compensator Designs

Designs one and two have guaranteed linear actuator performance by giving the actuator a force characteristic which will not violate either the force limit imposed by the LDCM stroke limit or the LDCM force limit. This, however, gives these two designs low relative position response at the higher frequencies.

Designs one and two have the same relative position and force characteristics. They would be expected to perform similarly. Further analysis will show that they have similar excitation capability but because of the difference in the two designs, they add different amounts of damping to the mast modes have different disturbance characteristics.

Design three guarantees that the LDCM will not violate its stroke limit, however, it does not keep the commanded force within the LDCM force limit, allowing force saturation. The higher actuator bandwidth that this allows will not be entirely without drawbacks because of the force saturation that occurs.

5.0 System Performance

Using the LDCM to apply force to a flexible space structure gives a system with special characteristics. The availability of only a relative position measurement for actuator stabilization gives the system a feedback configuration of structure and actuator. The LDCM has physical limits which motivated the compensation design strategies. The COFS program, which includes both identification and control experiments, places certain requirements on performance of the LDCM actuator. The LDCM actuator should achieve the following design goals:

- follow sinusoidal input commands
- excite modes of the mast
- generate pure force signals
- add little damping to the mast modes

Using the LDCM actuator to achieve the largest amount of damping possible was not a goal of this research.

This chapter analyzes the ability of the LDCM actuator to perform these system goals. The ability of the actuator to follow input commands will be examined because it will be seen to affect the ability to excite the modes of the mast. The effect of the

feedback configuration of mast and actuator on the modes of the mast will be examined to show how the mast behavior is changed by mounting the actuators on it. Disturbance analysis is performed to show the effect of the measuring devices on the purity of force applied to the structure. Most of this analysis is performed by simulating the system of the mast with all of the actuators mounted on it.

5.1 System Simulation

Analytical analysis was used when possible to evaluate performance, but, because of the high order of the system and the nonlinearities present in the actuator, simulations were necessary for much of the analysis.

Figure 23 shows a shows a schematic diagram of the system as simulated for design one. Examining the diagram shows the elements included in the simulation of the system. The same elements were used in the simulations of designs two and three. The system included input command limiters so that the proof mass relative position could be kept within the LDCM stroke limit. The system included force limiters to simulate the effects of current saturation in the LDCM drive circuitry. The optical encoder was simulated by a quantizer so that the effect of the digital measurement accuracy could be examined.

Several simplifications can be noticed by examining the schematic diagrams. First, the force loop was replaced by a unity gain because the force loop has unity gain and zero phase throughout the frequency range of the mast modes. Second, the effect of back emf of the motor is ignored because the force and current compensation reduce it

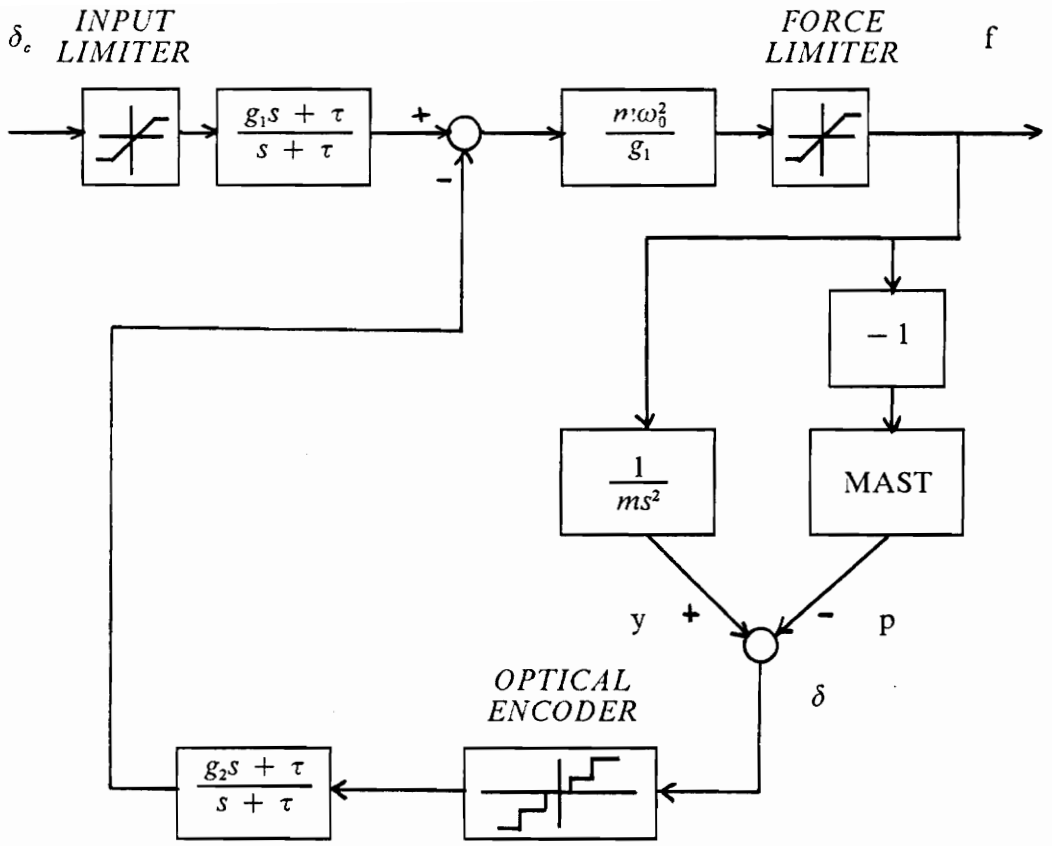

Figure 23. Block Diagram of the System as Simulated for Design One.

δ_c = command input
p = inertial position of mast
y = inertial position of proof mass
δ = relative position of proof mass
f = generated force
m = 11.6 kg Type I, 6.8 kg Type II
ω_0 = 4.681 Type I, 6.063 Type II
g_1 = 3
g_2 = 6
$\tau = \frac{3}{\sqrt{2}} \omega_0$

drastically, as shown in chapter two. Third, accelerometer dynamics were ignored because their bandwidth was very high compared to the mast mode frequencies.

The total system of the flexible mast with ten flexible modes and ten LDCM actuators can be represent by considering the signals on the schematic diagram to be vectors and the blocks to be matrices. The mast is modelled by the augmented state space shown in chapter three.

The system block diagram was used to write a state space model, including all nonlinearities, of the form

$$\dot{y}(t) = g\,(y(t)\,,\ \delta_c(t)\,,\ t)\ . \tag{5.1.1}$$

A fourth-fifth order Runge-Kutta differential equation solver with variable step size was used to get the system response from the model.

Typically, a sinusoidal relative position command was given at a mast mode frequency for five cycles at one actuator location to excite the structure. A zero command was then given to examine the free decay of the system. The actuator used for excitation of each mode was the one with the largest mode shape coefficient to give the maximum excitation. Torsional modes were excited by using a pair of actuators at the tip with opposite reference input commands.

5.2 *Dynamic Behavior*

The LDCM actuator has physical characteristics which place limits on the amount of force it can apply at a given frequency. These limits were used in deciding where to place the poles of the actuator with the actuator compensation. Designs one and two

keep the actuator within both the force and stroke limit of the LDCM and have bandwidth lower that several of the mode frequencies. Design three keeps the actuator within the stroke limit but allows force saturation to occur. Design three, though, has a higher bandwidth than designs one and two. The actuator bandwidth will be seen in this section to affect the actuator's ability to both follow input commands and excite the modes of the mast.

The LDCM is stabilized with the relative position feedback configuration. This configuration links the actuator to the structure in a feedback configuration, therefore, the actuator compensation will affect the behavior of the structure. This section will explain the effect of the three different compensator designs on the mast.

5.2.1 Actuator Input Following

The actuators mounted on the mast were to be able to excite the modes of the structure for identification experiments. Placing a sinusoidal command on an input should place a sinusoidal force on the mast and proof mass. Since the force applied to the proof mass and mast is related to the relative position of the proof mass, it is important for the proof mass relative position to be able to track sinusoidal input commands over the frequency range of the modes.

In order to measure each actuator design's ability to follow sinusoidal input commands, the position following error (PFE) was calculated as

$$PFE = \frac{1}{N}\sum_{n=0}^{N}\left(\frac{\delta_c(n) - \delta(n)}{mag\,(\,\delta_c\,)}\right)^2 \quad . \tag{5.2.1}$$

The difference between the relative position command and the relative position of the proof mass is normalized by the relative position command magnitude and squared. This is averaged over the total number of points in the simulation. The PFE gives a measure to use in comparison of the input following ability of the three compensator designs. The absolute magnitude of the PFE has little significance.

The PFE was calculated for each of the three designs. It was calculated at each of the x direction mode frequencies to see the change in actuator performance across the frequency range of operation. For designs one and two, full stroke input commands were given because the actuator compensation keeps the commanded force within the force limit of the actuator. For design three, the actuator compensation does not keep the commanded force within the LDCM force limit. Thus, two cases were run for design three. First, the command was limited, as derived earlier, to

$$\delta_c = \frac{f_{\max}}{m_{proof\,mass}\,\omega^2_{excitation}} \tag{5.2.2}$$

to keep the actuator within the actuator force limit. Second, design three was run with a full stroke command to show the effect of force saturation on the following ability of the actuator.

Table 2 shows the PFE values calculated for each actuator design at each x mode frequency. Designs one and two have very similar values of PFE. This is expected because the δ/δ_c bode plots for the two designs show that they have the same bandwidth. The values for design three show that there is a drastic change in the ability of the actuator to follow input commands when the actuator saturates in force.

Several things affect the PFE and should be pointed out in interpreting the PFE values. First, one major component of PFE comes from the phase lag between the input command and relative position response. Examining the δ/δ_c bode plots can help in

Table 2. Table of Position Following Error.

	Design 1	Design 2	Design 3	
	FULL COMMAND	FULL COMMAND	LIMITED COMMAND	FULL COMMAND
Mode	PFE	PFE	PFE	PFE
1x	0.079	0.049	0.001	0.001
2x	0.65	0.63	0.04	1.82
3x	0.56	0.54	0.34	0.94
4x	0.53	0.50	0.55	0.6

understanding the PFE values. For designs one and two, modes two, three, and four are all above the bandwidth of the compensator design and, therefore, have high phase lag between output and input. This is why designs one and two have much higher PFE values for modes two, three, and four than for mode one. This also explained why the values for the limited command case of design three gradually increase with excitation frequency. As the frequency of excitation approaches the bandwidth of the design, the phase lag between the output and input increases and, hence, the PFE increases.

Second, the transient response from relative position command to response affects the PFE. Design one and two have bandwidth of approximately 4 rad/sec. Design three has a bandwidth of approximately 45 rad/sec. When given commands at frequencies above their bandwidth, designs one and two have a transient before achieving sinusoidal relative position response. This shows up as higher values of PFE for modes two, three, and four. Design three has bandwidth equal to the highest mode frequency so does not show this transient in its relative position response.

Third, force saturation greatly affects the PFE because it causes nonsinusoidal force to be placed on the proof mass and structure. This is illustrated in the large difference between the PFE values between the case of limited command (no force saturation) and the case with force saturation for design three.

Figure 24 and Figure 25 show plots of the relative position response for each design with excitation at the third x mode frequency. Figure 24 shows the response for designs one and two. Figure 25 shows the response for the two cases of design three. Comparing these plots to the PFE values for the different designs can give a feeling for the significance of the PFE values.

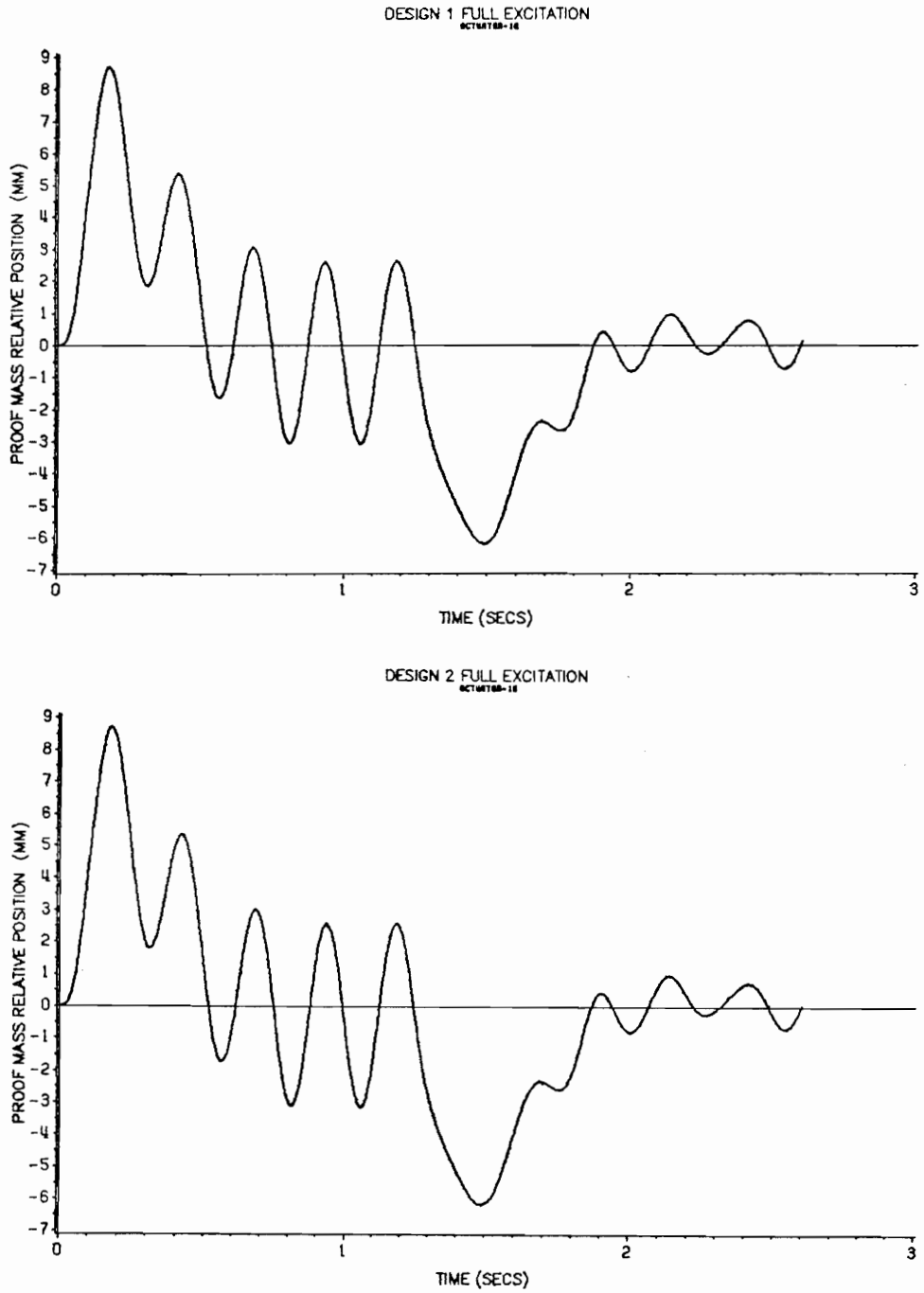

Figure 24. Simulations of Proof Mass Relative Position, Designs 1 and 2.: Top, Mode 3x Design 1; Bottom, Mode 3x Design 2

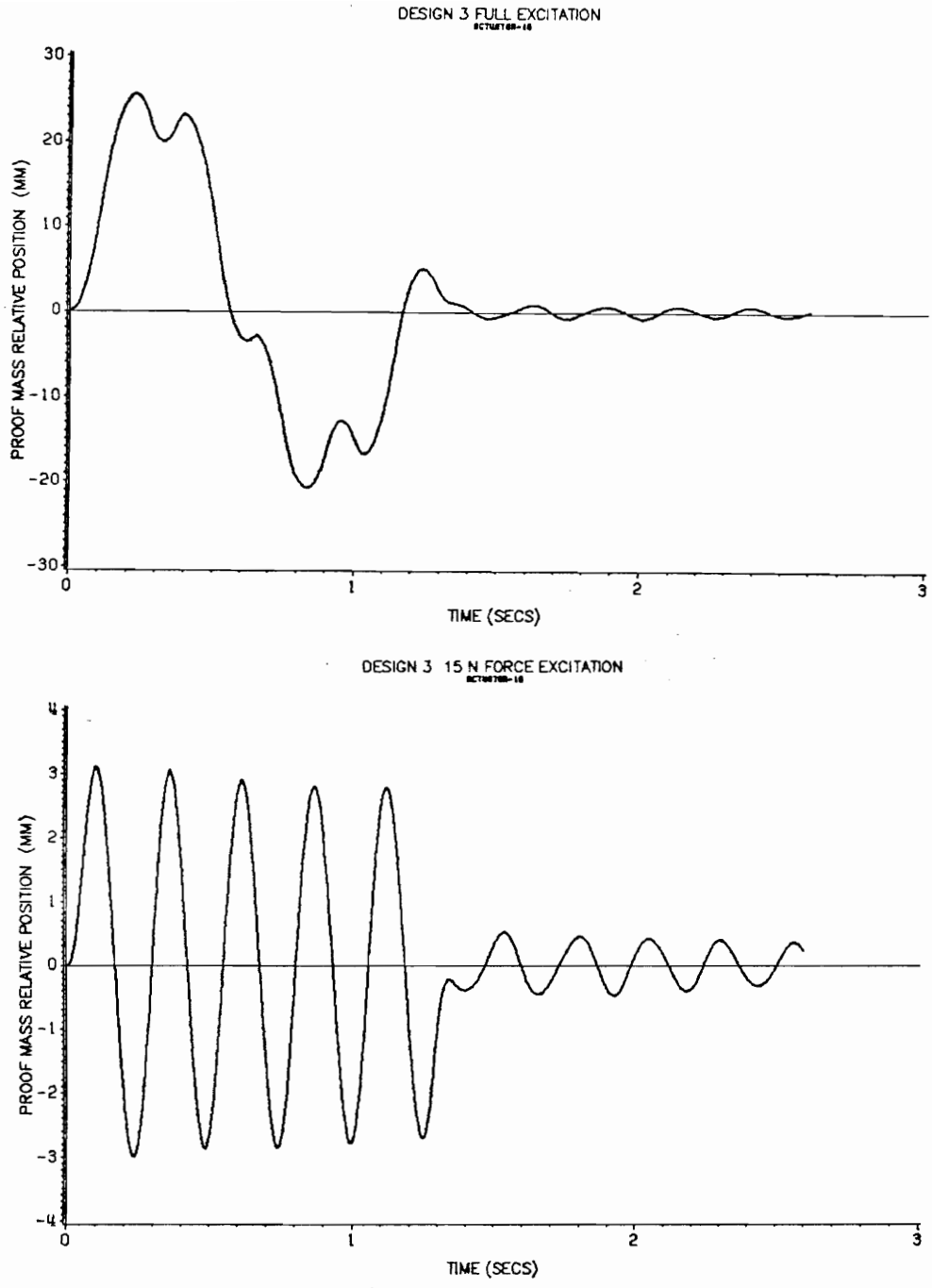

Figure 25. Simulations of Proof Mass Relative Position, Design 3.: Top, Mode 3x Full Command; Bottom, Mode 3x Limited Command

5.2.2 Mast Excitation Capability

The COFS program was proposed by NASA in order to examine flexible space structures. One set of proposed experiments was to excite the mast for model identification experiments. This subsection will examine each compensator design's ability to excite single modes of the mast.

Figure 26 shows a Bode plot of p/δ_e for a simplified system with one actuator and four mast modes for each of the three compensator designs. These plots show that the excitation of the mast is frequency dependent. The spikes in the response correspond to the mode frequencies of the mast. The mast response to excitation will be low except at these frequencies. Notice that there are zeros very close to the higher mode frequencies. Because of the closeness of these zeros, the magnitude of the mast response changes rapidly with frequency near the mode frequencies.

These bode plots are illustrative, however, they do not show the effects of the transient response of the actuator, the effect of force saturation, and the effect of having ten actuators placed on the structure. To assess the excitation capability of each of the three compensator designs, simulations were run for each of the designs at each of the x direction modes of the mast and at the torsional modes. The response for the y direction is very similar to that of the x modes.

The following set of plots shows the mast inertial position versus time for the x modes and torsional modes for each compensator design. Designs one and two were given full stroke excitation commands. Design three was given both full stroke commands and limited commands to show the effect of force saturation on the mast excitation capability.

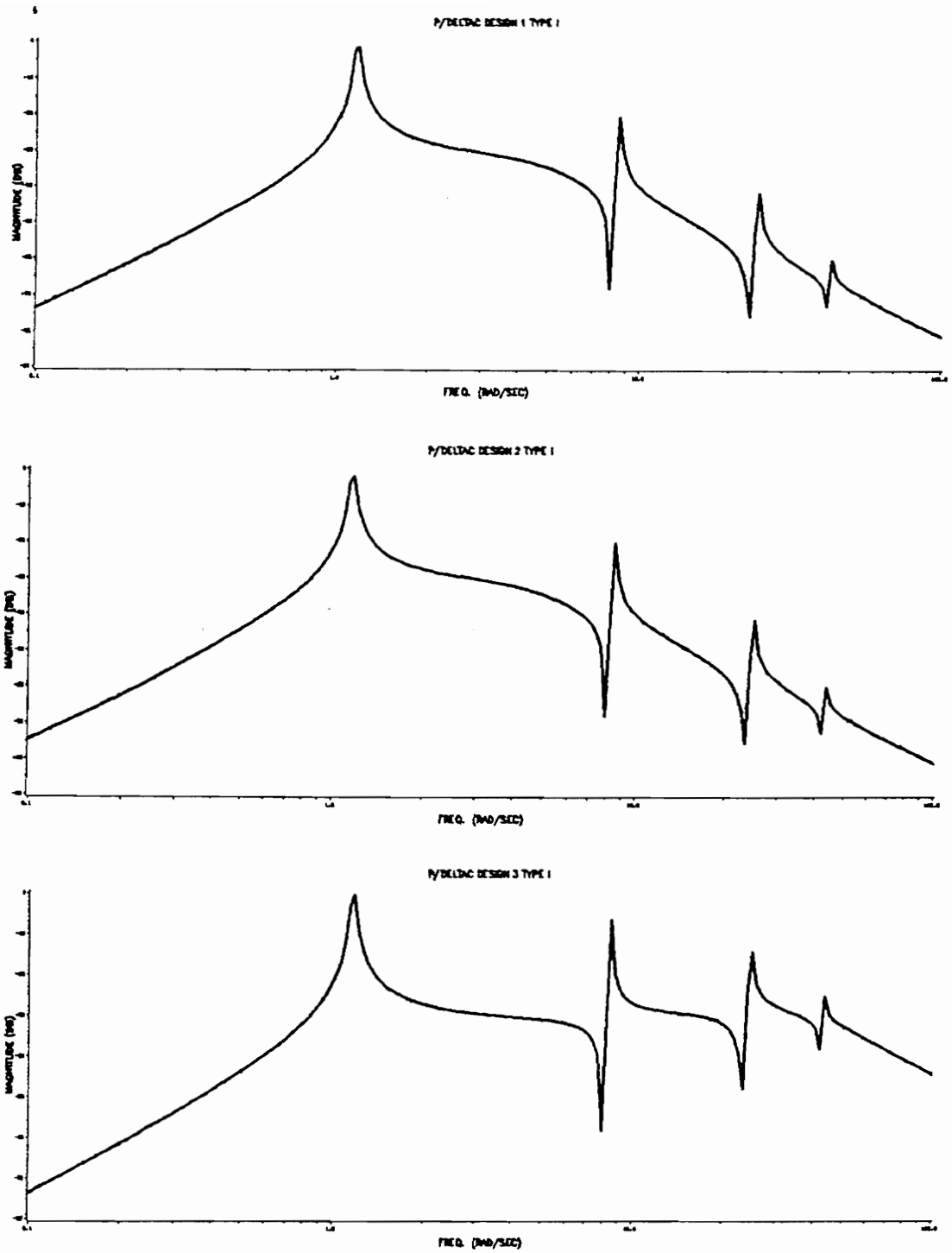

Figure 26. Bode Plot of p/deltac for the Three Compensator Designs.: Top, Design 1; Middle, Design 2; Bottom, Design 3

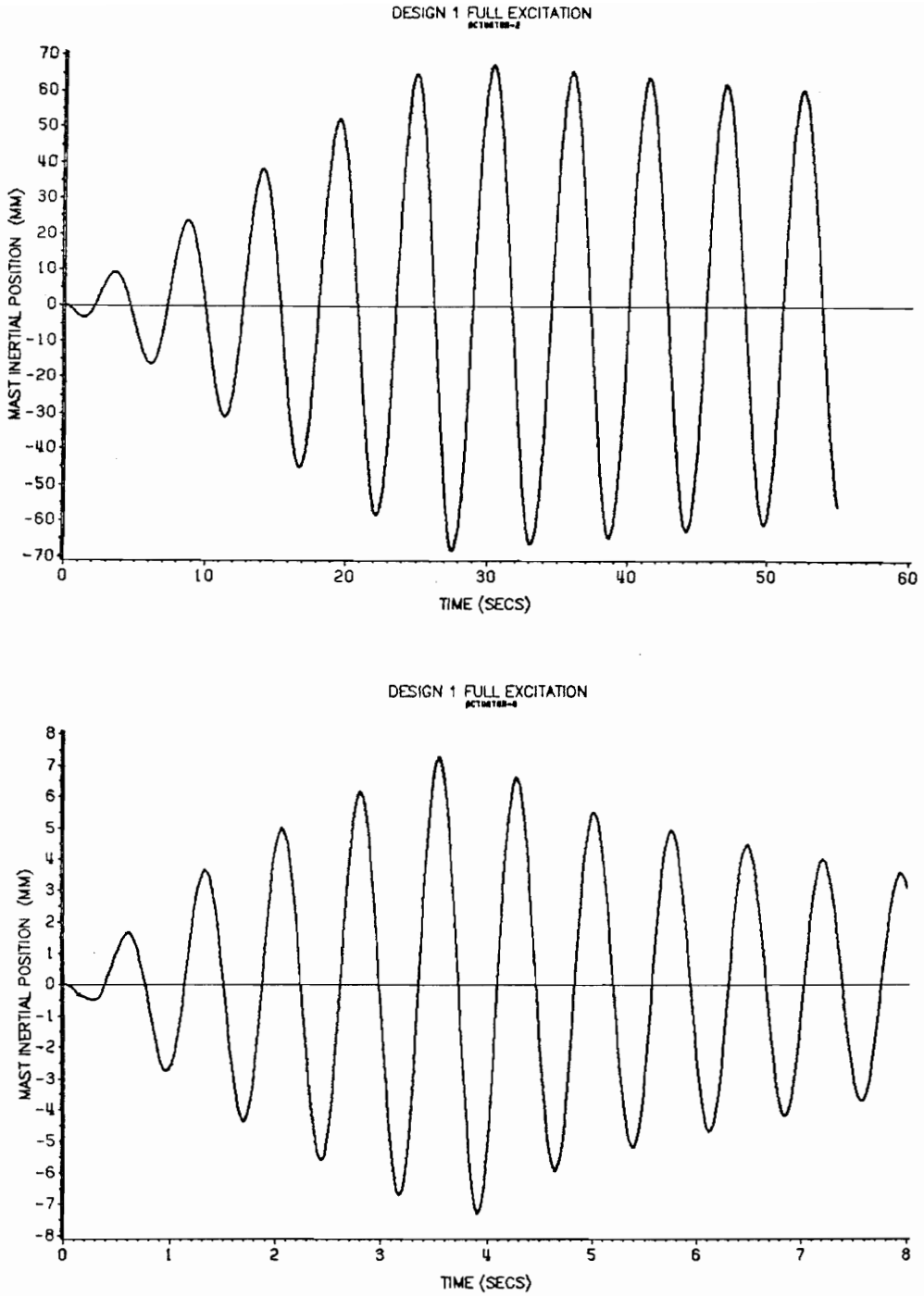

Figure 27. Simulations of Mast Inertial Position, Design One.: Top, $\delta_{c\,2,4} = 100.0 \sin 1.175t$

Bottom, $\delta_{c\,8} = 50.0 \sin 8.545t$

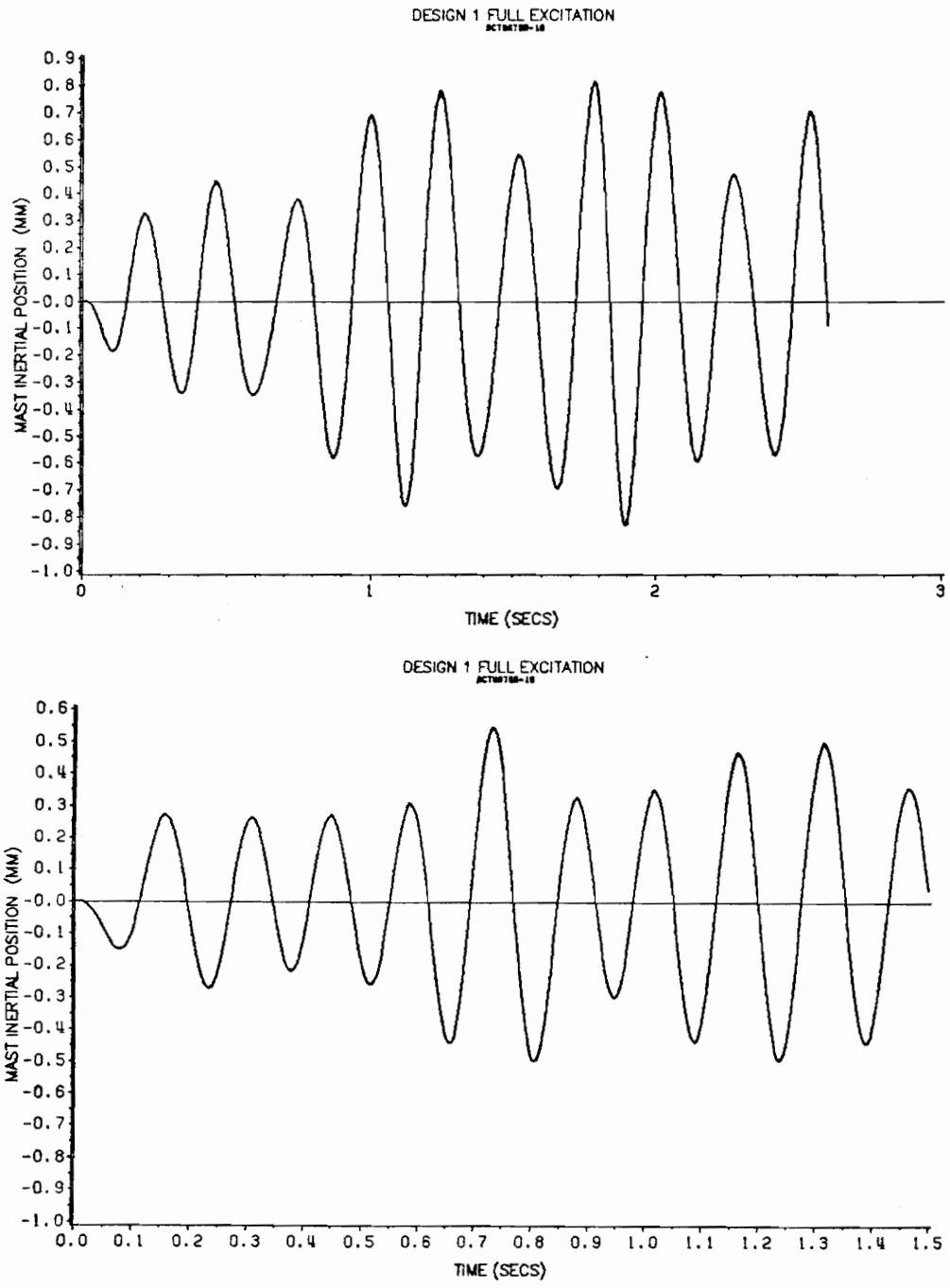

Figure 28. Simulations of Mast Inertial Position, Design One.: Top, $\delta_{c10} = 50.0 \sin 24.69t$

Bottom, $\delta_{c10} = 50.0 \sin 42.98t$

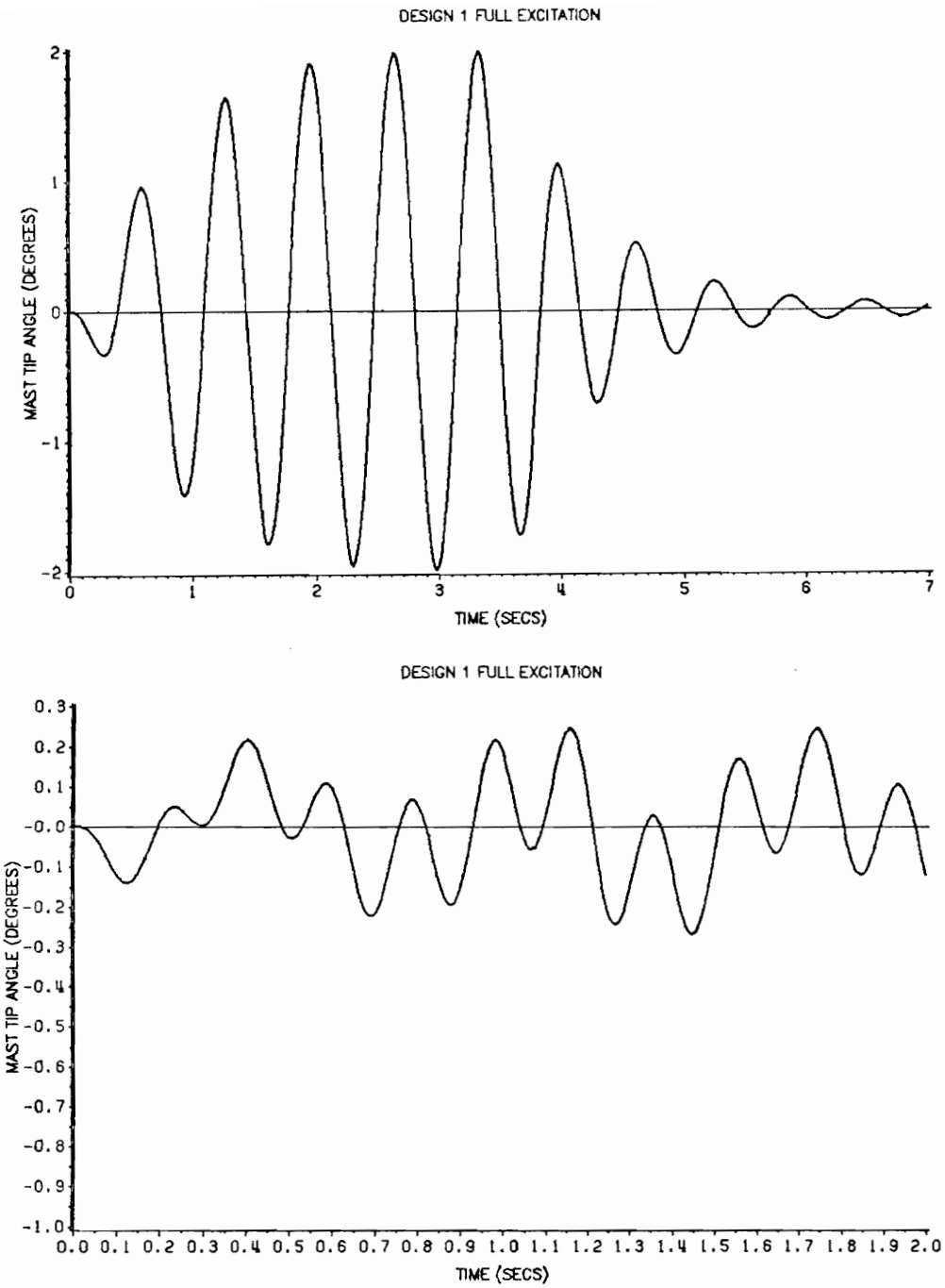

Figure 29. Simulations of Mast Tip Angle, Design One.: Top, $\delta_{c\,2,4} = \pm\ 100.0\ \sin 9.11t$

Bottom, $\delta_{c\,2,4} = \pm\ 100.0\ \sin 32.11t$

Figure 27, Figure 28, and Figure 29 show the mast excitation for design one. Figure 27 shows a plot of the mast position for the first and second x direction modes. Figure 28 shows a plot of the mast position for the third and fourth x modes. The position is shown at the location of the exciting actuator. Figure 29 shows a plot of the tip angle of rotation for excitation of the first and second torsional modes. Notice that, for the higher frequency modes, the third and fourth x modes and the second torsional mode, the mast excitation is not a single sinusoid. This is due to the input following ability of the actuator. The transient and phase lag in the relative position response at the higher frequencies cause multiple modes to be excited by the actuator. Notice also that, as the frequency of excitation increases, the magnitude of the mast excitation decreases. This is due to the rolloff in the relative position response at the higher frequencies.

Figure 30, Figure 31, and Figure 32 show the mast excitation for design two. Figure 30 shows a plot of the mast position for the first and second x direction modes. Figure 31 shows a plot of the mast position for the third and fourth x modes. The position is shown at the location of the exciting actuator. Figure 32 shows a plot of the tip angle of rotation for excitation of the first and second torsional modes. Notice that these plots show the same excitation characteristics as pointed out for design one. This is because the two compensator designs have the same bandwidth. The actuator's excitation capability is dependent mainly on the actuator bandwidth. Notice that, by comparing the second half of each plot between designs, it can be seen that the damping is different for the different designs. This will be explained in the next section.

Figure 33, Figure 34, and Figure 35 show the mast excitation for design three given full stroke excitation commands. As explained previously, this will cause force saturation at the higher frequencies. Figure 33 shows a plot of the mast position for the first and second x direction modes. Figure 34 shows a plot of the mast position for the

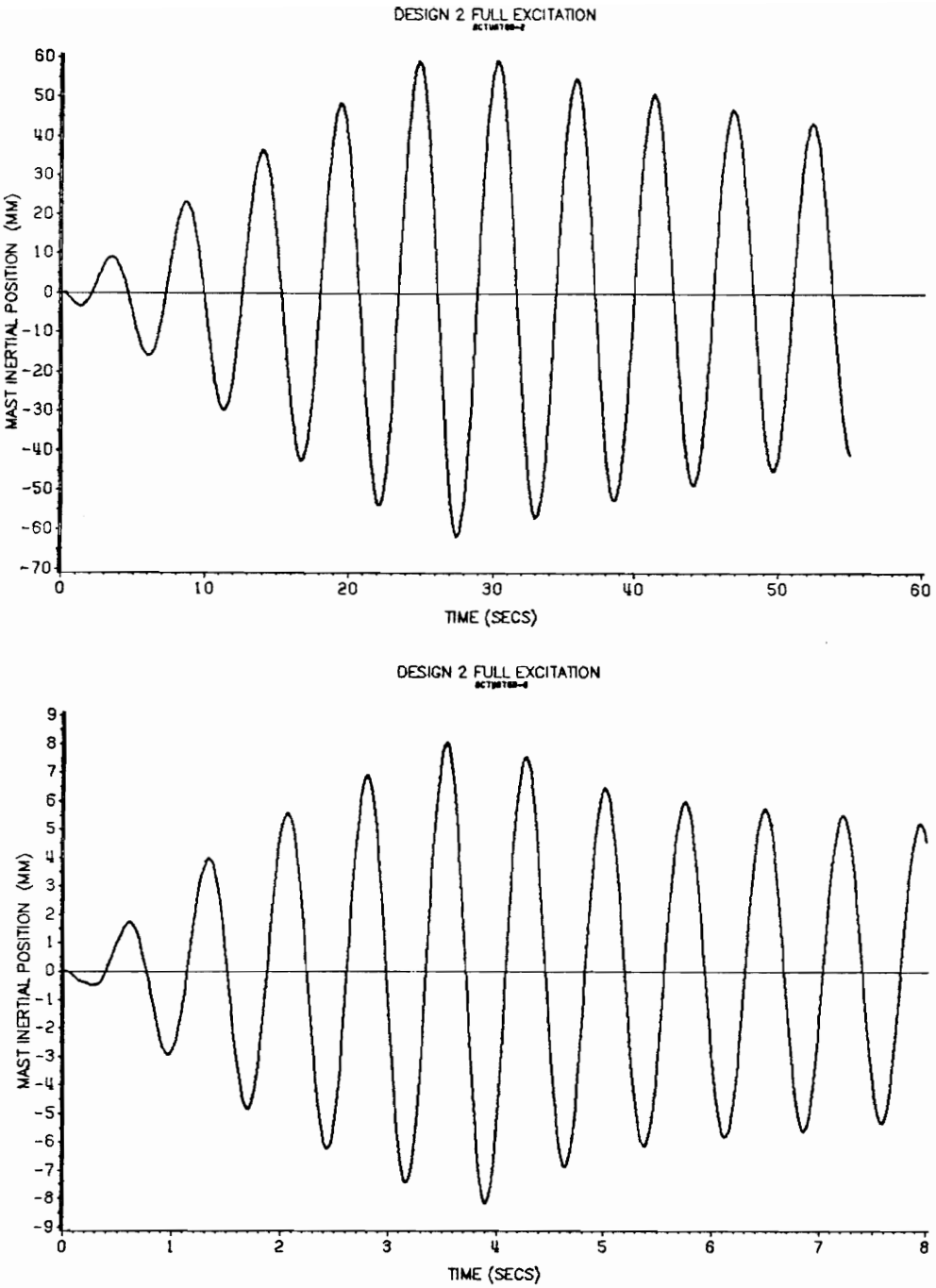

Figure 30. Simulations of Mast Inertial Position, Design Two.: Top, $\delta_{c\,2,4} = 100.0 \sin 1.175t$

Bottom, $\delta_{c\,8} = 50.0 \sin 8.545t$

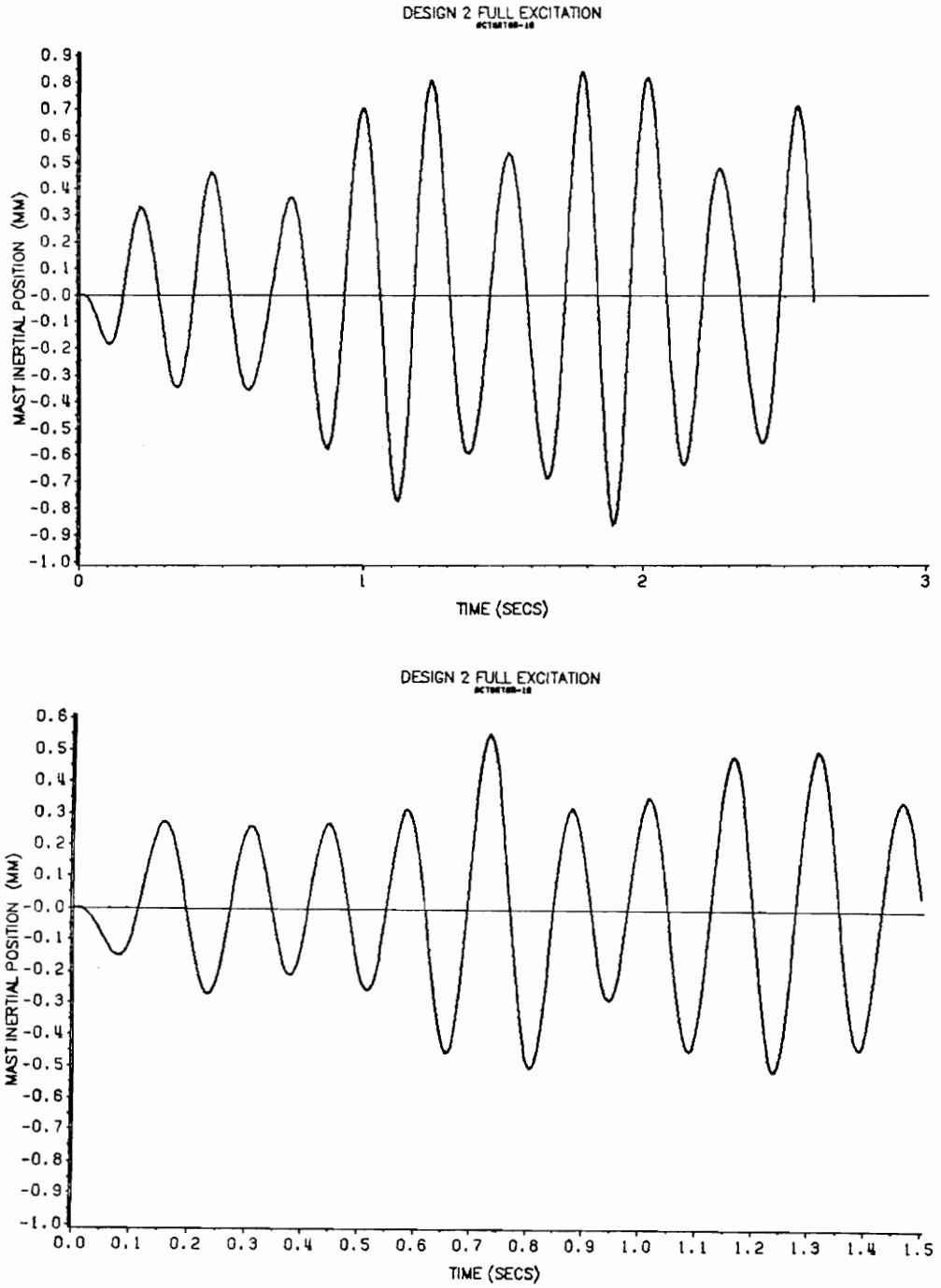

Figure 31. Simulations of Mast Inertial Position, Design Two.: Top, $\delta_{c10} = 50.0 \sin 24.69t$

Bottom, $\delta_{c10} = 50.0 \sin 42.98t$

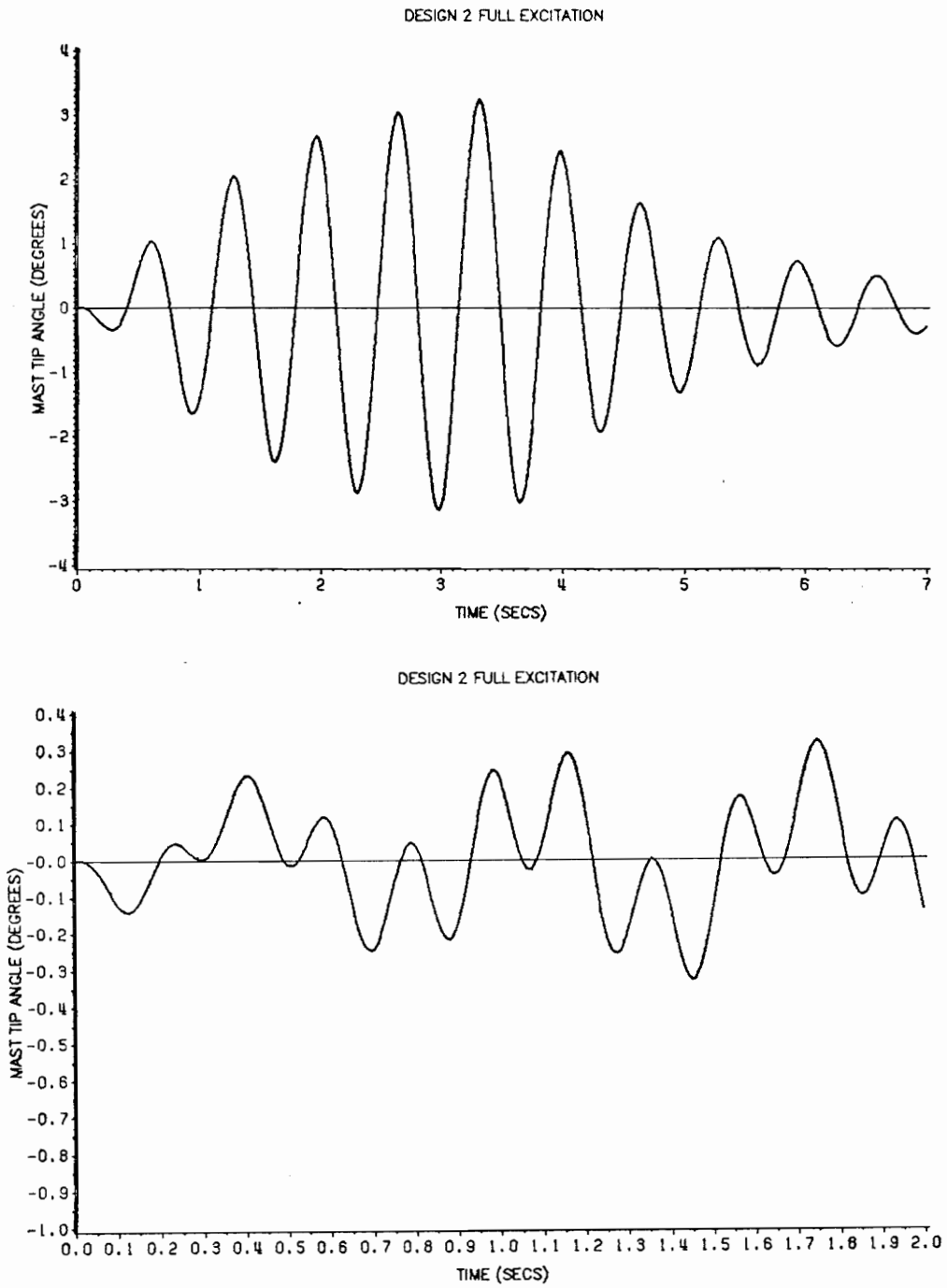

Figure 32. Simulations of Mast Tip Angle, Design Two.: Top, $\delta_{c\,2,4} = \pm\ 100.0\ \sin 9.11t$

Bottom, $\delta_{c\,2,4} = \pm\ 100.0\ \sin 32.11t$

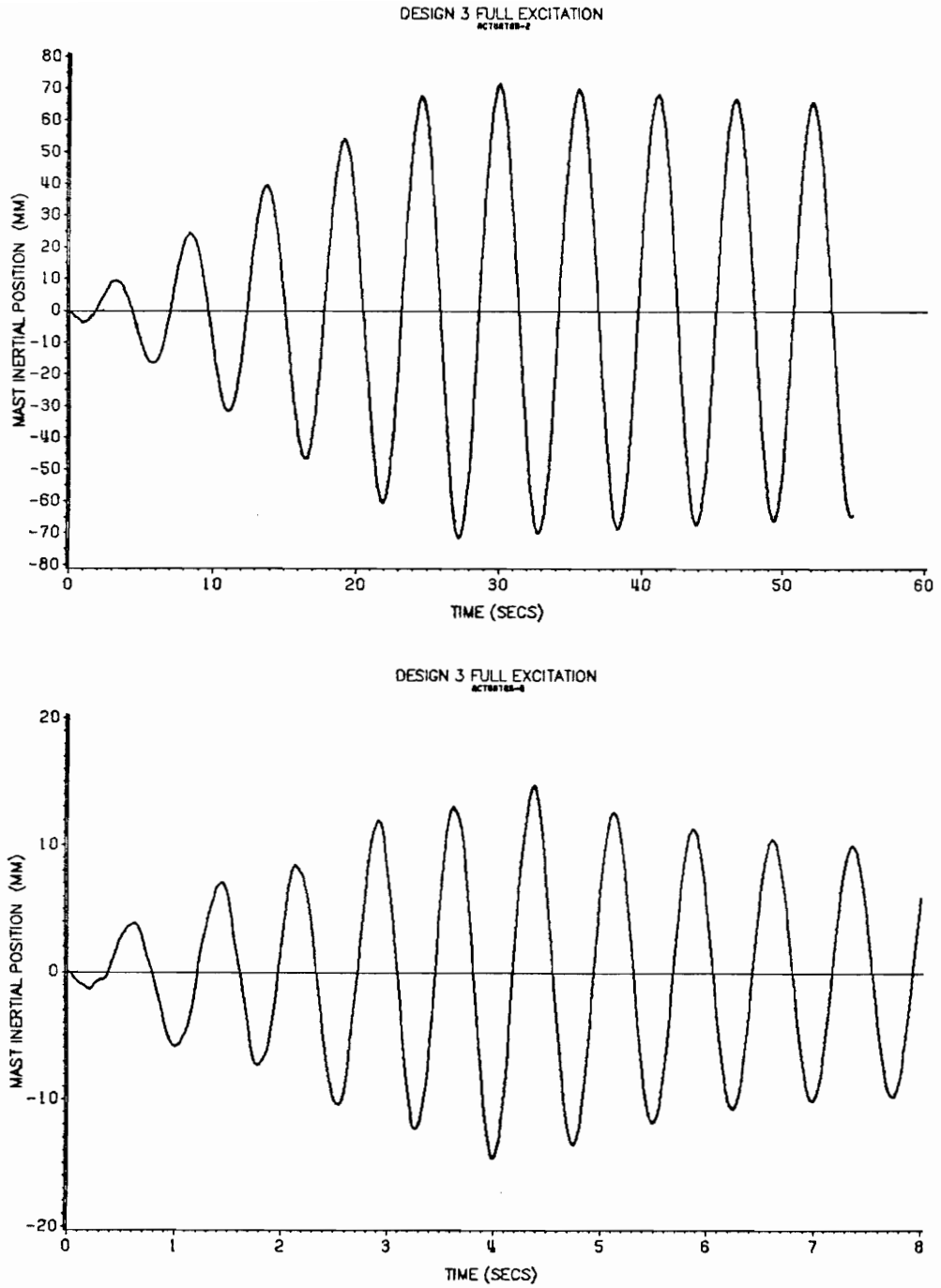

Figure 33. Simulations of Mast Inertial Position, Design Three.: Top, $\delta_{c\,2,4} = 100.0 \sin 1.175t$ Bottom, $\delta_{c\,8} = 50.0 \sin 8.545t$

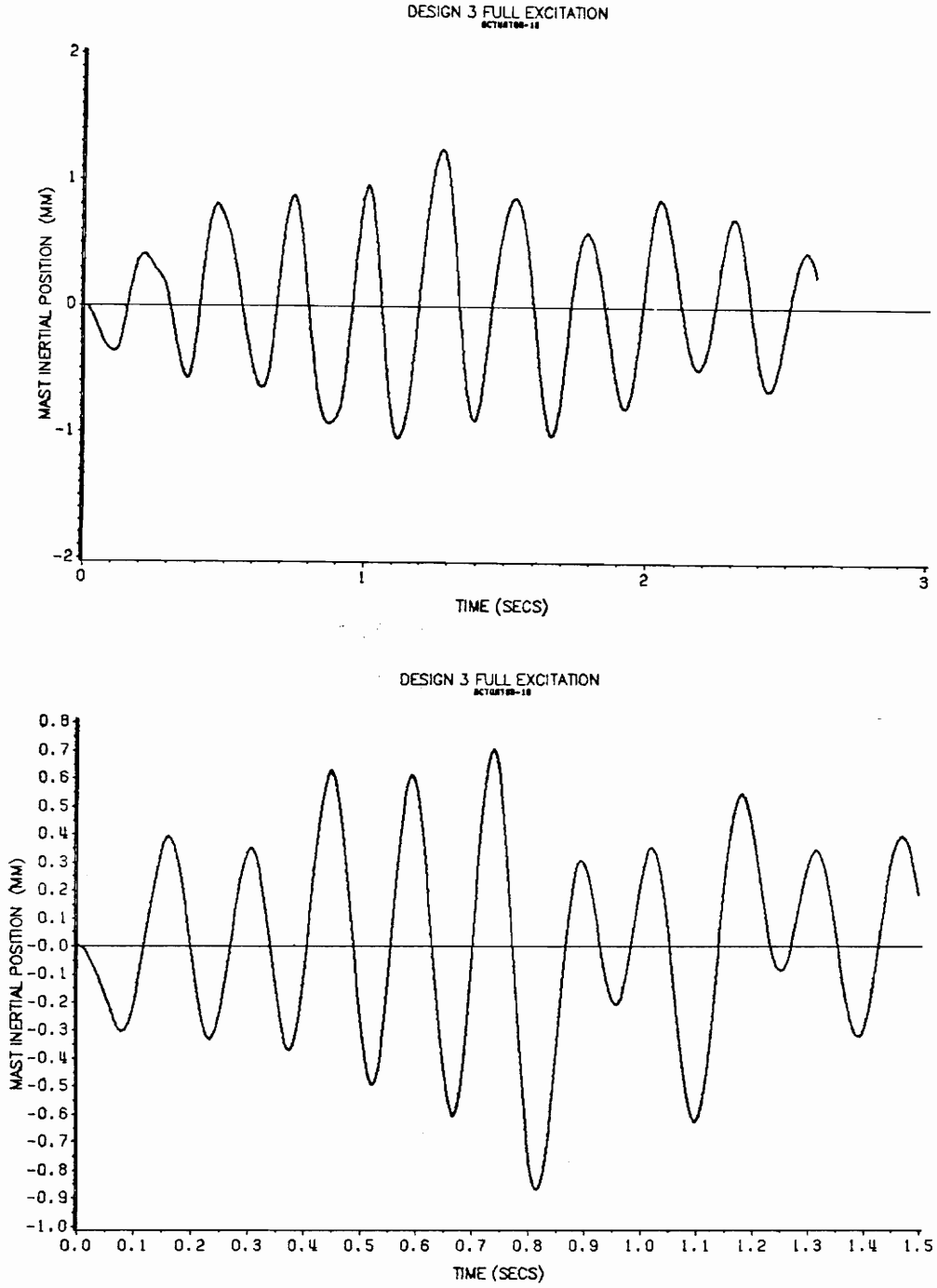

Figure 34. Simulations of Mast Inertial Position, Design Three.: Top, $\delta_{c10} = 50.0 \sin 24.69t$

Bottom, $\delta_{c10} = 50.0 \sin 42.98t$

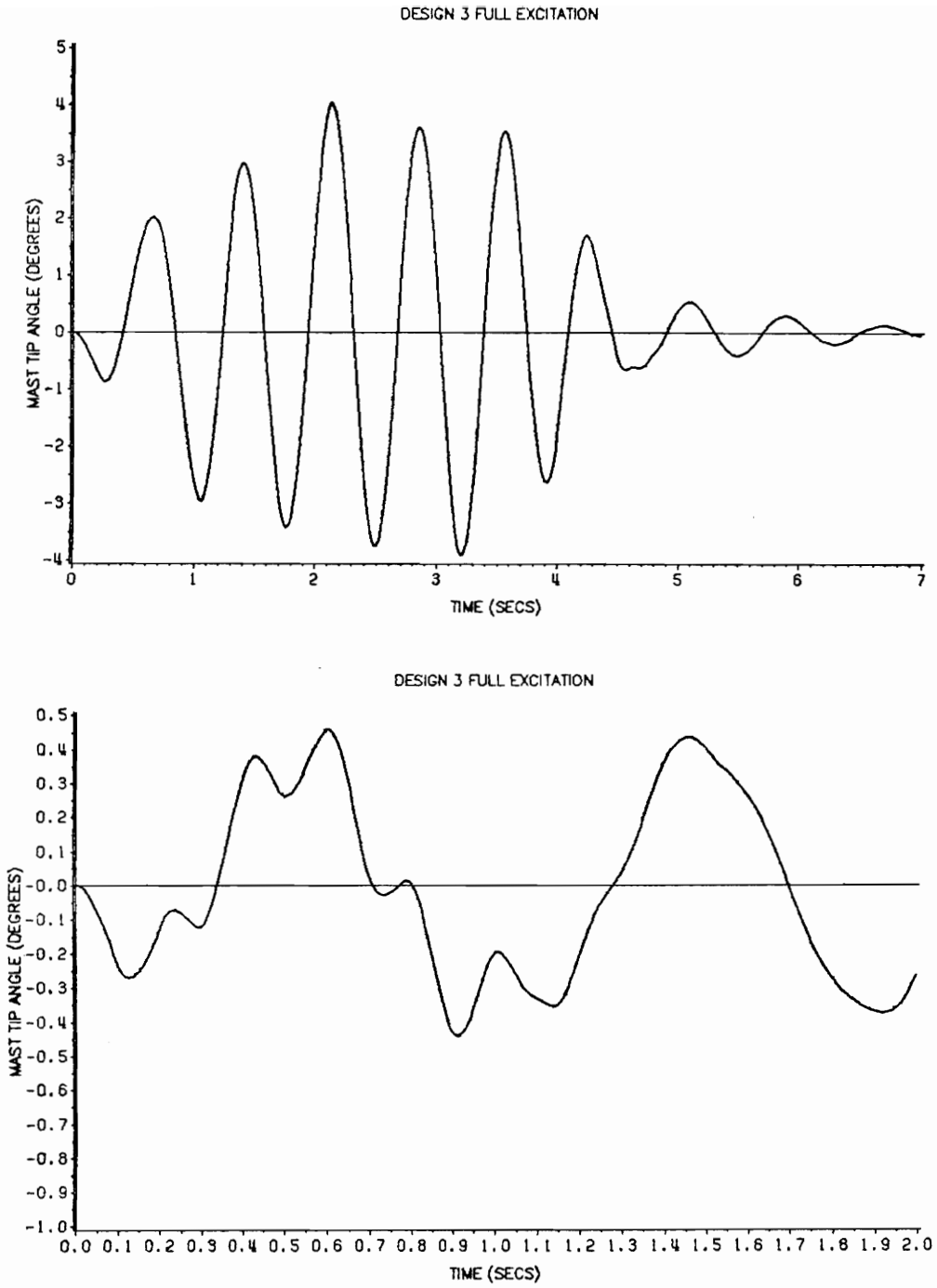

Figure 35. Simulations of Mast Tip Angle, Design Three.: Top, $\delta_{c\,2,4} = \pm 100.0 \sin 9.11t$

Bottom, $\delta_{c\,2,4} = \pm 100.0 \sin 32.11t$

third and fourth x modes. The position is shown at the location of the exciting actuator. Figure 35 shows a plot of the tip angle of rotation for excitation of the first and second torsional modes. Notice that the magnitude of the excitation is larger at the higher mode frequencies than for designs one and two. This is because the relative position response does not roll off until the highest mode frequency. Notice, however, that this excitation also shows multiple modes excited. This is because the force saturates at the higher excitation frequencies. This nonlinearity causes multiple modes to be excited.

Figure 36, Figure 37, and Figure 38 show the mast excitation for design three when the input command is limited to keep the actuator from saturating in force. The limit used,

$$\delta_{c\ limit} = \frac{F_{\max}}{m_{\text{proof mass}}\ \omega^2_{excitation}}\ , \tag{5.2.1}$$

was derived earlier. At the first x mode frequency, the stroke limit will not allow force saturation to occur so the mast position will look like the first plot in Figure 33. Figure 36 shows a plot of the mast position for the second x direction mode. Figure 37 shows a plot of the mast position for the third and fourth x modes. The position is shown at the location of the exciting actuator. Figure 38 shows a plot of the tip angle of rotation for excitation of the first and second torsional modes. Notice that the magnitude of mast excitation is similar to that of designs one and two for the higher frequency modes. This is because the same magnitude force is applied when the input is limited in this manner for design three as is applied in designs one and two. Notice, however, that the excitation at the higher frequencies is more purely a single sinusoid. This design with the limited input gives the most clean excitation of the higher frequency mast modes.

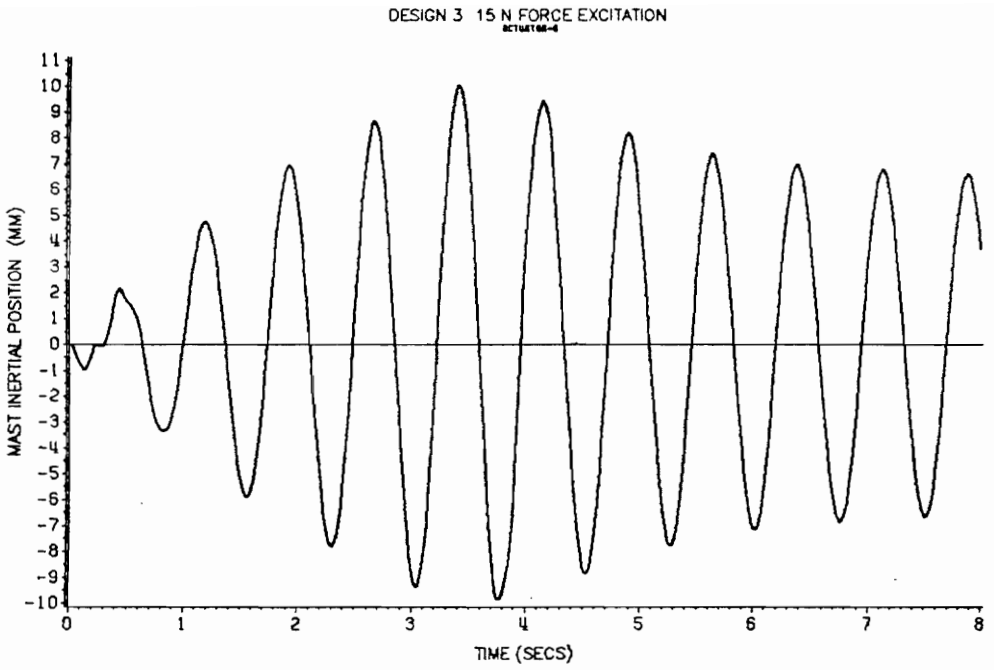

Figure 36. Simulations of Mast Inertial Position, Design Three.: $\delta_{c\,8} = 30.0 \sin 8.545t$

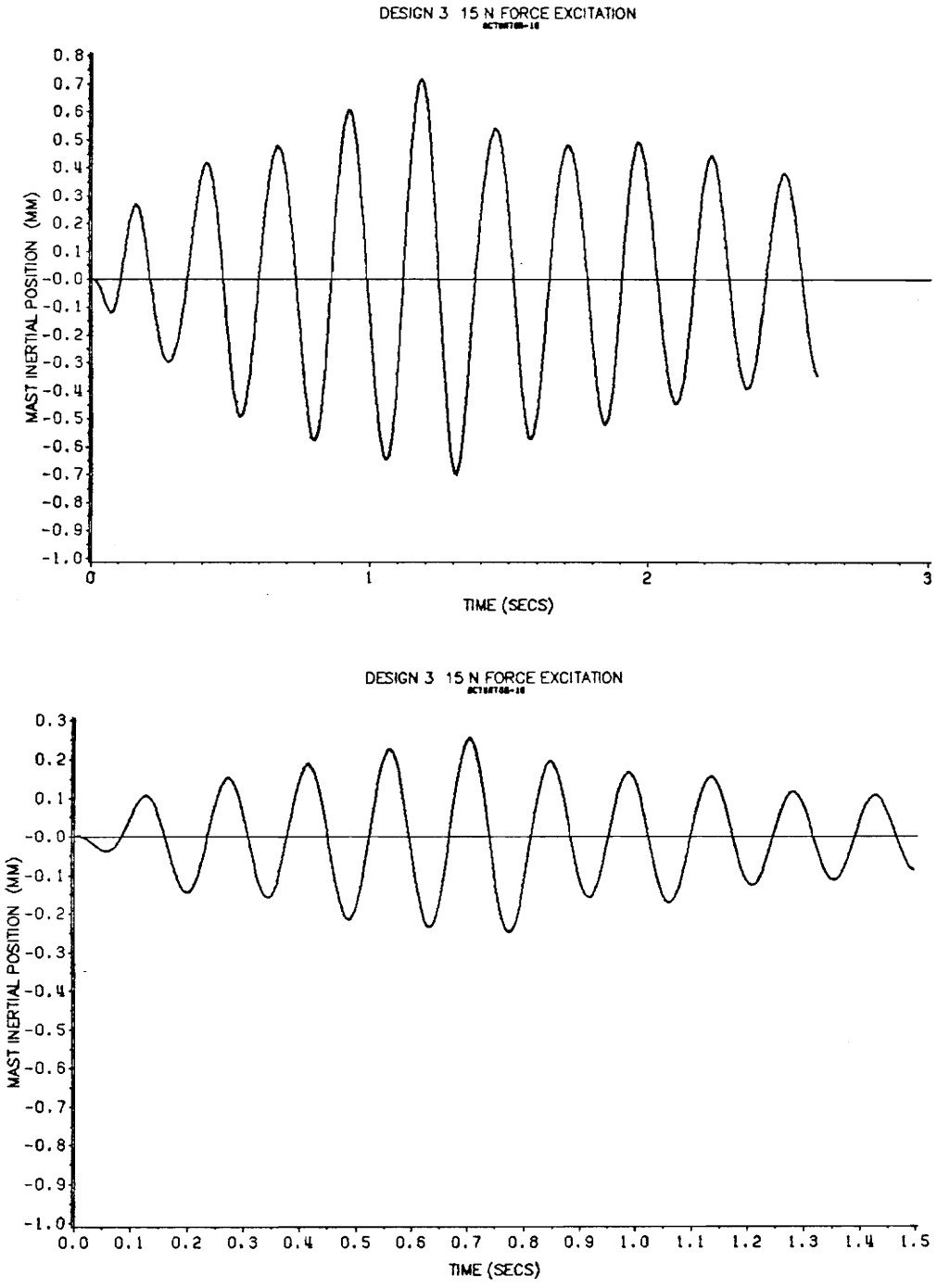

Figure 37. Simulations of Mast Inertial Position, Design Three.: Top, $\delta_{c\,10} = 3.6 \sin 24.69t$

Bottom, $\delta_{c\,10} = 1.2 \sin 42.98t$

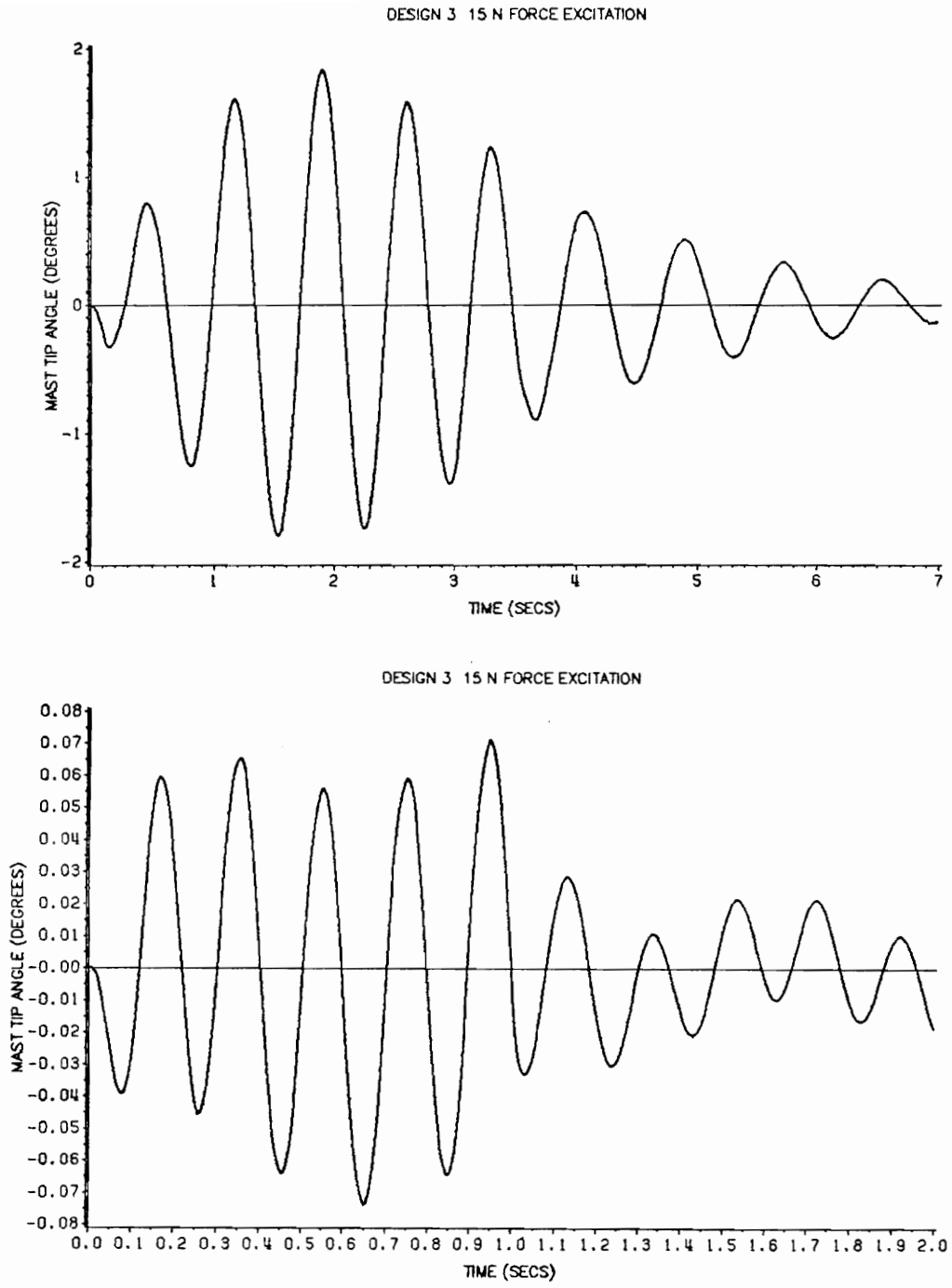

Figure 38. Simulations of Mast Tip Angle, Design Three.: Top, $\delta_{c\,2,4} = \pm 31.0 \sin 9.11t$

Bottom, $\delta_{c\,2,4} = \pm 2.5 \sin 32.11t$

The excitation capability of the three actuator designs may be summed up as follows. Designs one and two give poor magnitude mast excitation at the higher mode frequencies due to the low bandwidth of the actuator compensation. The low bandwidth also caused multiple modes to be excited when exciting the higher frequency modes. Design three increases the magnitude of the mast excitation capability, but, due to force saturation, multiple modes are still excited when exciting the higher frequency modes at full stroke. Placing a frequency dependent command limit on the input of design three keeps force saturation from occurring. However, design three must either contain the force saturation nonlinearity or the frequency dependent input command limit.

5.2.3 Feedback Configuration Effects

The LDCM actuator mounted on the flexible mast was open loop unstable. The only position measurement available for feedback was the proof mass relative position. This couples the actuator to the structure in a feedback configuration. This subsection details the effect of each compensator design on the modes of the mast.

Eigenvalue analysis was used to determine the effect of the actuator compensation on the frequency and damping of each mode of the mast. A state space realization was written for each dynamic element of the system block diagram. The augmented state space model was used for the mast. These realizations were connected according to the system block diagram, assuming no nonlinearities were present. A model of the form

$$\dot{x} = Ax + B\delta_c \tag{5.2.1}$$

$$\delta = Cx + D\delta_c$$

was formed for the total system with each compensator design. The eigenvalues of the A matrix were calculated to give the eigenvalues of the system including the mast, LDCM actuators, and actuator compensation. Table 3 shows the frequency and damping coefficient of each mode of the mast for the open loop case with no actuators mounted on the mast and for the three actuator compensation designs.

The amount of damping associated with each mode was also calculated from the simulations. The logarithmic decrement technique was used [11].

$$x_1 = p(t = t_1) \tag{5.2.2}$$

$$x_2 = p(t = t_2)$$

$$\alpha = \ln \frac{x_1}{x_2}$$

$$\zeta = \frac{\alpha}{\sqrt{(2\pi)^2 + \alpha^2}}$$

where x_1 and x_2 are the mast inertial position at two points one cycle apart and ζ is the damping factor. Table 4 shows a comparison of the damping values calculated from the eigenvalues and the values calculated from the simulations.

The damping values calculated from the simulations match the values calculated in the eigenvalue analysis very well. The damping could not be calculated from simulations of the high frequency modes for both designs one and two because, at higher excitation frequencies, the actuators do not excite single modes of the mast. It is not possible to apply the logarithmic decrement technique when multiple modes are excited. The good correlation between the damping values calculated two ways suggest that the values are correct.

Table 3. Table of Mast Mode Frequencies and Damping Coefficients.

Open Loop		With Actuator Compensation					
		Design 1		Design 2		Design 3	
Freq.	Damp	Freq.	Damp	Freq.	Damp	Freq.	Damp
rad/sec	%	rad/sec	%	rad/sec	%	rad/sec	%
1.175	0.2	1.134	0.437	1.136	1.24	1.138	0.312
1.521	0.2	1.488	0.503	1.492	1.04	1.493	0.291
8.168	0.3	8.213	2.03	8.212	1.26	8.008	0.967
8.545	0.3	8.598	1.90	8.592	1.17	8.369	0.973
9.111	0.5	9.970	11.2	9.650	6.09	7.460	4.93
23.69	0.5	23.74	0.602	23.72	0.547	23.42	2.04
24.69	0.5	24.75	0.594	24.72	0.543	24.25	2.14
32.11	0.5	32.46	0.850	32.31	0.660	29.16	16.1
41.47	0.5	41.53	0.537	41.50	0.517	41.56	2.99
42.98	0.5	43.04	0.536	43.01	0.516	43.13	3.00

Table 4. Table of Damping Coefficients

	Damping Coefficient, (%)					
Mode	Design 1		Design 2		Design 3	
	Eig.	Sim.	Eig.	Sim.	Eig.	Sim.
1x	0.437	0.4	1.242	1.23	0.312	0.32
1y	0.503	0.49	1.04	1.02	0.291	0.31
2x	2.03	1.9	1.26	1.2	0.967	0.96
2y	1.90	1.9	1.17	1.2	0.973	1.5
1T	11.2	12.5	6.09	6.3	4.93	5.1
3y	0.602	X	0.547	X	2.04	2.2
3x	0.594	X	0.543	X	2.14	2.0
2t	0.850	X	0.660	X	16.1	X
4y	0.537	X	0.517	X	2.99	3.3
4x	0.536	X	0.516	X	3.0	2.8

X signifies that the damping could not be calculated from the simulation.

Examining closely the values in Table 3 shows that both the frequency and the amount of the damping of the mast modes were changed by the addition of the actuator compensation.

In explaining this, it helps to consider a simplified system of one actuator mounted on the flexible mast. For each of the three compensator designs, the system block diagram can be manipulated into the general form shown in Figure 39. The input shown, i, is related to the relative position command, δ_c, by a lead block for design one and a constant for designs two and three. The transfer function $Q(s)$ represents the mast dynamics. The transfer function $G(s)$ is the transfer function f_{ST}/p taken from the system block diagram in Figure 23. Notice that this is the same transfer function as f/δ in the simplified block diagrams shown in the compensator design section.

This block diagram shows that compensating the LDCM actuator with the relative position feedback configuration is like placing feedback around the mast with compensation $G(s)$. Root locus techniques can be applied to achieve an understanding of how the actuator compensation affects the modes of the mast.

To understand how the mast modes are affected, the form of the mast dynamics, $Q(s)$, must be examined. Q(s) is the transfer function from force to mast position calculated from the state equations of the mast model. Each mode is represented by a pair of complex poles with very little damping. The total behavior of the mast is approximated by adding the effect of the modes. This gives a definite form to $Q(s)$,

$$Q(s) = \frac{K_1}{s^2 + 2\zeta_1\omega_1 s + \omega_1^2} + \ldots + \frac{K_N}{s^2 + 2\zeta_N\omega_N s + \omega_N^2} . \qquad (5.2.3)$$

Writing $Q(s)$ in pole-zero form will show that $Q(s)$ will have N pairs of poles and (N-1) pairs of zeros. Figure 40 shows a typical pole zero plot of mast dynamics containing 3

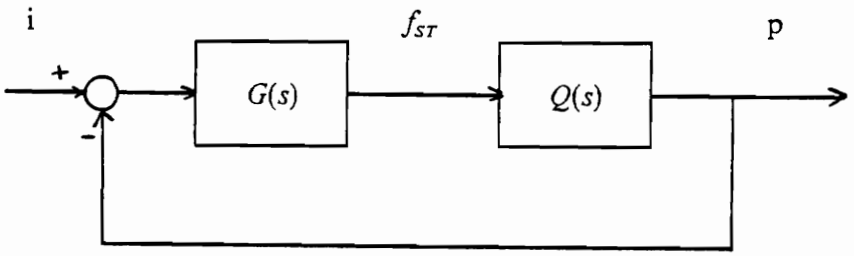

Figure 39. Block Diagram of Simplified System.

i = input command, zero for free decay
$Q(s)$ = transfer function representing mast dynamics
f_{ST} = force applied to structure
p = mast inertial position
$G(s) = f_{ST}/p$

modes. Notice that the poles and zeros are very close to the imaginary axis and that the poles and zeros alternate as one moves along the imaginary axis.

The departure angle of poles in a root locus plot describes the behavior of the poles of the system in a feedback configuration with low loop gain. The relative position feedback configuration places the mast in a feedback configuration with low loop gain so looking at the departure angles of the poles of $Q(s)$ will give a feeling for how the actuator compensation affects the poles of the mast dynamics.

When compensation is added in a feedback configuration, it adds poles and zeros to the plot of mast poles and zeros. The departure angle of a pole is calculated by placing a point near a pole on the pole zero plot [10]. Lines are then drawn from all poles and zeros to this point. The following equation must be satisfied and allows calculation of the angle from the nearest pole to the chosen point, the departure angle of that pole.

$$\sum \textbf{Angles from zeros} - \sum \textbf{Angles from poles} = 180 \qquad (5.2.4)$$

All angles are measured from the positive real axis. This can be broken up into the form shown below

$$\sum \textbf{Angles from mast zeros} + \sum \textbf{Angles from compensator zeros}$$

$$- \sum \textbf{Angles from mast poles} - \sum \textbf{Angles from compensator poles} = 180 \quad .(5.2.5)$$

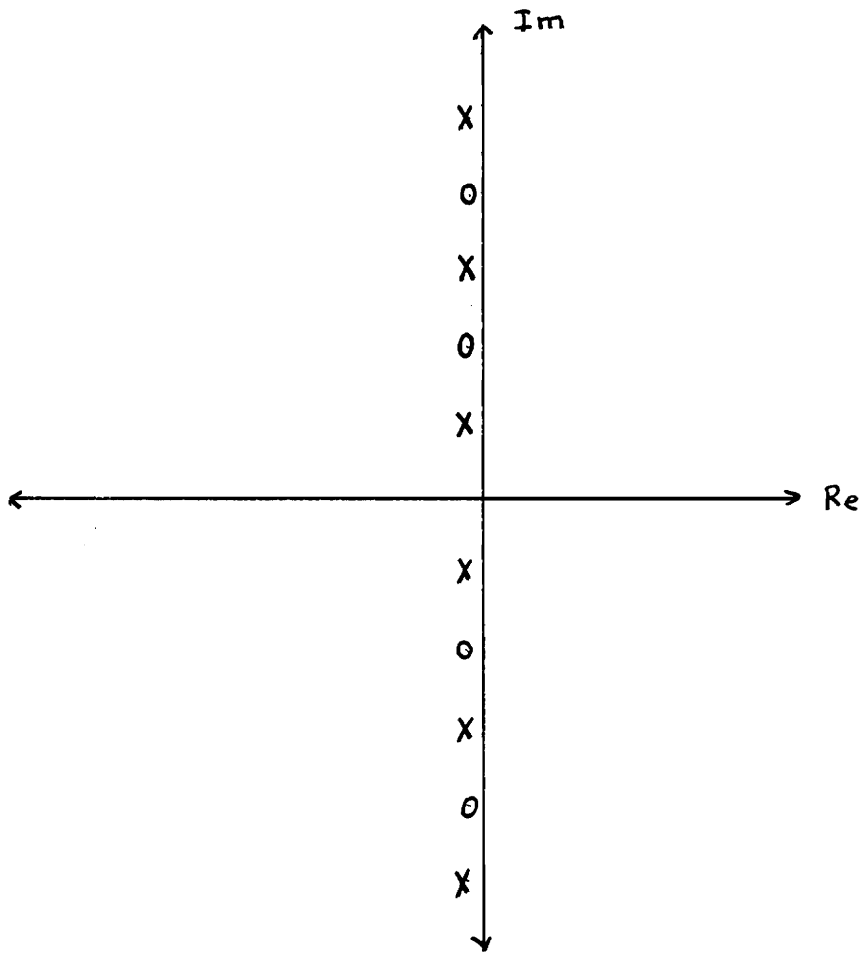

Figure 40. Plot of Mast Poles and Zeros

O = zero
X = pole

When calculating the departure angle, ϕ, of a mast pole above the real axis, it can easily be shown that, because of the special layout of mast poles and zeros, this simplifies to the approximate relation

$$\phi = 90 + \sum \text{Angles from compensator zeros} - \sum \text{Angles from compensator poles} . \tag{5.2.6}$$

It is well known that the phase of a transfer function at a frequency ω can be calculated by drawing lines from the poles and zeros of the transfer function to the point $j\omega$ and summing the angles in the following manner

$$\arg(G(j\omega)) = \sum \text{Angles from zeros} - \sum \text{Angles from poles} . \tag{5.2.7}$$

Since poles of the mast are very close to the imaginary axis, their location may be approximated by the point $j\omega_{mode}$. This allows a further approximation to be made in the calculation of the departure angle of the mast poles with compensation, $G(s)$, giving the approximate relation

$$\phi = 90 + \arg(G(j\omega_{mode})) . \tag{5.2.8}$$

This relation allowing the approximate calculation of the departure angle of mast poles in terms of the angle of the transfer function of the compensation is important in explaining how the relative position configuration affects the modes of the mast. Backing up to the system of one actuator mounted on the mast, it was seen that the actuator compensation was like placing the mast in a feedback configuration with compensation

$G(s) = f_{ST}/p$. This means that looking at the phase of the transfer function f_{ST}/p will give an explanation of how the actuator compensation affects the modes of the mast.

At mode frequencies where the phase is near zero, the departure angle will still be near 90 degrees and the mode frequency will shift up without added damping. For mode frequencies where the phase is near 90 degrees the departure angle will be near 180 degrees and the poles will be shifted towards the left half plane, adding the most damping. For mode frequencies where the phase is near 180 degrees, the mode frequency will shift down without added damping. This argument is shown to give a technique for finding the frequency range in which the actuator compensation has the most effect on the damping of the mast modes.

Several things combine to allow this argument to be used in explaining the effect of the LDCM actuators on the mast modes. First, placing the actuator on the mast in a relative position feedback configuration gives a feedback configuration of mast and actuator with low loop gain. Therefore, the departure angle of the mast poles describe their behavior in the system. Second, the unique configuration of the poles and zeros of the model for the mast allows a good approximation for the departure angles of the mast posed in terms of the phase of an actuator transfer function to be calculated. Third, the separability of the x, y, and torsional subsystems allow one to apply one actuator at a time to the mast in this manner to determine the effect of all of the actuators on the modes of the mast.

Figure 41 shows a plot of the phase of the transfer function f_{ST}/p for the three compensator designs. The vertical lines correspond to the mast mode frequencies. Examining this can be used to explain the relative amount of damping each of the compensator designed added to the mast modes. Examining this in conjunction with Table 3 helps explain the change in frequency and damping of the mast modes for the three compensator designs. For each compensator design, the most damping is added

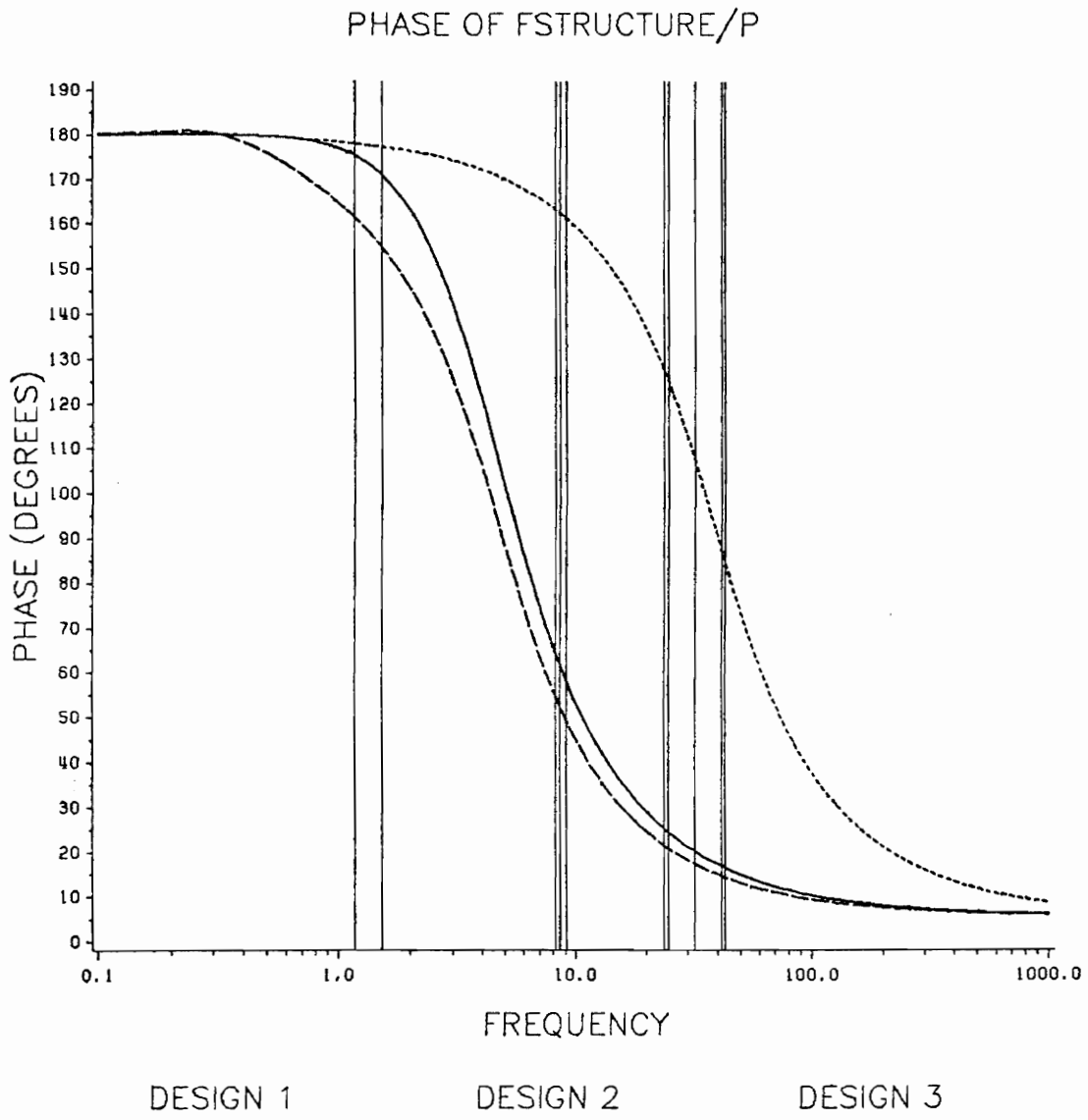

Figure 41. Plot of Phase of fstructure/p for the Three Designs.

when the phase of the transfer function f_{ST}/p is near 90 degrees. The phase of f_{ST}/p is the phase difference between the mast inertial position and the force applied to the mast so the most damping is added when the position and force are 90 degrees out of phase.

5.3 *Disturbance Analysis*

One of the proposed uses of the LDCM actuator in the COFS program was to excite the mast for model identification experiments. It is important for identification purposes to know what type of internal disturbances the system contains. The LDCM actuator, in the configuration used here, contains two sources of disturbance: the optical encoder and the proof mass accelerometer. The optical encoder provides a digital measurement of the relative position of the proof mass. Feeding back the digital measurement will add quantization noise to the system. The accelerometer which measures the proof mass acceleration generates internal noise. Since the accelerometer output is fed back in the force compensation of the LDCM and in the actuator compensation in designs two and three, the accelerometer adds noise to the system. This section details the amount of disturbance these two noise sources generate.

5.3.1 Position Measurement Quantization Noise

The optical encoder mounted on the bar of the LDCM gives a digital measurement of the relative position of the proof mass. This digital measurement is fed back in each of the three actuator compensation designs. Each time the encoder output steps in level,

a spike will be generated in the output force of the actuator. This subsection will compare the size of the force spikes for the three designs and determine the amount of noise these spikes generate in the force.

The magnitude of the force spikes may be used as a rough measure in comparing the amount of disturbance the digital measurement adds. The magnitude of the force spikes is related to the forward path gain from the encoder output to the generated force. In design one, the optical encoder is fed back through a lead compensator. Since the steps in the encoder output contain mostly high frequency components, the path gain at high frequencies determines the magnitude of the force spikes for design one. In both design two and three, the encoder output is fed back with constant gain, therefore, the forward path gain is a constant.

The magnitude of force spikes present in each of the three designs was calculated from the forward path gains and verified with simulations. Figure 42 shows a plot of force spike magnitude versus optical encoder resolution for each of the three designs. The relationship between encoder resolution and force spike magnitude is linear. A log scale was used on the plot because of the wide range of values.

Design three has the largest force spikes for a given encoder resolution due to the large feedback gains required to give the high bandwidth of the design. Design two has the smallest force spikes and design one has spikes which are slightly larger.

The force spike magnitude is good for comparisons of the three designs but it is not a good quantitative measure for the disturbance caused by the optical encoder. To give a quantitative measure of the amount of disturbance generated by the digital measurement of relative position, the power spectral density (PSD) of the generated force was calculated. A typical plot of the PSD of the force is shown in Figure 43. The background noise level is due to the force spikes.

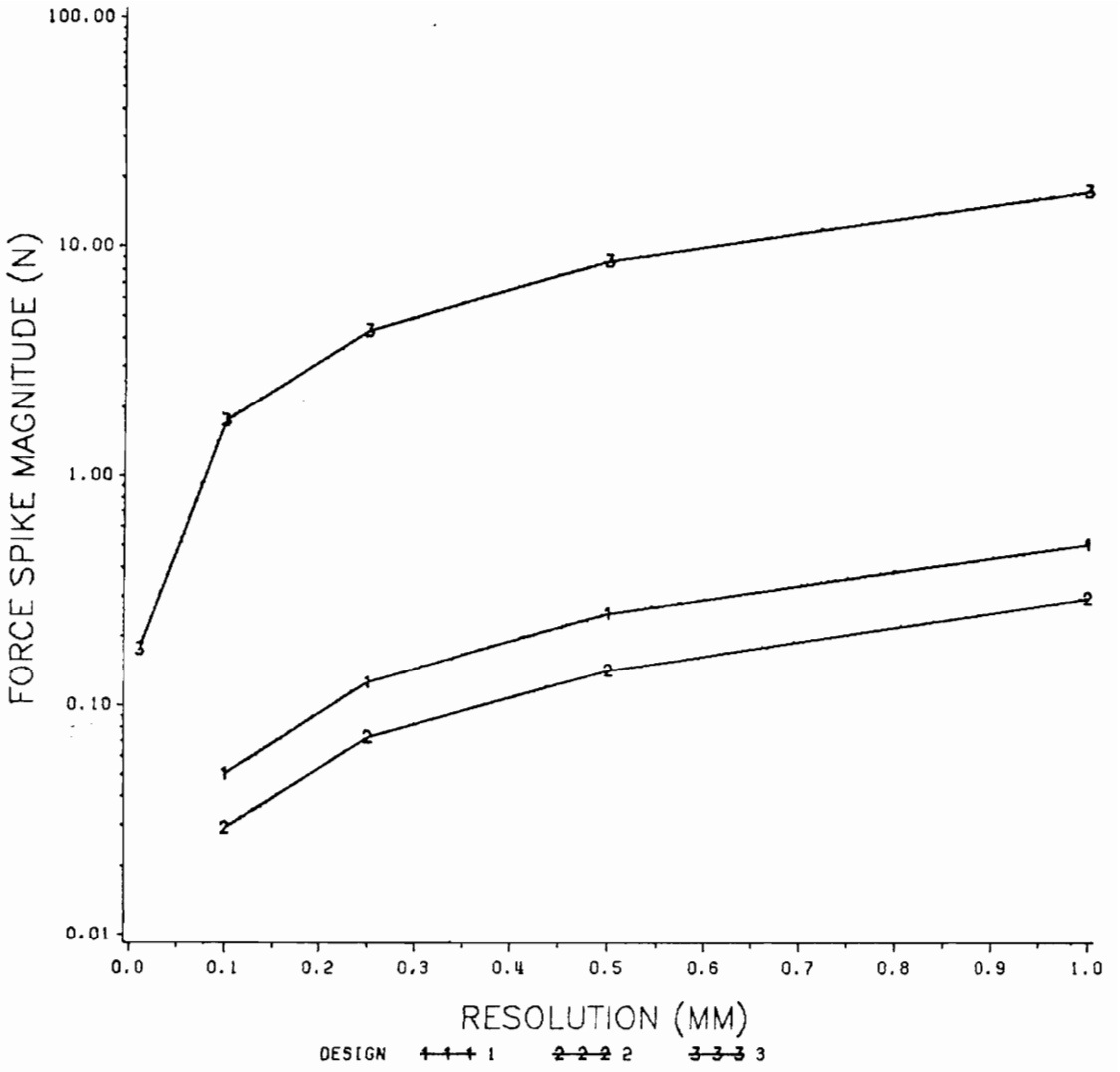

Figure 42. Effect of Encoder Resolution On Force Spike Magnitude

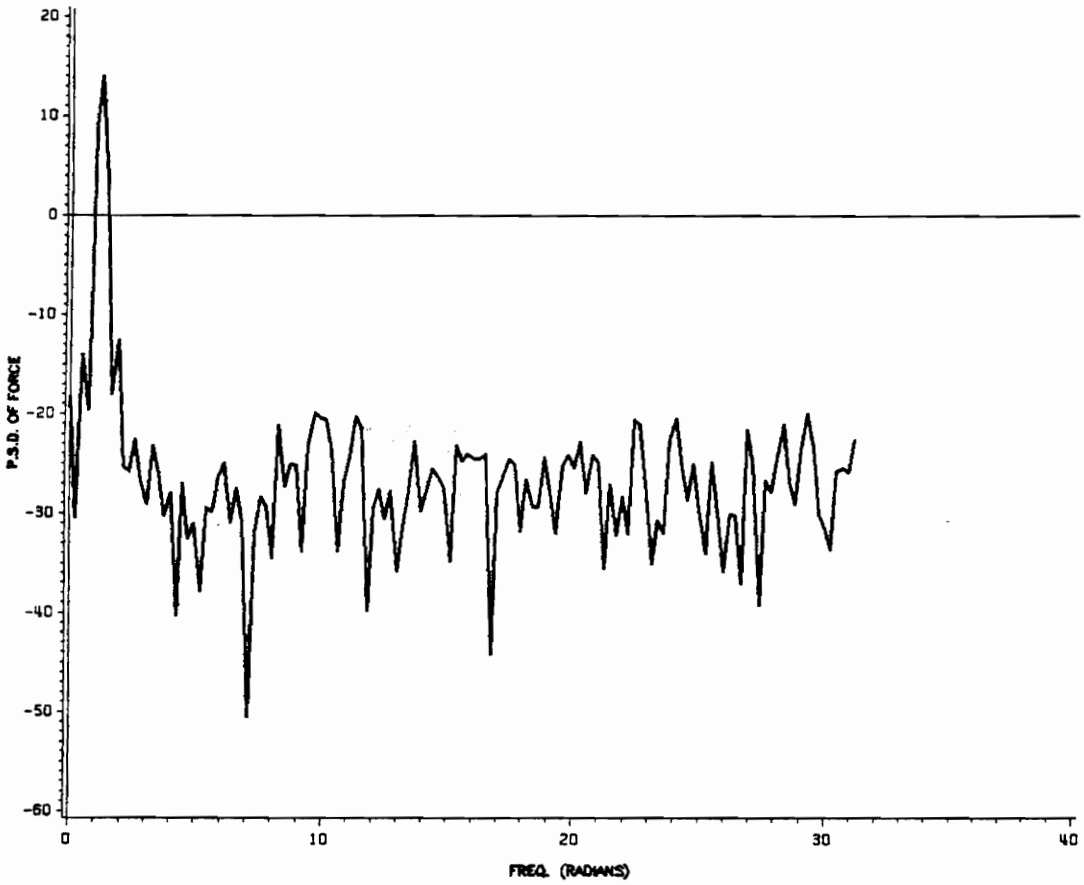

Figure 43. Power Spectral Density of LDCM Force During Excitation

The PSD of the force was calculated by using the DFT. First, a Bartlett window was applied to the data calculated from simulations. The DFT was then taken. Taking the magnitude squared of this over the number of data points gave the PSD [12],[13].

$$\hat{S}_{f_F}(\omega) = \frac{1}{N}\left|\sum_{n=0}^{N-1} f_n\, w_n\, e^{-j\omega n}\right|^2 \tag{5.3.1}$$

$$w_n = \left\{ \begin{array}{ll} \dfrac{2n}{N-1}, & 0 \le n \le \dfrac{N-1}{2} \\ 2 - \dfrac{2n}{N-1}, & \dfrac{N-1}{2} \le n \le N-1 \end{array} \right\}$$

$$\omega = \frac{2\pi k}{NT}, \quad 0 \le k \le N-1$$

where

f_n = force data

w_n = Bartlett window function

ω = frequency

T = sample time.

Simulations were run to calculate the force noise for various values of encoder resolution for each of the three compensator designs. Figure 44 shows a plot of the force noise versus encoder resolution for the different compensator designs. This plot shows the amount of noise the quantization disturbance will cause in the force for the three compensator designs.

Simulations were performed to look at the effect of force spikes on the different aspects of the system's performance. No appreciable effect could be seen in the actuator's input following ability. No effect, as well, could be seen in the amount of damping added to the mast modes. When the magnitude of the force spikes was very

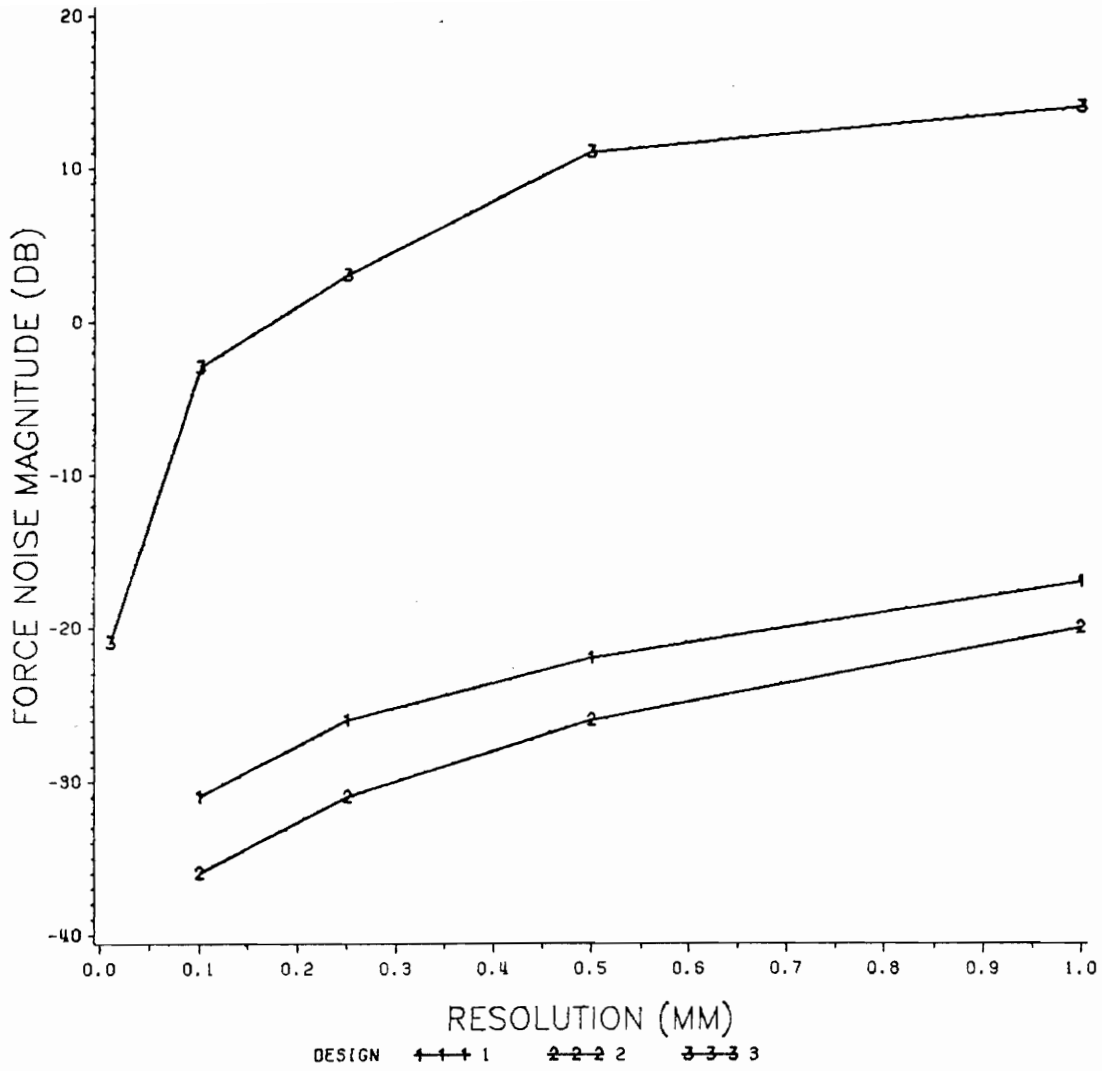

Figure 44. Effect of Encoder Resolution On Noise Generated By Force Spikes

large, for example, design three with resolution of 1 mm has spikes of 10 N magnitude, the force spikes led to the excitation of multiple modes of the mast. However, when the magnitude of the force spikes was small, this was unnoticeable.

The most significant effect of noise in the generated force would be apparent if accelerometers were used as measuring devices on the mast. Noise added to the force would be directly measured by the accelerometers.

5.3.2 Accelerometer Noise

The proof mass accelerometer is a source of disturbance within the LDCM system. Since the output of the accelerometer is used in feedback, any noise present on the output will cause disturbance. The output of the proof mass accelerometer is used in the force compensation of the LDCM. This is one place where the disturbance enters the system. Design one differs from designs two and three in that only the relative position measurement is used for actuator stabilization. Both design two and design three use the output of the proof mass accelerometer for actuator stabilization. For this reason, one would expect a difference in the amount of force noise due to the accelerometer noise for the three designs.

Simulations were performed to quantitatively determine the effect of the accelerometer noise on the generated force. Looking at the block diagram of the force compensation loop shows that the output of the accelerometer is fed back through a gain equal to the mass of the proof mass. The block diagram of actuator compensator designs two and three shows that the accelerometer output is fed back for actuator stabilization. These contributions were all taken into account in the simulations.

The accelerometer noise was assumed to be gaussian, zero mean, uncorrelated noise added to the accelerometer output. The variance was assumed to be P_{acc}. The power of the force output was calculated by

$$P_f = \sum_{n=0}^{N-1} f^2(n) \ . \tag{5.3.1}$$

The ratio P_f/P_{acc} was calculated for each of the three compensator designs for both type I and type II actuators. This ratio shows the relative amount of noise that a noisy accelerometer would add to the force generated by the actuator.

Table 5 shows values of the noise input output ratio P_f/P_{acc} for type I and type II actuators of each compensator design. These numbers were calculated with noise added to all of the accelerometer outputs. Examining these numbers gives some insight into the way the accelerometer noise enters the system. Notice that the numbers are very similar for all three compensator designs. This shows that the greatest amount of disturbance due to accelerometer noise enters the system through the force compensation loop. Using the accelerometer output for actuator stabilization in designs two and three adds only a small amount of disturbance. As explained in the section on position quantization disturbance, the significance of noise in the generated force will be in measuring the acceleration of the flexible mast since force noise is directly measurable in acceleration. Simulations were run to examine the combined effects of accelerometer noise and position quantization noise. The simulations showed the effects to be additive.

Table 5. Table of Accelerometer Noise Power Output Ratio.

	Force Noise Power Ratio, P_f/P_{acc} (dB)		
	Design 1	Design 2	Design 3
Type I	21.2	21.4	23.2
Type II	16.8	17.1	18.9

5.3.3 Blender Design

The optical encoder gives a digital measurement of the relative position of the proof mass. This digital measurement causes spikes in the force generated by the actuator. Another method of obtaining the relative position of the proof mass may be used to get rid of the problems caused by the digital measurement. This design, referred to as the blender design, allows another method of relative position measurement to be compared to the optical encoder.

Figure 45 shows a block diagram of the blender design. An accelerometer is placed on the base of the LDCM to give the mast acceleration. The output of this and the proof mass accelerometer are integrated and the difference formed to give the relative velocity of the proof mass. This is integrated to give an alternative measurement of the relative position of the proof mass. The integrators are approximated by first order lags to remove problems with DC offset. This alternative measurement of the proof mass relative position is blended with the optical encoder output by a pair of constants whose sum is unity. Changing the value of the blender constant, γ, allows a blending of the two measurements to analyze the effect of the alternative measurement method on the system performance. With $\gamma = 1$, the optical encoder measurement is fed back. With $\gamma = 0$, the relative position obtained from the accelerometers if fed back. This analysis was performed using the configuration of designs two and three. The results may be identically applied to design one as well.

The main goal in trying the configuration was to find a way of reducing the level of force noise caused by the force spikes. The effect of the different method of relative position measurement on the aspects of system performance evaluated previously was examined. Figure 46 shows a plot of the force spike magnitude versus blender constant,

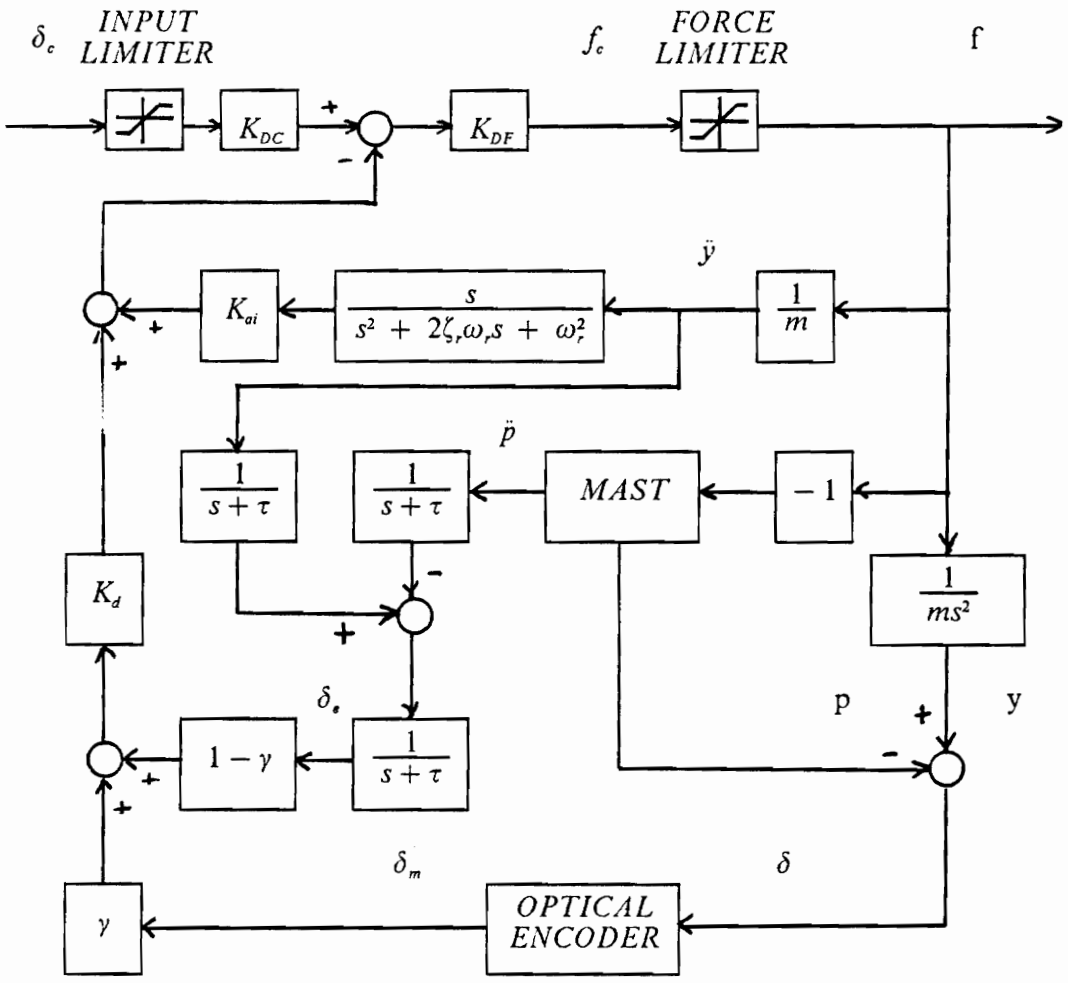

Figure 45. Block Diagram of System with Blender

δ_c = relative position command
f = generated force
f_c = commanded force
y = proof mass inertial position
p = mast inertial position
$\ddot{p}$ = mast acceleration
$\ddot{y}$ = proof mass acceleration
δ = proof mass relative position
δ_m = measured proof mass relative position
δ_e = estimated proof mass relative position
γ = blender constant
τ = 0.05

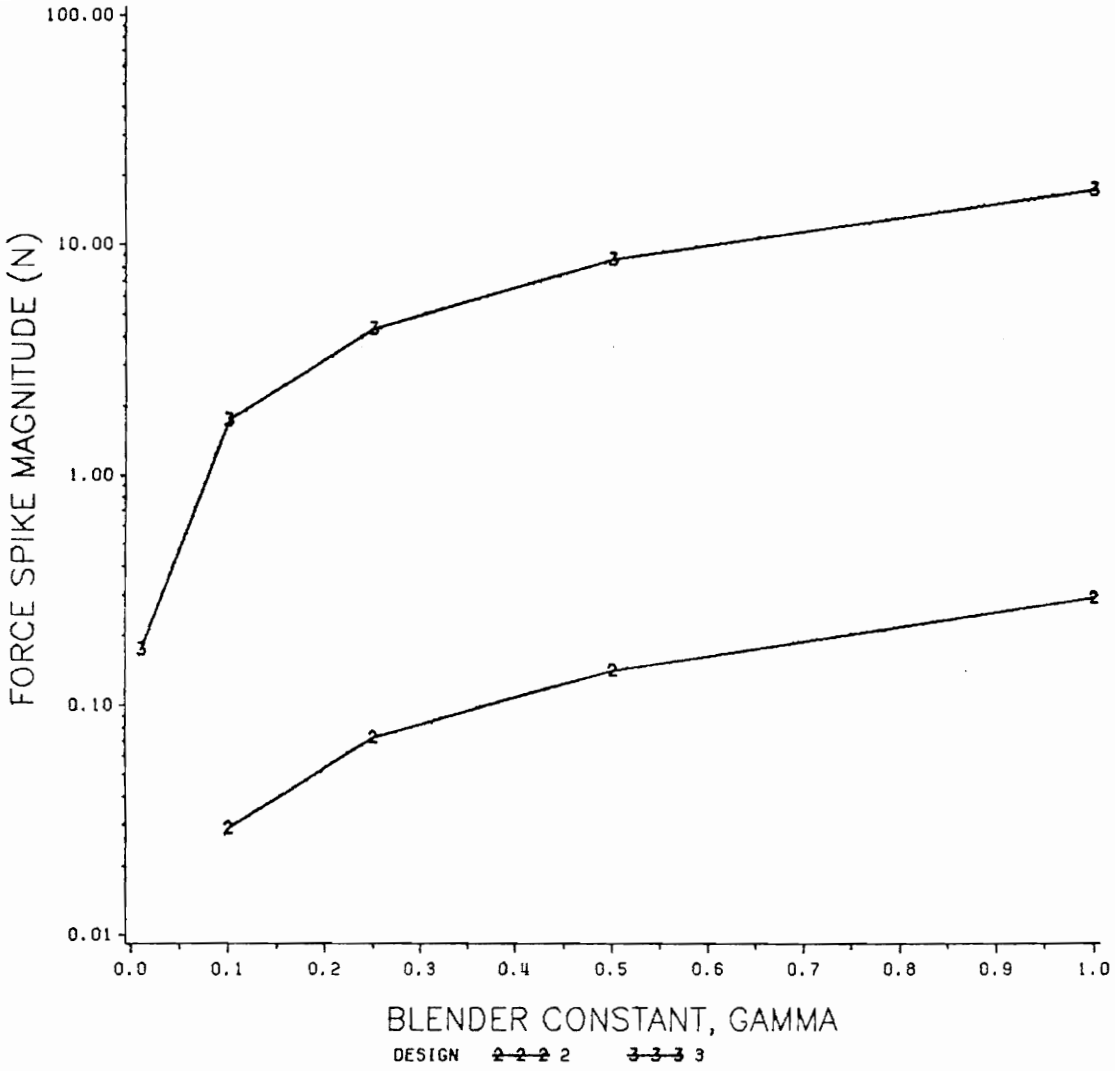

Figure 46. Effect of Gamma On Force Spike Magnitude

γ, with an optical encoder resolution of 1 mm for designs two and three. A logarithmic scale was used because of the large range of force spike magnitudes. This plot shows that changing γ gives the optical encoder an apparent resolution of γ times the actual resolution. Thus, the blender constant may be used to reduce the amount of force spiking. Figure 47 shows a plot of force noise magnitude due to force spiking versus blender constant. This shows how the blender constant, γ, can be used to achieve a specified level of force noise due to the digital measurement of relative position by the optical encoder.

The effect of the alternate method of measuring the relative position of the proof mass on the other aspects of system performance must be examined. This was done by looking at the effect of γ on the input following, mast excitation capability, damping and force noise due to accelerometer noise. Table 6 shows the effect of γ on the PFE for design two. The effect is the same for the other designs. The table shows that γ has an effect of the PFE only at low frequencies of excitation. This is due to the fact that first order lags are used to approximate integrators. The approximation is not as good at the lower frequencies so the measurement does not equal the actual value of the relative position.

The blender constant had no effect on the mast excitation capability of the different actuator designs. It had no effect, as well, on the amount of damping added to the modes of the mast. The blender design adds an accelerometer on the base of the LDCM. This would be expected to add to the amount of force noise caused by noise in the accelerometer outputs. Simulations were run with noise added to all the accelerometer outputs for $\gamma = 1$ and $\gamma = 0$ to show how much noise the extra accelerometer added. Table 7 shows the force noise to accelerometer noise power ratio for the case of $\gamma = 1$ and $\gamma = 0$. These values show that the extra accelerometer does not add a significant amount of noise to the force generated. Thus, the analysis performed showed that al-

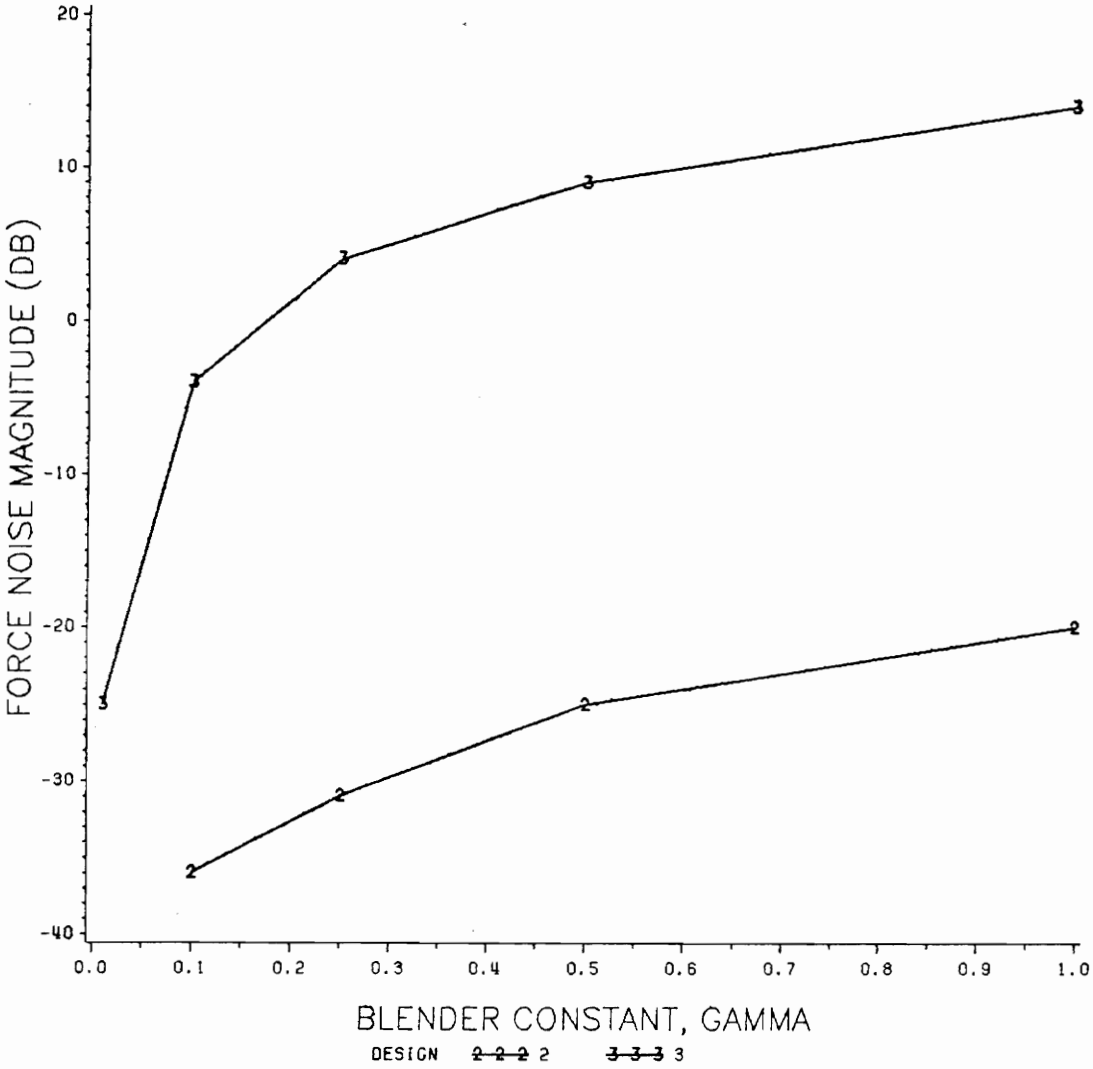

Figure 47. Effect of Gamma On Noise Generated By Force Spikes

Table 6. Table of Position Following Error versus Gamma.

Design 2

	Mode 1x	Mode 2x
γ	PFE	PFE
1.0	0.049	0.63
0.5	0.062	0.63
0.25	0.086	0.63

Table 7. Table of Force Noise Due To Accelerometer Noise, Blender Design.

	Design 2		Design 3	
	$\gamma = 1$	$\gamma = 0$	$\gamma = 1$	$\gamma = 0$
	P_f/P_{acc} (dB)	P_f/P_{acc} (dB)	P_f/P_{acc} (dB)	P_f/P_{acc} (dB)
Type I	21.4	21.7	23.2	24.0
Type II	17.1	17.2	18.9	19.4

ternate method of obtaining the relative position measurement from accelerometer measurements could be used to reduce the amount of force spiking in the system without significantly changing the system performance.

5.4 *Summary of System Performance*

The performance of the LDCM actuator was evaluated in reference to the COFS program goals. The actuator should follow sinusoidal input commands over the frequency range of the mast modes. The actuator should be able to excite modes of the mast. The actuator should generate clean force signals. Placing the actuator on the mast should not add damping to the mast modes. Simulations using a Runge-Kutta differential equation solver were used to evaluate the performance of the system.

The bandwidth of the compensated actuator was seen to be important in its ability to follow input commands and excite modes of the mast. Designs one and two performed similarly in these two capabilities due to their identical bandwidth. Designs one and two have transients in their relative position response at excitation frequencies higher than the actuator bandwidth. They also have low magnitude relative position response at the higher mode frequencies. The low magnitude relative position response causes these two design to be poor at exciting the higher frequency mast modes. The transients in relative position response cause multiple modes to be excited when the higher excitation frequencies are used.

Design three has much higher bandwidth than designs one and two. For full stroke commands at higher frequencies, design three does not follow sinusoidal input commands well because force saturation occurs. The magnitude of the relative position re-

sponse is higher than for designs one and two but because of force saturation, it is nonsinusoidal. The nonsinusoidal relative position response causes multiple modes to be excited, but, the magnitude of the mast excitation is much higher at the higher mode frequencies than for designs one and two.

Using a limited stroke command with design three keeps force saturation from occurring, causing the actuator to closely follow sinusoidal input commands. The following ability gradually gets poorer as the excitation frequency increases due to phase lag in the relative position response. This case gives the same magnitude mast excitation as designs one and two because the same amount of force is applied to the mast but this case excites single modes better because there is no transient in the relative position response.

Using a relative position measurement for actuator stabilization places the mast in the feedback path and, therefore, the actuator compensation will affect the modes of the mast. Eigenvalue calculation confirmed that both the mast mode frequencies and the amount of damping associated with each mode change. Damping values calculated from simulations matched well with the values calculated from eigenvalue analysis. Root locus techniques involving the departure angle of the mast poles were used to explain how the actuator compensation affects the modes of the mast. The most damping was added to modes at frequencies where the actuator applied force to the mast 90 degrees out of phase with the mast position. The frequencies where the most damping was added was near the bandwidth of the actuator compensation.

The digital output of the optical encoder caused spikes in the force generated by the LDCM actuator. These spikes were seen to cause wideband noise in the force. Design one had slightly larger spikes than design two. Design three had force spikes significantly larger than the other two designs because of the larger feedback gains needed to increase the actuator bandwidth. The force noise due to these spikes would

be directly measurable in accelerometers mounted on the mast but does not significantly affect other aspects of system performance.

Noise in the output of the accelerometers also caused noise in the force generated by the actuator. The primary contribution to this force noise was in the force compensation of the LDCM. In the force compensation loop, the accelerometer output is fed back with a gain equal to the mass of the proof mass. Since this is the primary source of force noise, the force noise values due to accelerometer noise for the three compensator designs are not significantly different.

Mounting an accelerometer on the mast (the LDCM base) gives an alternate method of obtaining the relative position of the proof mass. The measurement is good in the frequency range where the integrators used are a good approximation for an ideal integrator. This method of measuring the proof mass relative position does not cause spikes in the LDCM force. This method was also seen to only add a small amount of force noise due to accelerometer noise. This method did not have a significant effect on system performance in the frequency range where the integrators were good approximations for ideal integrators.

6.0 Conclusion

This thesis has examined a linear DC motor actuator for use in vibration suppression of a large space structure. The purpose was to fully describe the actuator and the effects that the actuator characteristics and the system configuration have on the use of this actuator.

Chapter two describes the linear DC motor. The physical limits of the LDCM, stroke length and power supply current, place limits on the amount of force the actuator can generate. The current and force compensation used in the LDCM actuator are described. This compensation removes the effects of back emf, friction, and cogging due to commutation.

Chapter three describes a proposed structure to use for analysis purposes. A finite element model accurate from 1 to 45 rad/sec is presented. Because the force compensation removes any motor dynamics, the actuator is seen to be unstable when placed on the mast. Two methods of actuator stabilization are available: inertial and relative position feedback. Relative position feedback is used because the relative position measurement is the only one available in space. The relative position feedback configuration couples the actuator to the structure in a feedback configuration.

Chapter four presents three different compensator designs for actuator stabilization. The actuator compensation is seen to guarantee that the LDCM stroke limit is not exceeded. The LDCM force limit is seen to limit the bandwidth of the actuator. Increasing the actuator bandwidth is seen to cause force saturation to occur.

Chapter five examines the performance of the LDCM actuator. The low bandwidth designs (one and two) are seen to give low magnitude mast excitation at the higher mode frequencies. Transients in the relative position response of these designs are seen to excite multiple mast modes. The higher bandwidth design (three) is seen to give higher magnitude mast excitation. The force saturation that occurs with this design is seen to cause nonsinusoidal relative position response which excites multiple mast modes.

The three compensator designs are seen to add damping to and change the frequency of the mast modes. Each design adds a different amount of damping. Root locus techniques examining the departure angles of the mast poles are used to explain the amount of damping added. This technique is powerful because it can be applied to any structure with a set of poles and zeros close to the imaginary axis. The analysis shows that the most damping is added to the modes in the frequency range where the phase lag between the mast position and the force applied to the mast is near 90 degrees.

The digital optical encoder measurement of the proof mass relative position is seen to cause spikes in the force generated by the actuator. Giving the actuator a wide bandwidth is seen to give significantly larger force spikes than lower bandwidth designs. Noisy accelerometer measurements also cause noise in the force generated by the actuator. The three designs have similar amounts of force noise from this source because the noise enters the system primarily through the force compensation of the LDCM. An alternate method of obtaining the proof mass relative position by adding

an accelerometer to the mast is seen to remove the force noise due to the digital measurement without significantly changing other aspects of the actuator's performance.

Some important conclusions may be drawn about using the LDCM actuator. When the actuator is equipped with current and force compensation, it requires stabilization when applied to a structure. The physical limits of the actuator are important in designing the actuator compensation. The limits give the actuator a maximum bandwidth if linear behavior is desired. The relative position feedback approach to actuator compensation links the structure and actuator in a feedback configuration. The measurements used for actuator compensation are a source of disturbance to the system.

This thesis has described the important characteristics of the LDCM actuator when it is used for vibration suppression of a large space structure. Future research should continue to examine the LDCM and concentrate an maximizing the vibration suppression capability of the actuator.

Appendix A. Computer Program for System Simulation

The system of the actuator mounted on the mast contains nonlinearities: force saturation and digital measurement quantization. Therefore, the system is described by a nonlinear differential equation of the form

$$\dot{y}(t) = g\,(y(t)\,,\ \delta_c(t)\,,\ t\,)\ .$$

A differential equation solving subroutine, DVERK, from the International Math and Statistical Library (IMSL), Inc., Houston, Texas was used to obtain the time response for the system. DVERK implements a fourth order Runge-Kutta method with variable step size. DVERK takes the state of the system defined at one time, $y(t_0)$, and propogates it forward one step in time to give $y(t_0 + h)$, where h is the step size. To use DVERK to calculate the time response of the system from $t = t_1$ to $t = t_2$, the DVERK subroutine must be called a number of times to move the system state from $t = t_1$ to $t = t_2$ in steps of h .

The DVERK subroutine requires a subroutine which calculates the derivative of the system state, therefore, the computer program used to simulate the system requires two parts. Part one is the main program which calls DVERK many times to step the system state through the desired simulation time. Part two is a subroutine which calculates the derivative of the system state.

Figure 48 shows a flowchart of the main program. The main program steps the system state through time and, at each time instant, calculates the signals of interest from the states of the system and prints them.

The subroutine calculates the derivative of the system state is just an implementation of the system differential equation (the system state equations)

$$\dot{y}(t) = g(y(t), \delta_c(t), t) .$$

with a small difference. DVERK requires a specific set of inputs and outputs for the derivative subroutine. The only inputs are the system state and the time at which the state is defined. This means that any input to the system must be written explicitly as a function of time and imbedded in the derivative subroutine. Also, any parameters which must be passed to the derivative subroutine, such as input parameters, must be passed to it by using a common storage area.

A listing of the computer program used to simulate the system with actuators with compensation design one follows. This implements the system shown in Figure 23. Also, a listing of the computer program used to simulate the system with actuators with compensation design two, including the blender, follows. This implements the system shown in Figure 45. Actuators with compensation design three may be simulated by adjusting the feedback gains to those from design three and using the same program. The only difference between the two programs are the state equations corresponding to the actuators and the equations used to calculate the signals of interest.

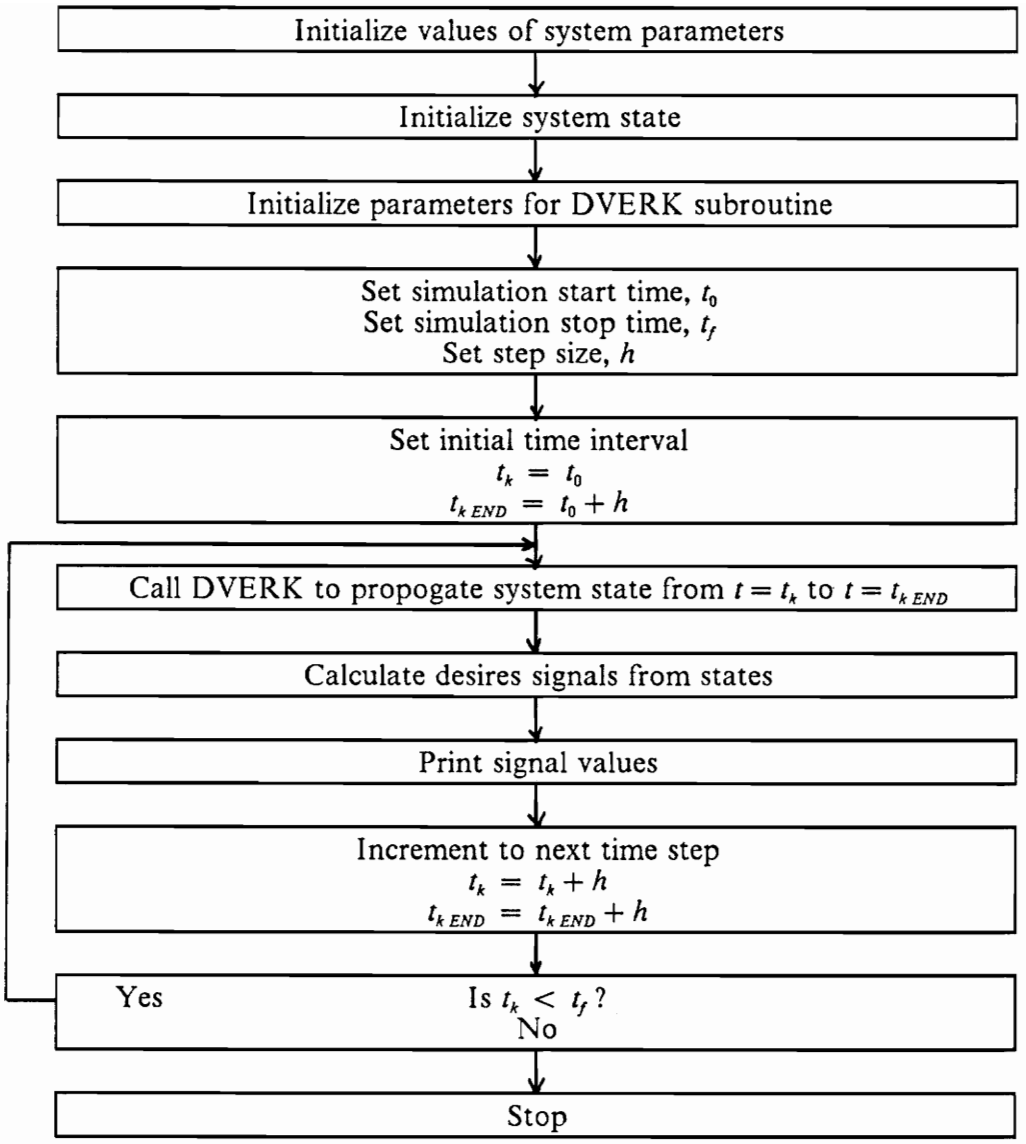

Figure 48. Flowchart of Simulation Computer Program

The system state equations and output equations for the signals of interest were derived by first writing a state space realization for each dynamic block on the system block diagram for a system with one mast mode and one actuator. The equations were combined according to the connections on the block diagram with the nonlinearities included. The equations were then expanded similarly to give a system with ten modes and ten actuators. The state and output equations were then written into the computer programs.

A.1 Simulation Program, Compensator Design One

```
      PROGRAM OPEN

      EXTERNAL E,YDOT

      COMMON ALPHA,OMEGA,ZETA,MASS,NMOD,NACT
      COMMON EXCON,EXCOFF,CONTON,CONOFF,XOMEGA,XAMP

      REAL*8 E

C             NUMBER OF STATES PASSED TO DVERK (DIFF EQ SOLV)
      INTEGER N
C             DIMENSION OF STATE + DERIVATIVE VECTORS
      INTEGER NW
C             ERROR PARAMETER FOR DVERK
      INTEGER IER
C             INPUT PARAMETAR FOR DVERK
      INTEGER IND
      INTEGER MM
      INTEGER I
      INTEGER J
C             NUMBER OF MODES IN MAST MODEL
      INTEGER NMOD
C             NUMBER OF ACTUATORS IN SYSTEM
      INTEGER NACT

      INTEGER III
      INTEGER K
C             WORK VECTOR FOR PSDCC
      INTEGER IWK(15150)
C             STEP TIME FOR DIFF EQ SOLVER
      REAL*8 T
      REAL*8 SUM
      REAL*8 ERROR
C             TIME WHERE CURRENT STATE IS VALID
      REAL*8 TK
C             STATE VECTOR
      REAL*8 Y(60)
C             TIME WHERE STATE IS DESIRED
      REAL*8 TKEND
C             ERROR TOLERANCE FOR EACH STEP
```

```
      REAL*8 TOL
C                 DVERK INPUT VECTOR
      REAL*8 C(24)
C                 DVERK WORK VECTOR
      REAL*8 W(60,20)
C                 DERIVATIVE OF STATE
      REAL*8 YPRIME(60)
C                 WORK VECTOR FOR PSDCC
      REAL*8 WK(15150)
      REAL*8 TIM
C                 PROOF MASS RELATIVE POSITION
      REAL*8 DEL(10)
C                 FORCE APPLIED TO PROOF MASS
      REAL*8 F(10)
C                 RELATIVE POSITION COMMAND
      REAL*8 DC(10)
C                 MAST INERTIAL POSITION
      REAL*8 P(10)
C                 MAST INERTIAL VELOCITY
      REAL*8 V(10)
C                 REFERENCE INPUT COMMAND
      REAL*8 R(10)
C                 NUMBER OF SECONDS IN SIMULATION
      REAL*8 SECS
C                 MASS OF PROOF MASS (ACT #)
      REAL*8 MASS(10)
C                 DAMPING OF EACH MAST MODE (MODE #)
      REAL*8 ZETA(10)
C                 MODE SHAPE COEFFICIENT (MODE #,ACTUATOR NUMBER)
      REAL*8 ALPHA(10,10)
C                 MODE FREQUENCY (MODE #)
      REAL*8 OMEGA(10)
C                 EXCITATION FREQUENCY (ACT #)
      REAL*8 XOMEGA(10)
C                 EXCITATION AMPLITUDE (ACT #)
      REAL*8 XAMP(10)
C                 SIMUALTION START TIME
      REAL*8 T0
C                 SIMULATION STOP TIME
      REAL*8 TF
C                 EXCITATION START TIME
      REAL*8 EXCON
C                 EXCITATION STOP TIME
      REAL*8 EXCOFF
C                 CONTROL START TIME
      REAL*8 CONTON
C                 CONTROL STOP TIME
```

```
      REAL*8 CONOFF
C                 PERIODOGRAM
      COMPLEX*16 PSDPER(0:1500)
C                 PSD WITH HAMMING WINDOW
      COMPLEX*16 PSDHAM(0:1500)
C                 PSD WITH BARTLETT WINDOW
      COMPLEX*16 PSDBAR(0:1500)

C                 ACTUATOR COMPENSATION PARAMETERS
      REAL*8 TAU
      REAL*8 G2
      REAL*8 G1
      REAL*8 OMG0

C                 HAMMING WINDOW VALUE
      REAL*8 WHAM
C                 BARTLETT WINDOW VALUE
      REAL*8 WBART

      REAL*8 SFFP(0:1500)
      REAL*8 SFFB(0:1500)
      REAL*8 SFFH(0:1500)
C                 VECTOR USED TO STORE DATA FOR PSD
      REAL*8 DELREL(1500)
      REAL*8 TMP

C                 TURN OFF UNDERFLOW INTERRUPTS
      CALL XUFLOW(0)

C                 THIS SECTION READS DATA FROM THE FILE MODEL.DAT

C                 READ MODE SHAPE COEFF  (MODE # , ACT # )
      DO 101 I = 1,10
       READ(2,*)(ALPHA(I,J),J = 1,10)
101   CONTINUE

C                 READ MODE FREQS   (MODE #)
      DO 102 I = 1,10
       READ(2,*)OMEGA(I)
102   CONTINUE

C                 READ DAMPING OF EACH MODE (MODE #)
      DO 103 I = 1,10
       READ(2,*)ZETA(I)
103   CONTINUE

C                 READ MASS OF EACH ACTUATOR (ACT #)
      DO 104 I = 1,10
```

```
      READ(2,*)MASS(I)
104   CONTINUE


C               THIS SECTION READS FROM AN INPUT FILE
C               WHICH DEFINES WHAT ACTUATORS WILL EXCITE
C               FOR WHAT TIMES AT WHAT FREQUENCIES

C               READ EXCITATION FREQ AND AMPLITUDE (ACT #)
      DO 105 I = 1,10
       READ(4,*)XOMEGA(I),XAMP(I)
105   CONTINUE

C               READ STEP TIME
      READ(4,*)T
C               READ SIMUALTION START TIME
      READ(4,*)T0
C               READ SIMULATION STOP TIME
      READ(4,*)TF
C               READ EXCITATION START TIME
      READ(4,*)EXCON
C               READ EXCITATION STOP TIME
      READ(4,*)EXCOFF
C               READ CONTROL START TIME
      READ(4,*)CONTON
C               READ CONTROL STOP TIME
      READ(4,*)CONOFF
C               READ NUMBER OF ACTUATOR WHERE PSD IS CALCULATED
      READ(4,*)NUMACT


C               DEFINE ACTUATOR COMPENSATION PARAMETERS
      G1 = 3.0
      G2 = 6.0

C               SET NUMBER OF MODES IN MODEL
      NMOD = 10
C               SET NUMBER OF ACTUATORS
      NACT = 10

      SECS = TF-T0
C               CALC NUMBER OF POINTS IN SIMULATION
      MM = INT(SECS/T)

C               CALC NUMBER OF STATES USED
      N = 2*NMOD + 4*NACT
C               SET PARAMETERS FOR DVERK
      NW = 60
```

```
      TOL = 0.0005
      IND = 1

C                INITIALIZE STATE TO ZERO
      DO 981 J = 1,N
      Y(J) = 0.0
981   CONTINUE

      ERROR = 0.0

C                TOP OF LOOP WHICH STEPS THE STATE THROUGH TIME
      DO 50 KK = 1,MM
C                TIME WHERE STATE IS KNOWN
       TK = T*FLOAT(KK-1) + T0
C                TIME WHERE STATE IS DESIRED
       TKEND = T*FLOAT(KK) + T0
C                SET INPUT PARAMETER FOR DVERK
       IND = 1
C
C                CALL DIFF EQ SOLVER TO PROPOGATE STATE FROM
C                TIME = TK TO TIME = TKEND
C
       CALL DVERK(N,YDOT,TK,Y,TKEND,TOL,IND,C,NW,W,IER)

C                CHECK FOR ERROR IN DVERK
      IF(IND.LT.0)GOTO 873

C                SET UP REFERENCE INPUT COMMAND
      IF(TK.GT.EXCON.AND.TK.LT.EXCOFF)THEN
C                IF IN EXCITATION STAGE, INPUT IS SINUSOIDAL
      DO 106 III = 1,10
       R(III) = XAMP(III)*SIN(XOMEGA(III)*TK)
106   CONTINUE
      ELSE
C                IF IN FREE DECAY STAGE, INPUT IS ZERO
      DO 107 III = 1,10
       R(III) = 0.0
107   CONTINUE
      ENDIF

C                CALCULATE MAST POSITION AND VELOCITY AT
C                EACH ACTUATOR LOCATION
      DO 10 J = 1,NACT
       P(J) = 0.0
       V(J) = 0.0
       DO 20 I = 1,NMOD
        P(J) = P(J) + ALPHA(I,J)*Y(2*I-1)
```

```
      V(J) = V(J) + ALPHA(I,J)*Y(2*I)
20    CONTINUE

C                 CALCULATE PROOF MASS RELATIVE POSITION
      DEL(J) = ( Y(2*NMOD+4*J-3) - P(J) )

C                 QUANTIZE TO SIMULATE OPTICAL ENCODER
      DEL(J) = E(DEL(J))
10    CONTINUE

C                 SAVE FORCE FOR PSD CALCULATION
      DELREL(KK) = F(NUMACT)

C                 SET RELATIVE POSITION COMMAND = REFERENCE INPUT
      DO 30 JJJ = 1,NACT
       DC(JJJ) = R(JJJ)
30    CONTINUE

C                 CALCULATE PFE
      ERROR = ERROR + ((DEL(NUMACT)-DC(NUMACT))/XAMP(NUMACT))**2

C                 IMPLEMENT INPUT COMMAND LIMITER
      DO 80 J = 1,NACT
       IF(ABS(DC(J)).GT.DCMAX(J))
     $       DC(J) = SIGN(DCMAX(J),DC(J))
80    CONTINUE

      TIM = TKEND

C                 CALCULATE FORCE GENERATED BY EACH ACTUATOR
      DO 70 J = 1,NACT

      F(J) = 250.0*( (Y(2*NMOD+4*J-1)-Y(2*NMOD+4*J))/G1
     $       + DC(J) - DEL(J)*G2/G1 )

C                 IMPLEMENT FORCE LIMITING OF LDCM
       IF(ABS(F(J)).GT.FMAX(J))F(J) =
     $                 SIGN(FMAX(J),F(J))

70    CONTINUE

C                 PRINT OUT SIGNALS AT EACH STEP IN
C                 TIME FOR PLOTTING
      DO 108  J = 1,NACT
       WRITE(10,1985)J,TIM,P(J)
       WRITE(11,1985)J,TIM,F(J)
       WRITE(12,1985)J,TIM,DEL(J)
       WRITE(13,1985)J,TIM,DC(J)
```

```
      WRITE(15,1985)J,TIM,V(J)
108   CONTINUE

C               END OF LOOP WHICH PROPOGATES THE STATE
C               THROUGH TIME
50    CONTINUE

C               THIS SECTION CALCULATES THE POWER SPECTRAL
C               DENSITY (PSD) OF A SIGNAL

C               DECIDE WHAT SECTION OF DATA TO USE
      K1 = INT(EXCON/T)
      K2 = INT(EXCOFF/T)
C               CALC NUMBER OF DATA POINTS
      MM = K2-K1
C               MULTIPLY EACH DATA POINT BY THE WINDOW VALUE
C               AND PUT IN A COMPLEX ARRAY
      DO 109 J = K1,K2
       K = J-K1
       IF(K.LT.(MM-1)/2)THEN
         WBART = 2.0*FLOAT(K)/FLOAT(MM-1)
       ELSE
         WBART = 2.0-2.0*FLOAT(K)/FLOAT(MM-1)
       ENDIF
       WHAM = 0.54-0.46*COS(2.0*3.14159*FLOAT(K)/FLOAT(MM-1))
       TMP = DELREL(J)
       PSDPER(K) = DCMPLX(TMP,0.0D0)
       PSDHAM(K) = DCMPLX(TMP*WHAM,0.0D0)
       PSDBAR(K) = DCMPLX(TMP*WBART,0.0D0)
109   CONTINUE
C               TAKE THE DFT OF THE WINDOWED DATA
      CALL FFTCC(PSDPER,MM,IWK,WK)
      CALL FFTCC(PSDHAM,MM,IWK,WK)
      CALL FFTCC(PSDBAR,MM,IWK,WK)

      DO 110 K = 0,MM-1
C               TAKE THE MAGNITUDE SQUARED AND NORMALIZE BY THE
C               NUMBER OF POINTS TO GET THE PSD
       SFFP(K) = CDABS(PSDPER(K))**2/FLOAT(MM+1)
       SFFH(K) = CDABS(PSDHAM(K))**2/FLOAT(MM+1)
       SFFB(K) = CDABS(PSDBAR(K))**2/FLOAT(MM+1)
C               PUT PSD IN DB
       SFFP(K) = 10.0*LOG10(SFFP(K))
       SFFB(K) = 10.0*LOG10(SFFB(K))
       SFFH(K) = 10.0*LOG10(SFFH(K))
110   CONTINUE

C               SET UP FREQUENCY PROPORTIONALITY CONSTANT
```

```
      TMP = 2.0*3.14159/T/FLOAT(MM)
C                 PRINT OUT THE DATA FOR PLOTTING
      DO 111 K = 0,(MM-1)/2
       WRITE(16,*)TMP*FLOAT(K),SFFP(K),SFFB(K),SFFH(K)
111   CONTINUE

C                 PRINT THE NORMALIZED PFE
      WRITE(*,*)ERROR/FLOAT(MM),'  SUM ( (DC(K)-DEL(K))/DC(K) )**2  '

1985  FORMAT(1X,I5,2(1X,E12.5))

      STOP
873   WRITE(*,*)'ERROR,  IND = ',IND
      STOP
      END



C                 THIS SUBROUTINE IMPLEMENTS THE MODEL BY
C                 CALCULATING THE DERIVATIVE OF THE STATE
C                 FROM THE STATE AND TIME, THE DIFF EQ
C                 SOLVER USES THIS ROUTINE TO PROPOGATE
C                 THE STATE THROUGH TIME

      SUBROUTINE YDOT(N,TK,Y,YPRIME)
      EXTERNAL E
      COMMON ALPHA,OMEGA,ZETA,MASS,NMOD,NACT
      COMMON EXCON,EXCOFF,CONTON,CONOFF,XOMEGA,XAMP

C                 EXCITATION START TIME
      REAL*8 EXCON
C                 EXCITATION STOP TIME
      REAL*8 EXCOFF
C                 CONTROL START TIME
      REAL*8 CONTON
C                 CONTROL STOP TIME
      REAL*8 CONOFF
C                 NUMBER OF STATES PASSED TO DVERK (DIFF EQ SOLV)
      INTEGER N
C                 NUMBER OF ACTUATORS IN SYSTEM
      INTEGER NACT
C                 NUMBER OF MODES IN MAST MODEL
      INTEGER NMOD
      INTEGER III
      REAL*8 E
      INTEGER I,J,K
      REAL*8 SUM
C                 TIME WHERE CURRENT STATE IS VALID
```

```
      REAL*8 TK
C                 STATE VECTOR
      REAL*8 Y(60)
C                 DERIVATIVE OF STATE
      REAL*8 YPRIME(60)

C                 REFERENCE INPUT COMMAND
      REAL*8 R(10)
C                 RELATIVE POSITION COMMAND
      REAL*8 DC(10)
C                 MAST INERTIAL POSITION
      REAL*8 P(10)
C                 MAST INERTIAL VELOCITY
      REAL*8 V(10)
C                 MODE SHAPE COEFFICIENT (MODE #,ACTUATOR NUMBER)
      REAL*8 ALPHA(10,10)
C                 RELATIVE POSITION MEASURED BY OPTICAL ENCODER
      REAL*8 DEL(10)
C                 MODE FREQUENCY (MODE #)
      REAL*8 OMGEGA(10)
C                 DAMPING OF EACH MAST MODE (MODE #)
      REAL*8 ZETA(10)
C                 MASS OF PROOF MASS (ACT #)
      REAL*8 MASS(10)
C                 EXCITATION AMPLITUDE (ACT #)
      REAL*8 XAMP(10)
C                 EXCITATION FREQUENCY (ACT #)
      REAL*8 XOMG(10)
C                 FORCE APPLIED TO PROOF MASS
      REAL*8 FC

C                 ACTUATOR COMPENSATION PARAMETERS
      REAL*8 OMG0
      REAL*8 G1
      REAL*8 G2
      REAL*8 TAU

C                 DEFINE ACTUATOR COMPENSATION PARAMETERS
      G1 = 3.0
      G2 = 6.0


C                 SET UP REFERENCE INPUT COMMAND
      IF(TK.GT.EXCON.AND.TK.LT.EXCOFF)THEN
C                 IF IN EXCITATION STAGE, INPUT IS SINUSOIDAL
      DO 101 III = 1,10
        R(III) = XAMP(III)*SIN(XOMEGA(III)*TK)
101   CONTINUE
```

```
      ELSE
C                 IF IN FREE DECAY STAGE, INPUT IS ZERO
      DO 102 III = 1,10
       R(III) = 0.0
102   CONTINUE
      ENDIF



C                 CALCULATE MAST POSITION AND VELOCITY AT
C                 EACH ACTUATOR LOCATION
      DO 10 J = 1,NACT
       P(J) = 0.0
       V(J) = 0.0
       DO 20 I = 1,NMOD
        P(J) = P(J) + ALPHA(I,J)*Y(2*I-1)
        V(J) = V(J) + ALPHA(I,J)*Y(2*I)
20     CONTINUE
C                 CALCULATE PROOF MASS RELATIVE POSITION
       DEL(J) =   Y(2*NMOD+4*J-3) - P(J)
C                 QUANTIZE TO SIMULATE OPTICAL ENCODER
       DEL(J) = E( DEL(J) )
10    CONTINUE

C                 SET RELATIVE POSITION COMMAND = REFERENCE INPUT
      DO 30 J = 1,NACT
       DC(J) = R(J)
30    CONTINUE

C                 IMPLEMENT INPUT COMMAND LIMITER
      DO 80 J = 1,NACT
       IF(ABS(DC(J)).GT.DCMAX(J))DC(J) = SIGN(DCMAX(J),DC(J))
80    CONTINUE

C                 THIS SECTION CALCULATES THE DERIVATIVE OF THE
C                 STATES OF THE SYSTEM IN TERMS OF THE STATES,
C                 INPUTS, AND FORCE

C                 THE STATES OF THE SYSTEM ARE ARRAINGED
C                 IN ORDER WITH THE MAST MODES FIRST, FOLLOWED
C                 BY THE MODES FOR THE ACTUATOR AND COMPENSATION

C                 THIS BLOCK OF EQUATIONS, THE FIRST ( 2 * NMOD )
C                 ARE THE STATES FOR THE MODES OF THE MAST
      DO 50 I = 1,NMOD
       YPRIME(2*I-1) = Y(2*I)
       SUM = 0.0
       DO 60 J = 1,NACT
```

```
      SUM = SUM + ALPHA(I,J)*(
     $    (Y(2*NMOD+4*J)-Y(2*NMOD+4*J-1))/G1 + DEL(J)*G2/G1
     $      - DC(J)   )
60    CONTINUE
      YPRIME(2*I) = -OMEGA(I)**2*Y(2*I-1)
     $          -2.0*ZETA(I)*OMEGA(I)*Y(2*I)

     $          + 250.0*SUM
50    CONTINUE

C               THIS BLOCK OF EQUATIONS, STARTING FROM 2*NMOD+1
C               ARE FOR THE ACTUATOR AND COMPENSATION
C               EACH ACTUATOR WITH COMPENSATION CONSISTS OF
C               7 STATES
      DO 70 J = 1,NACT

      OMG0 = (250.0/MASS(J))**0.5

      TAU = 3.0/(2.0)**0.5*OMG0

      YPRIME(2*NMOD+4*J-3) = Y(2*NMOD+4*J-2)

      YPRIME(2*NMOD+4*J-2) = OMG0**2*DC(J)
     $      + OMG0**2/G1*( Y(2*NMOD+4*J-1)-Y(2*NMOD+4*J) )
     $      - OMG0**2*G2/G1*DEL(J)

      YPRIME(2*NMOD+4*J-1) = -TAU*Y(2*NMOD+4*J-1) + TAU*(1.0-G1)*DC(J)

      YPRIME(2*NMOD+4*J) = -TAU*Y(2*NMOD+4*J) + TAU*(1.0-G2)*DEL(J)

70    CONTINUE

      RETURN
      END

C               THIS FUNCTION QUANTIZES THE ARGUMENT TO
C               SIMULATE THE DIGITAL MEASUREMENT OF THE
C               OPTICAL ENCODER
      FUNCTION E(X)
C               ARGUMENT
      REAL*8 X
C               ENCODER RESOLUTION
      REAL*8 R
      REAL*8 E
      REAL*8 TMP
C               SET ENCODER RESOLUTION TO 1 MM
      R = 1.00D-3
C               THIS FUNCTION ROUNDS TO THE NEAREST [RESOLUTION]
```

```
TMP = X/R + DSIGN(0.5D0,X)
E = R*FLOAT(INT(TMP))
END
```

A.2 Simulation Program, Compensator Designs Two and Three

```
      PROGRAM OPEN

      EXTERNAL E,YDOT

      COMMON ALPHA,OMG,ZETA,MASS,NMOD,NACT
      COMMON EXCON,EXCOFF,CONTON,CONOFF,XOMG,XAMP
      COMMON GAM,TAU,KAI,KD
      COMMON ZETAR,OMGR,FMAX,DCMAX,NI,NA
      COMMON KDC

C             WORK VECTOR FOR PSDCC
      INTEGER IWK(15150)
C             WORK VECTOR FOR PSDCC
      REAL*8 WK(15150)
C             NUMBER OF STATES PASSED TO DVERK (DIFF EQ SOLV)
      INTEGER N
C             DIMENSION OF STATE + DERIVATIVE VECTORS
      INTEGER NW
C             ERROR PARAMETER FOR DVERK
      INTEGER IER
C             INPUT PARAMETAR FOR DVERK
      INTEGER IND

      INTEGER MM

      INTEGER I,J,JJJ,III,K,KK
C             NUMBER OF MODES IN MAST MODEL
      INTEGER NMOD
C             NUMBER OF ACTUATORS IN SYSTEM
      INTEGER NACT
C             BLENDER CONSTANT
      REAL*8 GAM
C             ACTUATOR COMPENSATION PARAMETERS
      REAL*8 TAU
      REAL*8 KAI(10)
      REAL*8 KD(10)
      REAL*8 ZETAR
      REAL*8 OMGR
```

```
      REAL*8 KDC(10)
C                 FORCE LIMIT
      REAL*8 FMAX(10)
C                 INPUT LIMIT
      REAL*8 DCMAX(10)
C                 ACCELEROMETER NOISE
      REAL*8 NA
C                 STEP TIME FOR DIFF EQ SOLVER
      REAL*8 T

      REAL*8 SUM
C                 TIME WHERE CURRENT STATE IS VALID
      REAL*8 TK
C                 STATE VECTOR
      REAL*8 Y(109)
C                 TIME WHERE STATE IS DESIRED
      REAL*8 TKEND
C                 ERROR TOLERANCE FOR EACH STEP
      REAL*8 TOL
C                 DVERK INPUT VECTOR
      REAL*8 C(24)
C                 DVERK WORK VECTOR
      REAL*8 W(109,40)
C                 DERIVATIVE OF STATE
      REAL*8 YPRIME(109)

      REAL*8 TIM
C                 PROOF MASS RELATIVE POSITION
      REAL*8 DEL(10)
C                 FORCE APPLIED TO PROOF MASS
      REAL*8 F(10)
C                 RELATIVE POSITION COMMAND
      REAL*8 DC(10)
C                 MAST INERTIAL POSITION
      REAL*8 P(10)
C                 MAST INERTIAL VELOCITY
      REAL*8 V(10)
C                 REFERENCE INPUT COMMAND
      REAL*8 R(10)
C                 ESTIMATE OF RELATIVE POSITION FOR BLENDER
      REAL*8 DELE(10)
C                 NUMBER OF SECONDS IN SIMULATION
      REAL*8 SECS
C                 MASS OF PROOF MASS (ACT #)
      REAL*8 MASS(10)
C                 DAMPING OF EACH MAST MODE (MODE #)
      REAL*8 ZETA(10)
C                 MODE SHAPE COEFFICIENT (MODE #,ACTUATOR NUMBER)
```

```
      REAL*8 ALPHA(10,10)
C                MODE FREQUENCY (MODE #)
      REAL*8 OMG(10)
C                EXCITATION FREQUENCY (ACT #)
      REAL*8 XOMG(10)
C                EXCITATION AMPLITUDE (ACT #)
      REAL*8 XAMP(10)
C                SIMUALTION START TIME
      REAL*8 T0
C                SIMULATION STOP TIME
      REAL*8 TF
C                EXCITATION START TIME
      REAL*8 EXCON
C                EXCITATION STOP TIME
      REAL*8 EXCOFF
C                CONTROL START TIME
      REAL*8 CONTON
C                CONTROL STOP TIME
      REAL*8 CONOFF
C                PERIODOGRAM
      COMPLEX*16 PSDPER(0:1500)
C                PSD WITH HAMMING WINDOW
      COMPLEX*16 PSDHAM(0:1500)
C                PSD WITH BARTLETT WINDOW
      COMPLEX*16 PSDBAR(0:1500)

      REAL*8 TMP
C                HAMMING WINDOW VALUE
      REAL*8 WHAM
C                BARTLETT WINDOW VALUE
      REAL*8 WBART

      REAL*8 SFFP(0:1500)
      REAL*8 SFFB(0:1500)
      REAL*8 SFFH(0:1500)
C                VECTOR USED TO STORE DATA FOR PSD
      REAL*8 DELREL(1500)

C                TURN OFF UNDERFLOW INTERRUPTS
      CALL XUFLOW(0)

C                THIS SECTION READS DATA FROM THE FILE MODEL.DAT

C                READ MODE SHAPE COEFF  (MODE # , ACT # )
      DO 101 I = 1,10
        READ(2,*)(ALPHA(I,J),J = 1,10)
101   CONTINUE
```

```
C               READ MODE FREQS  (MODE #)
      DO 102 I = 1,10
       READ(2,*)OMG(I)
102   CONTINUE

C               READ DAMPING OF EACH MODE (MODE #)
      DO 103 I = 1,10
       READ(2,*)ZETA(I)
103   CONTINUE

C               READ MASS OF EACH ACTUATOR (ACT #)
      DO 104 I = 1,10
       READ(2,*)MASS(I)
104   CONTINUE

C               THIS SECTION READS FROM AN INPUT FILE
C               WHICH DEFINES WHAT ACTUATORS WILL EXCITE
C               FOR WHAT TIMES AT WHAT FREQUENCIES

C               READ EXCITATION FREQ AND AMPLITUDE (ACT #)
      DO 106 I = 1,10
       READ(4,*)XOMG(I),XAMP(I)
106   CONTINUE

C               READ STEP TIME
      READ(4,*)T
C               READ SIMUALTION START TIME
      READ(4,*)T0
C               READ SIMULATION STOP TIME
      READ(4,*)TF
C               READ EXCITATION START TIME
      READ(4,*)EXCON
C               READ EXCITATION STOP TIME
      READ(4,*)EXCOFF
C               READ CONTROL START TIME
      READ(4,*)CONTON
C               READ CONTROL STOP TIME
      READ(4,*)CONOFF

C               READ NUMBER OF ACTUATOR WHERE PSD IS CALCULATED
      READ(4,*)NUMACT

C               READ THE BLENDER CONSTANT FROM THE KEYBOARD
      READ(5,*)GAM

C               DEFINE ACTUATOR COMPENSATION PARAMETERS
      TAU = 1/20.0
      DO 98 J = 1,10
```

```
      IF(J.LE.4)THEN
        KAI(J) = .303
        KD(J) = 1.1439
        KDC(J) = 1.0
        FMAX(J) = 30.0D0
        DCMAX(J) = 15.0D-2
      ELSE
        KAI(J) = .2339
        KD(J) = 1.109
        KDC(J) = 1.0
        FMAX(J) = 15.0D0
        DCMAX(J) = 7.0D-2
      ENDIF
98    CONTINUE

      ZETAR = 1.0/SQRT(2.0)
      OMGR = 0.05*2.0*3.14159
C                 SET ACCELEROMETER NOISE TO ZERO
      NA = 0.0

C                 SET NUMBER OF MODES IN MODEL
      NMOD = 10
C                 SET NUMBER OF ACTUATORS
      NACT = 10

      SECS = TF-T0
C                 CALC NUMBER OF POINTS IN SIMULATION
      MM = INT(SECS/T)
C                 CALC NUMBER OF STATES USED
      N = 2*NMOD + 7*NACT
C                 SET PARAMETERS FOR DVERK
      NW = 109
      TOL = 0.0005
      IND = 1
C                 INITIALIZE STATE TO ZERO
      DO 981 J = 1,NW
      Y(J) = 0.0D0
981   CONTINUE

C                 TOP OF LOOP WHICH STEPS THE STATE THROUGH TIME

      DO 50 KK = 1,MM
C                 TIME WHERE STATE IS KNOWN
       TK = T*FLOAT(KK-1) + T0
C                 TIME WHERE STATE IS DESIRED
       TKEND = T*FLOAT(KK) + T0
C                 SET INPUT PARAMETER FOR DVERK
```

```
      IND = 1
C
C                 CALL DIFF EQ SOLVER TO PROPOGATE STATE FROM
C                 TIME = TK TO TIME = TKEND
C
      CALL DVERK(N,YDOT,TK,Y,TKEND,TOL,IND,C,NW,W,IER)

C                 CHECK FOR ERROR IN DVERK
      IF(IND.LT.0)GOTO 873

C                 SET UP REFERENCE INPUT COMMAND
      IF(TK.GT.EXCON.AND.TK.LT.EXCOFF)THEN
C                 IF IN EXCITATION STAGE, INPUT IS SINUSOIDAL
       DO 107 III = 1,10
        R(III) = XAMP(III)*SIN(XOMG(III)*TK)
107    CONTINUE
      ELSE
C                 IF IN FREE DECAY STAGE, INPUT IS ZERO
       DO 108 III = 1,10
        R(III) = 0.0
108    CONTINUE
      ENDIF

C                 CALCULATE MAST POSITION AND VELOCITY AT
C                 EACH ACTUATOR LOCATION
      DO 10 J = 1,NACT

       P(J) = 0.0
       V(J) = 0.0
       DO 20 I = 1,NMOD
        P(J) = P(J) + ALPHA(I,J)*Y(2*I-1)
        V(J) = V(J) + ALPHA(I,J)*Y(2*I)
20     CONTINUE

C                 CALCULATE PROOF MASS RELATIVE POSITION
       DEL(J) = ( Y(2*NMOD+7*J-6) - P(J) )
C                 QUANTIZE TO SIMULATE OPTICAL ENCODER
       DEL(J) = E(DEL(J))
C                 CALCULATE ESTIMATE OF REL POS FOR BLENDER
       DELE(J) = Y(2*NMOD+7*J)

10    CONTINUE
C                 SAVE FORCE FOR PSD CALCULATION
      DELREL(KK) = F(NUMACT)

C                 SET RELATIVE POSITION COMMAND = REFERENCE INPUT
      DO 115 J = 1,NACT
```

```
      DC(J) = R(J)
115   CONTINUE

C                 CALCULATE PFE
      ERROR = ERROR + ((DEL(NUMACT)-DC(NUMACT))/XAMP(NUMACT))**2

C                 IMPLEMENT INPUT COMMAND LIMITER
      DO 80 J = 1,NACT
       IF(ABS(DC(J)).GT.DCMAX(J))
     $       DC(J) = SIGN(DCMAX(J),DC(J))
80    CONTINUE

      TIM = TKEND

C                 CALCULATE FORCE GENERATED BY EACH ACTUATOR
      DO 70 J = 1,NACT

      F(J) = 250.0*(KDC(J)*DC(J)-NI-Y(2*NMOD+7*J-4)
     $            - KD(J)*(1.0-GAM)*Y(2*NMOD+7*J)
     $            -KD(J)*GAM*DEL(J)    )

C                 IMPLEMENT FORCE LIMITING OF LDCM
      IF(ABS(F(J)).GT.FMAX(J))F(J) =
     $                 SIGN(FMAX(J),F(J))

70    CONTINUE

C                 PRINT OUT SIGNALS AT EACH STEP IN
C                 TIME FOR PLOTTING
       DO 116 J = 1,NACT
        WRITE(10,1985)J,TIM,P(J)
        WRITE(11,1985)J,TIM,F(J)
        WRITE(12,1985)J,TIM,DEL(J)
        WRITE(13,1985)J,TIM,DC(J)
        WRITE(15,1985)J,TIM,V(J)
        WRITE(16,1985)J,TIM,DELE(J)
116    CONTINUE

C                 END OF LOOP WHICH PROPOGATES THE STATE
C                 THROUGH TIME
50    CONTINUE


C                 THIS SECTION CALCULATES THE POWER SPECTRAL
C                 DENSITY (PSD) OF A SIGNAL

C                 DECIDE WHAT SECTION OF DATA TO USE
      K1 = INT(EXCON/T)
```

```
      K2 = INT(EXCOFF/T)
C                 CALC NUMBER OF DATA POINTS
      MM = K2-K1
C                 MULTIPLY EACH DATA POINT BY THE WINDOW VALUE
C                 AND PUT IN A COMPLEX ARRAY
      DO 109 J = K1,K2
       K = J-K1
       IF(K.LT.(MM-1)/2)THEN
         WBART = 2.0*FLOAT(K)/FLOAT(MM-1)
       ELSE
         WBART = 2.0-2.0*FLOAT(K)/FLOAT(MM-1)
       ENDIF
       WHAM = 0.54-0.46*COS(2.0*3.14159*FLOAT(K)/FLOAT(MM-1))
       TMP = DELREL(J)
       PSDPER(K) = DCMPLX(TMP,0.0D0)
       PSDHAM(K) = DCMPLX(TMP*WHAM,0.0D0)
       PSDBAR(K) = DCMPLX(TMP*WBART,0.0D0)
109   CONTINUE
C                 TAKE THE DFT OF THE WINDOWED DATA
      CALL FFTCC(PSDPER,MM,IWK,WK)
      CALL FFTCC(PSDHAM,MM,IWK,WK)
      CALL FFTCC(PSDBAR,MM,IWK,WK)

      DO 110 K = 0,MM-1
C                 TAKE THE MAGNITUDE SQUARED AND NORMALIZE BY THE
C                 NUMBER OF POINTS TO GET THE PSD
       SFFP(K) = CDABS(PSDPER(K))**2/FLOAT(MM+1)
       SFFH(K) = CDABS(PSDHAM(K))**2/FLOAT(MM+1)
       SFFB(K) = CDABS(PSDBAR(K))**2/FLOAT(MM+1)
C                 PUT PSD IN DB
       SFFP(K) = 10.0*LOG10(SFFP(K))
       SFFB(K) = 10.0*LOG10(SFFB(K))
       SFFH(K) = 10.0*LOG10(SFFH(K))
110   CONTINUE

C                 SET UP FREQUENCY PROPORTIONALITY CONSTANT
      TMP = 2.0*3.14159/T/FLOAT(MM)
C                 PRINT OUT THE DATA FOR PLOTTING
      DO 111 K = 0,(MM-1)/2
       WRITE(16,*)TMP*FLOAT(K),SFFP(K),SFFB(K),SFFH(K)
111   CONTINUE

C                 PRINT THE NORMALIZED PFE
      WRITE(*,*)ERROR/FLOAT(MM),'  SUM ( (DC(K)-DEL(K))/DC(K) )**2 '

1985  FORMAT(1X,I5,2(1X,E12.5))
```

```
      STOP
873   WRITE(6,*)'ERROR,  IND = ',IND
      STOP
      END

C               THIS SUBROUTINE IMPLEMENTS THE MODEL BY
C               CALCULATING THE DERIVATIVE OF THE STATE
C               FROM THE STATE AND TIME, THE DIFF EQ
C               SOLVER USES THIS ROUTINE TO PROPOGATE
C               THE STATE THROUGH TIME

      SUBROUTINE YDOT(N,TK,Y,YPRIME)
      EXTERNAL E
      COMMON ALPHA,OMG,ZETA,MASS,NMOD,NACT
      COMMON EXCON,EXCOFF,CONTON,CONOFF,XOMG,XAMP
      COMMON GAM,TAU,KAI,KD
      COMMON ZETAR,OMGR,FMAX,DCMAX,NI,NA
      COMMON KDC

C               EXCITATION START TIME
      REAL*8 EXCON
C               EXCITATION STOP TIME
      REAL*8 EXCOFF
C               CONTROL START TIME
      REAL*8 CONTON
C               CONTROL STOP TIME
      REAL*8 CONOFF
C               NUMBER OF STATES PASSED TO DVERK (DIFF EQ SOLV)
      INTEGER N
      INTEGER III
C               NUMBER OF ACTUATORS IN SYSTEM
      INTEGER NACT
C               NUMBER OF MODES IN MAST MODEL
      INTEGER NMOD
      INTEGER I,J,JJ,K
      REAL*8 TMPP
C               BLENDER CONSTANT
      REAL*8 GAM
C               ACTUATOR COMPENSATION PARAMETERS
      REAL*8 TAU
      REAL*8 KAI(10)
      REAL*8 KD(10)
      REAL*8 ZETAR
      REAL*8 OMGR
      REAL*8 KDC(10)
C               FORCE LIMIT
      REAL*8 FMAX(10)
C               INPUT LIMIT
```

```
      REAL*8 DCMAX(10)
C                 ACCELEROMETER NOISE
      REAL*8 NA
      REAL*8 SUM
C                 TIME WHERE CURRENT STATE IS VALID
      REAL*8 TK
C                 STATE VECTOR
      REAL*8 Y(109)
C                 DERIVATIVE OF STATE
      REAL*8 YPRIME(109)
C                 REFERENCE INPUT COMMAND
      REAL*8 R(10)
C                 RELATIVE POSITION COMMAND
      REAL*8 DC(10)
C                 MAST INERTIAL POSITION
      REAL*8 P(10)
C                 MAST INERTIAL VELOCITY
      REAL*8 V(10)
C                 MODE SHAPE COEFFICIENT (MODE #,ACTUATOR NUMBER)
      REAL*8 ALPHA(10,10)
C                 RELATIVE POSITION MEASURED BY OPTICAL ENCODER
      REAL*8 DEL(10)
C                 MODE FREQUENCY (MODE #)
      REAL*8 OMG(10)
C                 DAMPING OF EACH MAST MODE (MODE #)
      REAL*8 ZETA(10)
C                 MASS OF PROOF MASS (ACT #)
      REAL*8 MASS(10)
C                 EXCITATION AMPLITUDE (ACT #)
      REAL*8 XAMP(10)
C                 EXCITATION FREQUENCY (ACT #)
      REAL*8 XOMG(10)
C                 FORCE APPLIED TO PROOF MASS
      REAL*8 F(10)

C                 SET UP REFERENCE INPUT COMMAND
      IF(TK.GT.EXCON.AND.TK.LT.EXCOFF)THEN
C                 IF IN EXCITATION STAGE, INPUT IS SINUSOIDAL
        DO 101 III = 1,10
          R(III) = XAMP(III)*SIN(XOMG(III)*TK)
101     CONTINUE
      ELSE
C                 IF IN FREE DECAY STAGE, INPUT IS ZERO
        DO 102 III = 1,10
          R(III) = 0.0
102     CONTINUE
      ENDIF
```

```
C               CALCULATE MAST POSITION AND VELOCITY AT
C               EACH ACTUATOR LOCATION
      DO 10 J = 1,NACT

       P(J) = 0.0
       V(J) = 0.0
       DO 20 I = 1,NMOD
        P(J) = P(J) + ALPHA(I,J)*Y(2*I-1)
        V(J) = V(J) + ALPHA(I,J)*Y(2*I)
20     CONTINUE

C               CALCULATE PROOF MASS RELATIVE POSITION
       DEL(J) =  Y(2*NMOD+7*J-6) - P(J)
C               QUANTIZE TO SIMULATE OPTICAL ENCODER
       DEL(J) =  E( DEL(J) )

10    CONTINUE

C               SET RELATIVE POSITION COMMAND = REFERENCE INPUT
       DO 107 J = 1,NACT
        DC(J) = R(J)
107    CONTINUE

C               IMPLEMENT INPUT COMMAND LIMITER
      DO 80 J = 1,NACT
       IF(ABS(DC(J)).GT.DCMAX(J))DC(J) = SIGN(DCMAX(J),DC(J))
80    CONTINUE

C               CALCULATE FORCE GENERATED BY EACH ACTUATOR
      DO 90 J = 1,NACT

       F(J) = 250.0*(   KDC(J)*DC(J) - NI - Y(2*NMOD+7*J-4)
     $              - KD(J)*(1.0-GAM)*Y(2*NMOD+7*J)
     $              -KD(J)*GAM*DEL(J)    )

C               IMPLEMENT FORCE LIMITING OF LDCM
       IF(ABS(F(J)).GT.FMAX(J))F(J) =
     $                 SIGN(FMAX(J),F(J))

90    CONTINUE


C               THIS SECTION CALCULATES THE DERIVATIVE OF THE
C               STATES OF THE SYSTEM IN TERMS OF THE STATES,
C               INPUTS, AND FORCE
```

```
C               THE STATES OF THE SYSTEM ARE ARRAINGED
C               IN ORDER WITH THE MAST MODES FIRST, FOLLOWED
C               BY THE MODES FOR THE ACTUATOR AND COMPENSATION

C               THIS BLOCK OF EQUATIONS, THE FIRST ( 2 * NMOD )
C               ARE THE STATES FOR THE MODES OF THE MAST
      DO 50 I = 1,NMOD

       YPRIME(2*I-1) = Y(2*I)

       SUM = 0.0
       DO 60 J = 1,NACT
        SUM = SUM + ALPHA(I,J)*F(J)
60     CONTINUE

       YPRIME(2*I) = -OMG(I)**2*Y(2*I-1)
     $          -2.0*ZETA(I)*OMG(I)*Y(2*I)
     $          - SUM

50    CONTINUE

C               THIS BLOCK OF EQUATIONS, STARTING FROM 2*NMOD+1
C               ARE FOR THE ACTUATOR AND COMPENSATION
C               EACH ACTUATOR WITH COMPENSATION CONSISTS OF
C               7 STATES
      DO 70 J = 1,NACT
C               SET UP JJ TO INDEX INTO THE CORRECT BLOCK OF
C               STATES FOR EACH ACTUATOR
      JJ = 2*NMOD+7*J

      YPRIME(JJ-6) = Y(JJ-5)

      YPRIME(JJ-5) = F(J)/MASS(J)

      YPRIME(JJ-4) = -2.0*ZETAR*OMGR*Y(JJ-4) + Y(JJ-3)
     $          + KAI(J)*F(J)/MASS(J) + KAI(J)*NA

      YPRIME(JJ-3) = -OMGR**2*Y(JJ-4)

      SUM = 0.0
      DO 108 I = 1,NMOD
       SUM = SUM + ALPHA(I,J)*YPRIME(2*I)
108   CONTINUE

      YPRIME(JJ-2) = -TAU*Y(JJ-2) + SUM

      YPRIME(JJ-1) = -TAU*Y(JJ-1) + F(J)/MASS(J) + NA
```

```
      YPRIME(JJ) = Y(JJ-1) - Y(JJ-2) - TAU*Y(JJ)

70    CONTINUE

      RETURN
      END


C                THIS FUNCTION QUANTIZES THE ARGUMENT TO
C                SIMULATE THE DIGITAL MEASUREMENT OF THE
C                OPTICAL ENCODER
      FUNCTION E(X)
C                ARGUMENT
      REAL*8 X
C                ENCODER RESOLUTION
      REAL*8 R
      REAL*8 E
      REAL*8 TMP
C                SET ENCODER RESOLUTION TO 1 MM
      R = 1.00D-3
C                THIS FUNCTION ROUNDS TO THE NEAREST [RESOLUTION]
      TMP = X/R + DSIGN(0.5D0,X)
      E = R*FLOAT(INT(TMP))
      END
```

References

[1] Card, M. F., Anderson, W. W., "Technical Issues In Dynamics and Control of Large Space Structures", *34th Congress of the International Astronautical Federation*, Budapest, Hungary, Oct. 10-15, 1983, Paper No. 83-404.

[2] Forward, R. L., "Electronic Damping of Orthogonal Bending Modes In A Cylindrical Mast-Experiment", *Journal of Spacecraft and Rockets*, Vol. 18, No. 1, Jan.-Feb. 1981.

[3] Bailey, T., Hubbard, J. E., "Distributed Piezoelectric-Polymer Active Vibration Control of a Cantilever Beam", *Journal of Guidance, Control, and Dynamics*, Vol. 8, No. 5, Sept.-Oct. 1985.

[4] Aubrun, J. N.,Margulies, G., *Gyrodampers for Large Space Structures*, NASA CR-NAS1-14887-Task 6, Feb. 1979.

[5] Mills, R. A., "Active Vibration Control Of A Cantilevered Beam: A Study of Control Actuators", *34th Congress of the International Astronautical Federation*, Budapest, Hungary, Oct. 10-15, 1983, Paper No. ST 83-11.

[6] Aubrun, J. N., Margulies, G., *Low-Authority Control Synthesis for Large Space Structures*, NASA CR-NAS1-14887, May 1982.

[7] Zimmerman, D. C., Horner, G. C., Inman, D. J., "Microprocessor Controlled Force Actuator", *Journal of Guidance, Control, and Dynamics*, Jan.-Feb. 1988.

[8] Zimmerman, D. C., Inman, D. J., "Actuator Structure Interactions" *Proceedings of the Second NASA/DOD Control/Structure Interaction Technology Conference*, Nov. 17-19, 1987.

[9] Haviland, J. K., Politansky, H., Lim, T. W., Pilkey, W. D., "The Control of Linear Proof-Mass Dampers" *Proceedings of the Sixth VPI&SU/AIAA Symposium on Dynamics and Control of Large Structures*, Blacksburg, VA, June 29 - July 1, 1987.

[10] Kuo, B., *Automatic Control Systems*, Prentice Hall, Englewood Cliffs, NJ, 1982.

[11] Meirovitch, L., *Elements of Vibration Analysis*, Mcgraw-Hill, New York, 1986.

[12] Oppenheim, A., Schafer, R., *Digital Signal Processing*, Prentice-Hall, Englewood Cliffs, NJ, 1975.

[13] Orfandis, S., *Optimum Signal Processing, An Introduction*, MacMillan, New York, 1985.

Vita

Mr. Ide was born in San Diego, CA in 1963. He grew up and lived in Endwell, NY until March, 1980. He graduated from high school in June, 1981 in Waynesboro, VA.

Mr. Ide received a T. Marshall-Hahn Engineering Merit Scholarship and attended Virginia Polytechnic Institute and State University (Virginia Tech) for his undergraduate work. While at Virginia Tech, he participated in the co-op program with IBM in Endicott, NY. He received his Bachelor of Science in Electrical Engineering, Summa Cum Laude, in September, 1985.

Mr. Ide worked for Sanders Associates in Nashua, NH from September, 1985 to September, 1986. He returned to Virginia Tech in September, 1986 to pursue his Master of Science in Electrical Engineering.

Mr. Ide is a member of Tau Beta Pi, Eta Kappa Nu, Phi Kappa Phi, and the IEEE ASSP Society.